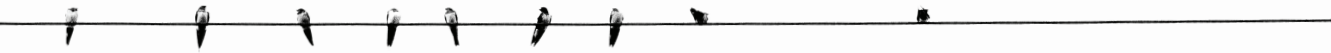

COST ALLOCATION AND RISK MANAGEMENT IN RENEWABLE ELECTRICITY NETWORKS

Bo Tranberg

PhD Dissertation

January 2019

Danske Commodities

AARHUS UNIVERSITY
DEPARTMENT OF ENGINEERING

COST ALLOCATION AND RISK MANAGEMENT IN RENEWABLE ELECTRICITY NETWORKS

Bo Tranberg
Department of Engineering, Aarhus University
Danske Commodities

PhD Dissertation

January 2019

1st Edition, January 2019

Bo Tranberg
Department of Engineering
Aarhus University
Inge Lehmanns Gade 10
DK-8000 Aarhus C

This document was typeset in LaTeX.

Cover design by Maria Sedykh.
Cover photo by Danielle MacInnes on Unsplash.

Contents

Summary v

Preface ix

Acknowledgments xiii

1 General introduction 1

Part I
Cost allocation in renewable electricity networks 5

2 Introduction 7
- 2.1 Motivation 7
- 2.2 Methods 8
- 2.3 Main findings 13

3 Decompositions of injection patterns 15
- 3.1 Introduction 15
- 3.2 Methods of flow allocation 18
- 3.3 Power flow decomposition 25
- 3.4 Conclusion 31

4 Flow-based nodal cost allocation 35
- 4.1 Introduction 35
- 4.2 Modelling and methods 36
- 4.3 Flow-based nodal cost allocation 47
- 4.4 Results 49
- 4.5 Conclusion and outlook 56

5 Flow-based analysis of storage usage 59
- 5.1 Introduction 59
- 5.2 Power system modelling 60
- 5.3 Flow tracing 62
- 5.4 Results 64
- 5.5 Discussion & conclusions 68

6 Real-Time Carbon Accounting 71
6.1 Introduction 71
6.2 Methods 72
6.3 Results 76
6.4 Conclusion 78

Part II
Managing wind risk 81

7 Introduction 83
7.1 Motivation 83
7.2 Methods 85
7.3 Main findings 87

8 Managing volumetric risk of long-term power purchase agreements 89
8.1 Introduction 89
8.2 Modeling framework 91
8.3 Modeling power spot price and wind power production 99
8.4 Application to risk management 113
8.5 Conclusion 127

9 Concluding remarks 129

Appendices 135

A A simplified model of a highly renewable European electricity network 135

B Copulas 137
B.1 Information matrices 137
B.2 Derivations of copula scores 138
B.3 Mapping functions copulas 142

C Supplementary material 143
C.1 Carbon intensities 143
C.2 Flow tracing 148
C.3 Additional results 150

Bibliography 159

Summary

As part of the efforts to mitigate climate change, there has been rapidly increasing share of renewable power generation in the European electricity system. In the interest of bridging the gap between corporate and academic research interests, this PhD project presents a research collaboration on renewable electricity systems between Aarhus University and the energy trading company Danske Commodities.

The first part of this dissertation has the perspective of a central planner exploring the optimal system design based on simplified fundamental models of the European electricity system. The aim is to determine the optimal locations and capacities of renewable generation sources while keeping the system reliable and cost-efficient. A subsequent step is to allocate the costs associated with the investments needed for the optimal electricity system of the future. I apply power flow tracing techniques for allocation of transmission system usage, cost allocation of generation capacities as well as consumption-based carbon accounting.

In the second part, the perspective is changed to that of individual investors in renewable generation technologies, specifically wind turbines. I apply econometric models in the form of copulas to jointly model wind power production and power spot price. The goal is for an energy trading company to minimize the risk associated with long-term wind power purchase agreements, which, in turn, minimizes the risk of investors in these wind turbines. This provides additional incentives for similar investments and thereby increasing the share of renewable power generation in the European electricity system.

Applying physical and financial models to different aspects of the European electricity system has led to insights on the differences between the two modeling perspectives. The central planning perspective is useful when exploring pragmatic solutions to the overall design of the European electricity system of the future, but provides no guidance for the individual actors in the system. In contrast, an investor in renewable generating assets focuses on a set of business goals with little regard to their impact on the overall electricity system.

The link between the two perspectives is the policy makers, who regulate the electricity system. The results from system models using the central planning

perspective can be used by the policy makers as guidelines to provide the right incentives for investors, and other actors in the system, such that the current European electricity system develops towards the optimal and sustainable system of the future.

Resume

Der er sket en hastig stigning i andelen af vedvarende energikilder i det europæiske elsystem som følge af bestræbelserne på at formindske klimaforandringer. Dette PhD-projekt er et forskningssamarbejde mellem Aarhus Universitet og energihandelsselskabet Danske Commodities med det formål at bygge bro imellem erhvervsmæssige og akademiske forskningsinteresser med hensyn til det europæiske elsystem.

Første del af afhandlingen har en central planlæggers perspektivet, som udforsker det optimale systemdesign baseret på simplificerede fundamentale modeller for det fremtidige europæiske elsystem. Målet er at fastlægge de optimale placeringer og kapaciteter af vedvarende energikilder og samtidigt sørge for at systemet er pålideligt og omkostningseffektivt. Et efterfølgende skridt er at allokere omkostningerne i forbindelse med de nødvendige investeringer for at nå det optimale fremtidige system. Jeg anvender flow-tracing metoder til at allokere brugen af transmissionsnetværket, allokering af omkostninger ved generationskapaciteter og et forbrugsbaseret CO_2-regnskab.

I anden del skifter perspektivet til individuelle investorer i vedvarende energikilder, specifikt vindmøller. Jeg anvender økonometriske modeller i form af copulaer til at lave en fælles model for vindproduktion og spotprisen i elmarkedet. Målet for en energihandelsvirksomhed er at minimere risikoen i forbindelse med længerevarende fastpriskontrakter for vindenergi, som derved minimerer risikoen for investorer i vindmøller. Dette giver incitament til yderligere investeringer i vedvarende energikilder, som dermed forøger andelen af vedvarende energi i det europæiske elsystem.

Anvendelsen af fysiske og finansielle modeller til forskellige aspekter af det europæiske elsystem har ført til indsigt i forskellene mellem de to perspektiver. En central planlæggers perspektiv er brugbart til at udforske pragmatiske løsninger til det overordnede design af det fremtidige europæiske elsystem, men giver ingen vejledning for individuelle aktører i systemet. I modsætning fokuserer individuelle investorer i vedvarende energikilder på et sæt af forretningsmål uden at tage højde for disses effekt på det overordnede elsystem.

Forbindelsen imellem de to perspektiver er politikerne, som regulerer elsystemet. Resultaterne fra modeller med perspektivet af en central planlægger kan bruges

af politikerne som inspiration til at implementere de rette incitamenter for investorer, og andre aktører i systemet, sådan at det nuværende europæiske elsystem udvikler sig mod det optimale, fremtidige, bæredygtige system.

Preface

This dissertation presents the results of a research collaboration between Aarhus University and Danske Commodities. Throughout this project, I have spent approximately half of my time at each party. The purpose of the project has been to bridge the gap between corporate and academic research interests within the fields of energy system modeling and electricity trading. This has put me in a unique position to learn from, and draw on, expert knowledge from Aarhus University in relation to analyses carried out for Danske Commodities and vice versa, which has proven valuable for both organizations during the project.

Researching future scenarios for the European electricity system using fundamental energy system models, while being part of Danske Commodities, has enabled me to concurrently evaluate the practical applicability of my research. It has also highlighted the differences between the central planner perspective of energy system models and the perspective of individual investors in the electricity system. Furthermore, the contrast between the requirements and deadlines of an operational organization and the thorough and comprehensive nature of academic research has been challenging. It has also helped qualify the corporate as well as academic aspects of my research.

In my time at Danske Commodities, I have contributed to several quantitative business analyses all focusing on improving the business case of long-term wind power purchase agreements. The main outcome of this work was the development of a new model for pricing and hedging long-term wind power purchase agreements, which was subsequently implemented in the business. The development of this model also led to an academic publication, which is included here.

The following is dedicated to presenting my academic contributions. During this project, I have contributed to 10 academic publications. The five most important of these are highlighted as individual chapters. The dissertation is split into two parts. The first part presents the results of my work on energy system models at Aarhus University. The second part presents the results of my work on pricing and risk management of long-term wind power purchase agreements at Danske Commodities. In addition to written contributions, I have presented my work at three conferences and internally at Vestas and NRGi.

INCLUDED ARTICLES

The following is a list of academic contributions in order of appearance in this dissertation. These articles constitute chapters 3–6 and 8. They have all been, or are in the process of being, peer reviewed. The articles have been typeset differently than they appear in the respective journals to appear coherently here. Equations and figures are numbered within each chapter and references appear in a combined bibliography at the end.

Decompositions of injection patterns for nodal flow allocation in renewable electricity networks, Mirko Schäfer, Bo Tranberg, Sabrina Hempel, Sefan Schramm and Martin Greiner, *European Physical Journal B*, 2017 [1].

I took main responsibility for the analysis and provided a minor contribution to the writing process.

Flow-based nodal cost allocation in a heterogeneous highly renewable European electricity network, Bo Tranberg, Leon J. Schwenk-Nebbe, Mirko Schäfer, Jonas Hörsch and Martin Greiner, *Energy*, 2018 [2].

This article was prepared in coordination with the master's thesis work of Leon J. Schwenk-Nebbe. I supervised the project in collaboration with professor Martin Greiner. Mirko Schäfer and I shared the responsibility for organizing, adapting and writing the work into a format suitable for publication as a journal article.

Flow-Based Analysis of Storage Usage in a Low-Carbon European Electricity Scenario, Bo Tranberg, Mirko Schäfer, Tom Brown, Jonas Hörsch and Martin Greiner, *15th International Conference on the European Energy Market (EEM)*, 2018 [3].

This article builds on previous work by Tom Brown and Jonas Hörsch. I took main responsibility for the analysis and subsequently writing the work into a format suitable for publication as a conference article.

Real-time carbon accounting method for the European electricity markets, Bo Tranberg, Olivier Corradi, Bruno Lajoie, Thomas Gibon, Iain Staffell and Gorm Bruun Andresen, Submitted to *Energy Strategy Reviews* [4].

This is a collaboration with Tomorrow to showcase the carbon accounting methodology of the electricityMap[1]. Olivier Corradi and Bruno Lajoie provided system

[1] www.electricitymap.org

data from the electricityMap and Thomas Gibon extracted carbon intensity data from the ecoinvent database. I took main responsibility for the analysis and subsequently writing the work into a format suitable for publication as a journal article.

Managing Volumetric Risk of Long-term Power Purchase Agreements, Bo Tranberg, Rasmus Thrane Hansen and Leopoldo Catania, Submitted to *Energy Economics*, 2018 [5].

This article was prepared in coordination with the master's thesis work of Rasmus Thrane Hansen. I initiated and later supervised the project in collaboration with assistant professor Leopoldo Catania. I took main responsibility for organizing, adapting and writing the work into a format suitable for publication as a journal article.

ADDITIONAL ARTICLES

The following is a list of academic contributions during this project that are not included in this dissertation.

Power Flow Tracing in Complex Networks, Mirko Schäfer, Sabrina Hempel, Jonas Hörsch, Bo Tranberg, Stefan Schramm and Martin Greiner, *New Horizons in Fundamental Physics*, 2017 [6].

Optimal heterogeneity in a simplified highly renewable European electricity system, Emil H. Eriksen, Leon J. Schwenk-Nebbe, Bo Tranberg, Tom Brown and Martin Greiner, *Energy*, 2017 [7].

Allocation of nodal costs in heterogeneous highly renewable European electricity networks, Mirko Schäfer, Leon J. Schwenk-Nebbe, Jonas Hörsch, Bo Tranberg and Martin Greiner, *2017 14th International Conference on the European Energy Market (EEM)*, 2017 [8].

Statistical meandering wake model and its application to yaw-angle optimisation of wind farms, Emil Thøgersen, Bo Tranberg, Jürgen Herp and Martin Greiner, *Journal of Physics: Conference Series*, 2017 [9].

Power flows in complex renewable energy networks, Mirko Schäfer, Bo Tranberg and Martin Greiner, Contribution to *FIAS International Symposion on Discoveries at the Frontiers of Science 2017, To appear* [10].

CONFERENCE PRESENTATIONS

Market integration of renewables - Challenges facing traders. Presented at the CoNDyNet Industry Workshop: From Research to Application. November 2016. Frankfurt, Germany.

Statistical meandering wake model and its application to yaw-angle optimisation of wind farms. Presented at WIND ENERGY DENMARK 2017. October 2017. Herning, Denmark.

Flow-based analysis of storage usage in a low-carbon European electricity scenario. Presented at the 15th International Conference on the European Energy Market. June 2018. Łódź, Poland.

CORPORATE PRESENTATIONS

Challenges with increasing renewables. Presented at Vestas. October 2016.

Power markets: past, present, future. Presented at Vestas. October 2017.

Wind power purchase agreements. Presented at NRGi. November 2017.

Electricity markets: past, present, future. Presented at Vestas. September 2018.

Acknowledgements

First and foremost, I would like to thank Kristian Gjerløv-Juel and Martin Greiner for making this project possible and believing that I was the right candidate. I would also like to thank Gorm Bruun Andresen for his wise words towards the end of the project.

Thanks to everyone at Danske Commodities who introduced me to the world of finance and energy trading and patiently answered my endless questions.

A big thank you to my PhD colleagues Hailiang Liu, Kun Zhu, Magnus Dahl and Smail Kozarcanin for helpful discussions related to issues inside as well as outside the office.

To my colleagues from abroad Jonas Hörsch, Mirko Schäfer and Tom Brown: Thanks for everything!

1

General introduction

It is widely acknowledged that human activities, in the form of greenhouse gas (GHG) emissions, have led to changes in the global climate, specifically in the form of global warming [11]. Global warming negatively impacts our environment, e.g., by increasing the frequency and intensity of extreme weather events. To mitigate climate change, many countries are now transitioning the energy system away from traditional fossil-fuel power plants to low-carbon renewable technologies such as hydro, solar and wind power generation.

This wide acknowledgment of climate change has not always existed. It all began in 1983 when the United Nations (UN) formed the World Commission on Environment and Development. It was a response to several global environmental challenges not being adequately addressed following the 1972 United Nations Conference on the Human Environment. The output of the commission was the report *Our Common Future* published in 1987 [12]. The report is particularly known for the modern definition of *sustainable development*:

> Sustainable development is development that meets the needs of the present without compromising the ability of future generations to meet their own needs.
>
> ...
>
> Thus, the goals of economic and social development must be defined in terms of sustainability in all countries – developed or developing, market-oriented or centrally planned [12].

The work of the commission and the publication of the report had an impact on subsequent UN conventions leading to the adoption of the *Kyoto Protocol* in 1997. This led to 193 countries committing to reduce greenhouse gas concentration in the atmosphere to "a level that would prevent dangerous anthropogenic interference with the climate system" [13].

In 2011, the European Union set an ambitious long-term goal to reduce greenhouse gas emissions by 80–95% by 2050, compared to 1990 levels [14]. This goal was reinforced in 2015 by the *Paris Agreement* with the long-term goal to hold the increase in the global average temperature well below 2°C above pre-industrial levels and to limit the temperature increase to 1.5°C above pre-industrial levels [15].

In 2018, The Intergovernmental Panel on Climate Change (IPCC) published a special report on the impacts of global warming of 1.5°C above pre-industrial levels and related global greenhouse gas emission pathways [11]. The report suggests zero GHG emissions by 2050 in all scenarios to meet the goals of the Paris Agreement. It further suggests net negative CO_2 emission from 2050 onwards.

In November 2018, the European Union [16] adopted a new long-term vision for a climate neutral economy by 2050 in line with the Paris Agreement. It concludes with the statement:

> Internationally, over the coming year the EU should expand its cooperation closely with its international partners, so that all parties to the Paris Agreement develop and submit a long-term national mid-century strategy by 2020 in the light of the recent IPCC Special report on 1.5°Celsius [16].

It is clear from this time line that the view on climate change has escalated significantly during the last three decades. A large contribution to the GHG emissions comes from the energy sector. More than 80% of the global electricity generation has been originating from fossil fuel for several decades [17]. As a result, electricity and heat production account for 25% of global GHG emissions [18]. In order to mitigate the GHG emissions from electricity production, it has been suggested for a decade that the electricity system should undergo a transition away from fossil-fueled power plants to renewable sources, e.g., hydro, solar, and wind power [19–25].

Such a transition is currently in progress in many countries. However, it is not without challenges. Power generated from renewable sources like hydro, solar, and wind depends on variable weather patterns and is, thus, variable. For a system to fully rely on renewable generation, it needs flexibility mechanisms to balance this variability. Such flexibility can be provided by large-scale storage units providing flexibility over time, and long-range transmission lines providing flexibility in space across large geographical areas [26, 27].

The focus of this dissertation is to explore solutions to the challenges mentioned above by: 1) investigating the optimal layout of renewable generation capacities (assuming cooperation between the European countries and subsequently allocate costs based on actual usage), and 2) improving risk management of long-term wind power purchase agreements. These two points of focus are addressed in Part 1 and Part 2, respectively.

OUTLINE

This dissertation is split in two parts as follows.

Part 1: The first part has the perspective of a central planner exploring the optimal system design based on simplified fundamental models of the European electricity system. The aim is to determine the optimal locations and capacities of renewable generation sources while keeping the system reliable and cost-efficient. A subsequent step is to allocate the costs associated with the investments needed for the optimal electricity system of the future. Flow tracing is the central methodology for the cost allocation mechanisms. When the optimal system has been found, it is up to the policy makers to implement policies that provide incentives for individual investors such that the current electricity system develops towards the optimal system of the future. Such policy implications are outside the scope of this dissertation.

Part 2: In the second part, the perspective is that of individual investors in renewable generation technologies in particular wind turbines. The purpose is to improve the risk management associated with the variable nature of wind production. The goal is for an energy trading company to minimize the risk associated with long-term wind power purchase agreements, which, in turn, minimizes the risk of investors these wind turbines. This provides additional incentives for similar investments and thereby increasing the share of renewable power generation in the European electricity system.

Chapter 9: This chapter provides a general conclusion to the work presented in Part 1 and Part 2.

Part I

Cost allocation in renewable electricity networks

2

Introduction

2.1 MOTIVATION

The European Union has set a goal to reduce carbon emissions by 80%–95% in 2050 compared to 1990 levels [14]. Reaching this goal requires the entire European energy system to undergo a massive change, decreasing the share of traditional fossil-fuel power plants and increasing the share of variable renewable sources such as hydro, solar and wind.

Such a shift from traditional power plants with scheduled production to variable renewable sources disrupts the traditional planning ability of the electricity system since all aspects become dependent on the feed-in of renewable electricity, which, in turn, depends on the weather conditions. In the following, electricity and power are used interchangeably.

Electricity systems with high shares of variable renewables have a high need of flexibility to ensure security of supply. Flexibility can be provided by long-range power transmission allowing pooling of resources across large geographical areas, storage units providing flexibility over time, fossil-fueled backup peaker plants e.g. gas turbines, or coupling the electricity system to other parts of the energy sector e.g. heating and transport.

The main research questions for the sustainable European electricity system of the future with a high share of renewables are:

1. How much renewable generation, transmission, and storage capacity should be installed?
2. Where should it be installed?
3. Who benefits from the renewable generation capacities and added flexibility of transmission and storage?

4. Who should pay for the necessary investments?

The first two questions are approached by modeling the fundamental physical and economic aspects of the electricity system. The perspective of the modeling applied is that of cooperation between the European countries with the objective to minimize the total system cost and not the costs of individual countries. Cooperation refers to renewable generation capacities being placed according to the best weather resources. This results in a need for additional transmission and storage capacity to balance the supply and demand on an hourly basis across the countries in the model.

Answering the latter two questions should incorporate a measure of the grid usage associated with power import and export between the involved countries. These questions can be answered using power flow tracing methods. Flow tracing follows the path of power flows through the transmission network connecting the location of generation with the location of consumption, thereby mapping the path in between. Flow tracing provides a measure of the share of transmission grid usage for each generation technology for each country. This measure can be used to quantify the benefits from additional installed generation capacities as well as the added flexibility of transmission and storage capacities.

2.2 METHODS

The four articles presented in this part follow a similar methodology. All use flow tracing methods for different applications. The first three articles apply flow tracing to outputs of energy system models whereas the last article applies flow tracing to a historical sample of real-time system data.

2.2.1 Electricity system modeling

The main purpose of energy system models is planning of current and future systems. Here, I focus exclusively on future scenarios for the European electricity system with high shares of renewable electricity generation. Due to the variable nature of renewable electricity generation with patterns on diurnal, synoptic and seasonal time-scales, these models must decide on the dispatch of generation, storage and imports/exports to continually balancing the electricity supply and demand.

I start with a simplified model of the European electricity network, in which each country is modeled as an aggregated node and transmission lines are aggregated

to single links between neighboring countries. The model is further simplified in such a way that all countries have the same share of renewable generation relative to the individual electricity demand. This is referred to as renewable penetration and the assumption is that the average electricity generation from wind and solar combined is equal to the average demand for each country – a scenario for 2050 in accordance with the EU climate goals. Additionally, the mix between wind and solar generation is fixed to 0.7 for all countries meaning that 70% of the renewable generation comes from wind. Fixing the renewable penetration and mix between wind and solar to the same value for all countries leads to a homogeneous layout. I also explore heterogeneous layouts of renewable generation capacities, which ensure that wind turbines and solar photovoltaics are installed in the locations with the best weather resources for maximum utilization and cost-optimal investments. Only three generation technologies are considered: variable solar and wind, as well as a generic dispatchable backup power for balancing. Time series for wind and solar production as well as electricity demand are used to determine the hourly nodal power balances, imports, exports and backup power needed. These are not determined by an optimization, but rather what is known as *synchronized balancing* in which the balancing assigned for every hour to each country is proportional to its average demand [28]. This way all countries are forced to cooperate on balancing the variability of the renewable power generation.

In a later study, I consider the techno-economic optimization model PyPSA [29] to determine the optimal investments in generation and storage capacities as well as dispatch. The objective is to minimize the total system cost in a low-carbon 2050 scenario for the European electricity system. This model features a set of six generation technologies and three storage technologies. Additionally, it features a higher spatial resolution of 64 nodes representing 33 European countries, which enables capturing patterns on regional scales within larger countries. The network topology considered in this study is based on clustering the full transmission network of Europe. For a discussion on network aggregation methods and the role of spatial scale in electricity system modeling, see [30].

While the studies presented here focus exclusively on the power sector, other studies have started investigating the effects of coupling with other sectors like heating and transport through electric vehicles and heat pumps [31, 32].

Extensions of the transmission grid beyond Europe and interconnecting the continents has been proposed to utilize renewable sources far from load centers [33] and to balance the variability of renewable power generation on a global

scale [34].

In addition to studying future electricity system scenarios, another important aspect is to model the transition from the current system. This provides policy makers with the necessary insights to implement policies that encourage investments in the right places at the right time for the system to follow an optimal transition path towards being fully renewable. The transmission needs during the transition of a European power system are studied in [35]. The roles of energy storage, grid exchange and flexible electricity generation in a transition towards a 100% renewable electricity system in the Baltic region is studied in [36]. The transition across the entire energy system for Germany towards 100% renewable in 2050 is studied in [25], finding the transition to be possible both from a technical and economic perspective. Additionally, two ambitious studies have modeled the global transition towards 100% renewable energy systems [24,37].

Recently, the usage of energy system models has received criticism, questioning the feasibility of a 100% renewable electricity system [38]. A detailed literature review shows that none of the raised issues are critical for feasibility or viability and that "each issue can be addressed at low economic cost, while not affecting the main conclusions of the reviewed studies" [39].

2.2.2 Power flow tracing

Flow tracing was formalized in the late 1990s by Bialek [40] and Kirschen [41] independently of each other. Following the deregulation of electricity markets flow tracing was introduced as a method to assess the impact of a specific generator or load on the power system. The initial proposed application of flow tracing was for transmission loss allocation [40]. Bialek proposed a method based on solving linear equations. Kirschen's method is based on an iterative approach where the problem is solved using recursive equations. A recent comparison of the two approaches, in relation to cost allocation in distribution networks, found that Bialek's method had a higher accuracy for determining distribution factors than Kirschen's method [42].

Both approaches require that Kirchhoff's current law (KCL) be satisfied for all nodes in the network i.e. the sum of currents flowing into a node equals the sum of currents flowing out. Additionally, both approaches introduce the *proportional sharing* principle, which states:

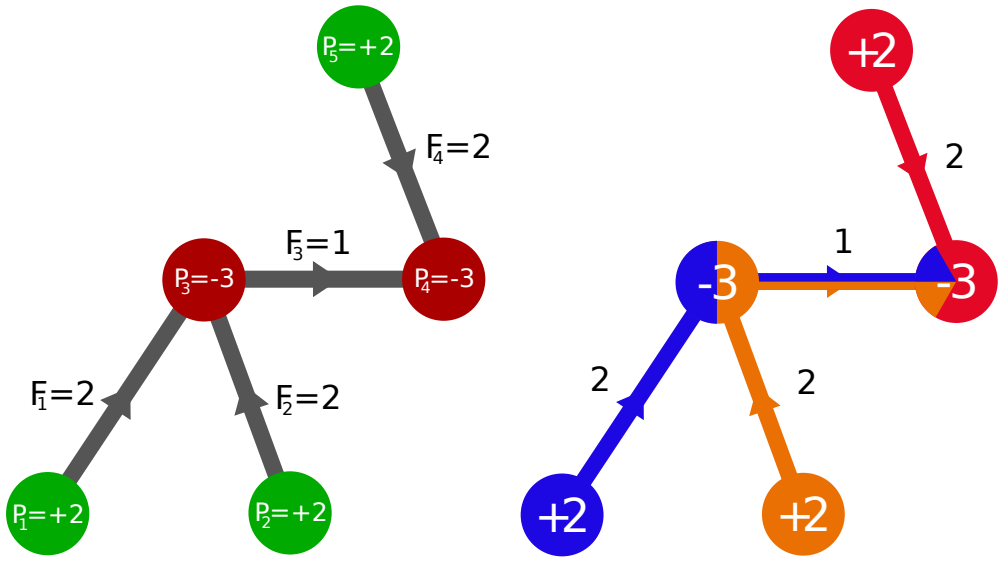

Figure 2.1: Nodal power balances and import/export (left). Flow tracing applied to exports (right). Reproduced from [43].

> If the proportion of the inflow which can be traced to generator i is x_i, then the proportion of the outflow which can be traced to generator i is also x_i [41].

An analogy to the KCL and proportional sharing principle is the mixing of water flows in pipe systems. An example of the proportional sharing principle is shown in Figure 2.1. The left part shows an example of three exporting nodes (1, 2, 5) and two importing nodes (3, 4) as well as power flows on the connecting links. The right part shows that the exports from node 1 and 2 mixes equally at node 3 and subsequently serves the load of node 3 with the remainder being exported to serve the load of node 4.

The proportional sharing principle is also referred to as *average participation* in the literature. It has been criticized since it considers total flows on each transmission line not allowing for supposition of opposing counter flows [44]. An alternative approach to flow tracing is the *marginal participation* method, which is based on power transfer distribution factors (PTDFs). This method considers the "sensitivity of each branch's active power flow to changes in the power balances of the nodes" [44]. Bialek presents three ways of rationalizing the use of the proportional sharing principle in [45]. The conclusions of his

arguments are:

1. For loss allocation to be fair, the sharing must be linearly proportional to the power flow

2. The proportional sharing principle coincides with the Shapley value from cooperative game theory when considering loss allocation as a coalition game

3. An argument based on the maximum entropy principle leads to proportional sharing of the mixing within each node

Considering the above criticism and rationalization of the proportional sharing principle, it is proposed for the application of transmission usage allocation in large-scale electricity networks due to its intuitiveness and lack of additional parameters [46].

In efforts to successfully implement the European Internal Electricity Market, cross-border tariffs were replaced by the Inter-Transmission System Operator Compensation (ITC) mechanism in 2004. The purpose of the mechanism is to provide compensation to transmission system operators for the costs associated with losses incurred by, and making infrastructure available to, cross-border flows of electricity [47–49]. Initially, the mechanism used a *postage stamp* method for infrastructure usage and a *With and Without* (WWT) method for loss allocation [48]. The postage stamp method allocates the transmission usage to each participant according to the its power injected/withdrawn in proportion to the total power injected/withdrawn in the system. The WWT method compares the flows through a country's transmission network with the flows in case all transits between third parties are removed. For a thorough description and comparison of these and other flow allocation methods, see [44,50,51]. Both of the initially used methods in the ITC mechanism have limitations and have been criticized in a number of studies, particularly for the lack of a "logical link between actual transits and the ITC charges" [49,52].

The Agency for the Cooperation of the Energy Regulators (ACER) was tasked to develop a new compensation mechanism by 2014. ACER published a "recommendation on a new regulatory framework for ITC" in 2013, concluding that a new regulatory framework should be developed to replace the existing methods [53]. However, to this day, there has been no agreement on a new method for the ITC. Studies comparing several different methods for flow allocation in

relation to the ITC mechanism have all recommended to use the proportional sharing flow tracing [50,51,54].

The following chapters present applications of flow tracing based on Bialek's method. These applications include: transmission usage, cost allocation and carbon accounting. Transmission usage is a direct output of flow tracing. Cost allocation and carbon accounting are both based on identifying trading partners (importers/exporters) and subsequently multiplying the exchanged power with infrastructure and operations costs for cost allocation or carbon emission intensity for carbon accounting.

2.3 MAIN FINDINGS

The first study acknowledges the limitation of proportional sharing flow tracing that it only considers the total flow on each transmission line and does not allow studying counter flows. It proposes two alternative methods by decomposing injection patterns that can be associated with individual contracts. These two new variants are compared with the ordinary flow tracing by calculating the transmission grid usage for every country for each of the three methods. The three methods reveal different flow allocation patterns for individual hours, but the results are similar when averaged over the entire time series. This is mostly driven by the average imports and exports of each country.

The second study explores optimal heterogeneous placement of renewable generation capacity with the objective to minimize total system cost. It is found that an optimal heterogeneous layout, which places the renewable generation in the places with favorable weather resources, reduces the system levelized cost of electricity (LCOE). Nodal LCOEs are explored using flow tracing. Capital and operational costs associated with power generation as well as transmission capacity costs are allocated based on exported and imported power. It is found that cooperation in the form of exporting excess power and heterogeneous placement of generation capacity not only reduces the system LCOE, but also reduces the nodal LCOE for all countries compared to a case without cooperation (no transmission). In the case of cooperation and a heterogeneous layout, the net exporters are the main beneficiaries.

The third study presents an application of flow tracing that is extended to include the charging and discharging of storage units. Using flow tracing, it is possible to determine the composition of storage inflow with respect to the different generation technologies. It is found that battery storage is predominantly used

by solar power. Hydrogen storage is almost completely charged with power from onshore and offshore wind power. The results of flow tracing confirm the intuition from the spatial distribution of generation and storage capacities. For the three considered storage technologies (battery, hydrogen and pumped hydro), most of the discharged power is consumed locally within the discharging node. However, when the discharged power is exported, it tends to be transmitted several hundred kilometers suggesting the importance of storage to provide flexibility across the transmission system given sufficient transmission capacities.

The fourth study uses flow tracing to construct a consumption-based carbon emission accounting method for a historical sample of real-time system data. Substantial differences are found between the production-based (from the local generation mix) and consumption-based carbon accounting for many of the EU28 countries studied. The differences between the two accounting approaches and the associated impact of imports on consumption-based carbon intensity emphasize the importance of including cross-border flows for increased transparency regarding carbon emission accounting of electricity.

3

Decompositions of injection patterns for nodal flow allocation in renewable electricity networks

This chapter is published as "Decompositions of injection patterns for nodal flow allocation in renewable electricity networks" by Mirko Schäfer, Bo Tranberg, Sabrina Hempel, Sefan Schramm and Martin Greiner in the European Physical Journal B [1].

3.1 INTRODUCTION

In view of climate change and the finite time horizon and political instability of fossil fuel supply, the transition towards a sustainable energy system is one of the main challenges for our modern society. As of today, wind and solar power generation are mature technology options which can provide electricity on a large scale at increasingly competitive costs [55]. Nevertheless, the fluctuating nature of these renewable generation technologies requires a new energy system design compared to past and present infrastructures, which are mostly based on centralised dispatchable fossil fuel power generation. Elaborate computational models seek to capture the respective relevant physical, technological and economical boundary conditions [56].

Applied Theoretical Physics can contribute another perspective to this challenge. By focussing on simplified, more abstract models it is often possible to identify the fundamental relationships and key dynamics of larger complex systems, and to develop and test new methods and concepts.

One focus for this kind of approach has been on network representations of electricity systems, which assess for instance structural properties [57] or the topological robustness of power grids [58,59]. Another strong line of research

investigates synchronisation properties of power grid models [60–63], for instance under decentralisation [64] or link removal [65].

In contrast, the modelling approach which we term 'complex renewable energy networks' addresses the analysis and design of energy systems with a high share of renewable generation. The renewable generation as well as the electricity consumption in these models is based on realistic data, whereas the system representation (constituents and network structure), the backup power dispatch and the power flow equations are simplified. In this context, the optimal mix between solar and wind power generation [66], the influence of storage and an associated phase transition [67,68], or the benefit of power transmission have been investigated [35,69].

The transmission needs associated with the smoothing of spatial fluctuations of renewable power generation [69] provide a strong motivation to analyse the flow patterns occurring in complex renewable energy networks. The necessary transmission infrastructure crucially depends on the geographical distribution of load and generation capacities, and on the spatio-temporal correlations in the renewable generation patterns, in particular for wind power generation [70,71]. Flow allocation methods assign a share of the total power flow to the individual importing and/or exporting nodes in the system, thus providing valuable information about their role in the overall flow pattern and an estimate of their usage of transmission capacity. These techniques are to some degree related to measures which relate the collective dynamics of a network to small parameter changes of the system [72], in particular with respect to robustness against link failures [65]. The method of flow tracing for instance has been discussed in the context of the transmission system operator compensation mechanism regarding transient cross-border flows in the European power grid [51,53]. In [43] this allocation method, also known as average participation, has been applied to a simplified model of the European electricity grid. From a complex networks perspective, flow tracing can be understood as a directed diffusion process on the directed acyclic flow graph [6,43,73]. The partial flows assigned to the respective exporting or importing nodes are thus always oriented in the same direction as the total power flow. This might be in contradiction with individual market transactions between importers and exporters, which can produce counter flows in the opposite direction.

Figure 3.1 illustrates this limitation of the flow tracing approach. In the depicted system state, Germany (DE) is a net exporter of electricity, whereas France (FR) is a net importer. This situation suggests the possibility of a trade contract between

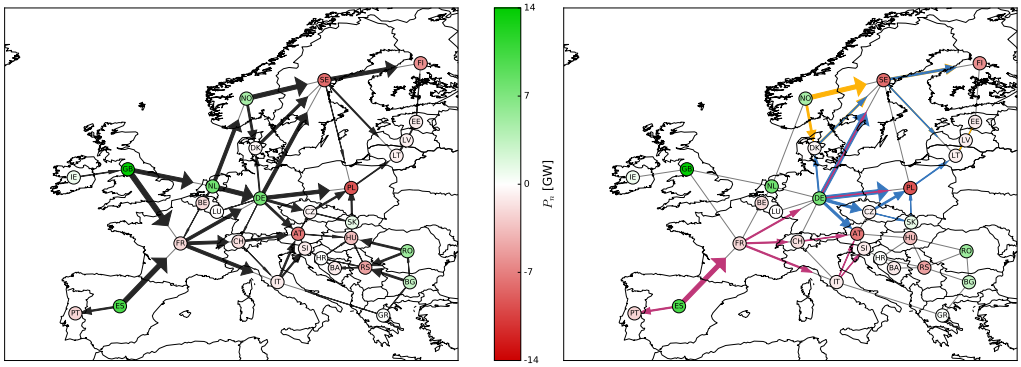

Figure 3.1: Flow tracing: Illustration of the partial flows of Germany (DE), Norway (NO), and Spain (ES) at an exemplary time step in a simplified model of the European electricity system. The nodes are colour-coded according to the magnitude of their exports (green) and imports (red) at this time, respectively. The left figure shows the total power flows in the system. The partial power flows assigned to Germany (blue), Norway (orange), and Spain (purple) based on the flow tracing method are displayed in the right figure. The size of the arrows for partial flows are scaled to the maximal partial flow of the respective country. For clarity only arrows for partial flows larger than a small threshold equal to 5% of the largest partial flow occuring in the system are shown.

these countries, leading to an associated *partial* power flow from Germany to France. Since the *total* power flow is oriented from France to Germany, such a contract and the associated partial flow cannot be represented by the flow tracing method. In this article we propose an alternative approach to flow and transmission capacity allocation based on decompositions of injection patterns. These decompositions allow to associate partial flows to individual transactions between importers and exporters, and factor in explicitly the patterns of nodal imports and exports. Here we use the decomposition method to analyse power flows in highly renewable electricity systems, but this technique can also be adapted to other models of networked systems, in which line flows depend linearly on nodal injections (for instance hydraulic networks [74], vascular networks [75], or network diffusion [76]).

This article is organized as follows: After briefly reviewing the linearised power flow equations, Sec. 3.2 provides a description of the flow tracing method and introduces the decomposition method of injection patterns. Two specific implementations (proportional and random contract decomposition) are described, and the conceptual differences to flow tracing are discussed. Sec. 3.3 compares

flow tracing and the decomposition method of injection patterns in the context of a simplified model of a highly renewable European electricity network, which is specified in more detail in Appendix A. A conclusion and outlook is given in Sec. 3.4.

3.2 METHODS OF FLOW ALLOCATION

Flow allocation methods attribute a share of the total power flow on a network to the net power in- or outflow associated with a specific node or subset of nodes [51]. Due to the indistinguishability of the electrical power flow in the network, such an attribution in general is not unique and has to be based on intuitive algorithms. In the following sections we briefly state the linearised power flow equations [77] and review the tracing method of flow allocation [40,41, 43,78]. We then introduce decompositions of injection patterns as an alternative way of allocating power flows, which is based on a decomposition of the net power inflows and outflows, and discuss this method in a comparison with the flow tracing approach.

3.2.1 The DC power flow equations

The majority of todays power grid infrastructure can be represented as AC networks. Although the power flow in these AC networks is governed by the full AC power flow equations, for the stable network operation the so-called DC approximation can be applied [77]. The directed active power flow $F_{m\to n}$ on a link from node m to n is then given by

$$F_{m\to n} = b_{mn}\left(\theta_m - \theta_n\right) , \tag{3.1}$$

with θ_n the voltage angle at node n and b_{mn} the line susceptance of the link. The voltage phase angles have to fulfill the linear equations

$$P_n = \left(\sum_m b_{nm}\right)\theta_n - \sum_m b_{nm}\theta_m = \sum_m B_{nm}\theta_m , \tag{3.2}$$

where we have introduced the nodal susceptance matrix B_{nm} with

$$B_{nm} = \begin{cases} -b_{nm} & \text{if } n \neq m \\ \sum_m b_{nm} & \text{if } n = m \end{cases} , \tag{3.3}$$

and P_n denotes the net power injection at node n. In the present article we consider a coarse-grained model of the European electricity grid and for simplicity

set $b_{nm} = 1$ for all links [28]. In this case, the nodal susceptance matrix B_{nm} corresponds to the Laplacian of the network [73].

In the DC approximation P_n represents the input to the calculation of the power flows. Solving Eq. (3.2) then yields the voltage phase angles, which via Eq. (3.1) determine the power flow on the links of the network. The resulting linear relationship between injection pattern and power flow can be expressed using the matrix of *power transfer distribution factors* H_{ln} (PTDF matrix):

$$F_l = \sum_n H_{ln} P_n \ . \tag{3.4}$$

Here we use the index $l = l(m,n)$ for the link between nodes m and n. The PTDF matrix $\mathbf{H}$ can be calculated as

$$\mathbf{H} = \mathbf{\Omega K}^T \mathbf{B}^\dagger \ , \tag{3.5}$$

where $\mathbf{B}^\dagger$ denotes the Moore-Penrose pseudo inverse of the nodal susceptance matrix $\mathbf{B}$, the diagonal matrix $\mathbf{\Omega}$ contains the line susceptances on the links l, and $\mathbf{K}^T$ is the transposed incidence matrix with

$$K_{ln}^T = \begin{cases} 1 & \text{if link } l \text{ starts at node } n \ , \\ -1 & \text{if link } l \text{ ends at node } n \ , \\ 0 & \text{otherwise .} \end{cases} \tag{3.6}$$

Note that Eq. (3.2) with Eq. (3.1) yields the law of flow conservation at the nodes:

$$P_n = \sum_m b_{nm} \left(\theta_n - \theta_m\right) \tag{3.7}$$

$$= \sum_m F_{n\to m} - \sum_k F_{k\to n} \ . \tag{3.8}$$

The left part of Fig. 3.1 shows the DC power flows at a specific point in time for a simplified model of the European transmission network (see Appendix A). Note that the power flows form a directed acyclic network without loops, which transports power from the exporting nodes (sources) to the importing nodes (sinks) of the system.

3.2.2 Flow Tracing

The method of flow tracing dissects the total flow pattern into strands originating from the different generators [40,41,43,78]. If one visualises the power flow as a water flow from source nodes (net generators) to sink nodes (net loads), a specific

colour can be added to the flow originating from the individual generators. These colour flows then will propagate and mix downstream throughout the total flow, until they end up in the loads at the different sink nodes. The colour mix on the connecting links then represents the partial flows attributed to the generators at the source nodes. This process corresponds to a directed diffusion process on the directed acyclic graph representing the power flows in the network [43,73]. The right part of Fig. 3.1 illustrates the share of the total power flow allocated to two exporting countries in a simplified European transmission network using this flow tracing approach. Note that these partial flows always point in the same direction as the total flow.

Using a more formal description of this method, one seeks the share $P^-_{n,s}$ of the load P^-_n and the share $F^{(s)}_{k\to n}$ of the total power flow $F_{k\to n}$, which can be traced back to the generation P^+_s at node s. Here the notation $P^+_n = P_n$ for an exporting generator n with $P_n > 0$, and $P^-_n = -P_n$ for an importing load n with $P_n < 0$ is used. That is, the total flow pattern $F_{k\to n}$ and the injection pattern P_n containing the nodal exports and total imports is the input for this method. The tracing algorithm then yields as outputs the partial flows $F^{(s)}_{n\to k}$ and the composition of the imports $P^-_{n,s}$ according to the origin of the corresponding power flow. For the method of flow tracing one first assumes partial flow conservation:

$$\delta_{n,s}P^+_n + \sum_k F^{(s)}_{k\to n} = P^-_{n,s} + \sum_m F^{(s)}_{n\to m} \ . \tag{3.9}$$

Additionally it has to be determined how these incoming or locally generated shares of the total flow are distributed to the local load and to the downstream neighbours. By following the principle of *proportional sharing* it is usually assumed that all incoming fractions are equally mixed and passed on [40]. This can be written as

$$\delta_{n,s}P^+_n + \sum_k q^{(s)}_k F_{k\to n} = q^{(s)}_n P^-_n + \sum_m q^{(s)}_n F_{n\to m} \ , \tag{3.10}$$

where $q^{(s)}_n$ is what we term – following the colour flow visualization – the colour mix passed on at node n, and $P^-_{n,s} = q^{(s)}_n P^-_n$. The colour mixtures can be calculated iteratively starting from pure sources without any inflows, or by interpreting Eq. (3.10) as a matrix equation and solving for $q^{(s)}_n$ [6,46]. Following this method of tracing based flow decomposition the partial flow on line l to the generator n is attributed as

$$F^{(n)}_l = q^{(n)}_{t(l)} F_l \ . \tag{3.11}$$

For the notation it is assumed that the directed links l are orientated along the total power flow F_l, and $t(l)$ denotes the tail of the directed link l, that is the node at its origin.

The description of flow tracing in the last paragraphs attributes partial flows to the net generating nodes (exporters) in the network. Flow allocation to importers can be obtained by inverting both the injection pattern $P_n \to -P_n$ and the flow pattern $F_l \to -F_l$, and then apply the flow tracing algorithm to these inverted patterns. It is also straightforward to consider a generalisation of the flow tracing method which follows the power originating from specific generation technologies or inflow distributions at the source nodes [6, 46].

3.2.3 Decomposition of injection patterns into import/export patterns

The method of flow tracing dissects the *total power flow* in the network, making use of a directed diffusion process following the principles of flow conservation and proportional sharing. The linearity of the power flow equations in Eq. (3.4) suggests an alternative decomposition of the power flow pattern, based instead on a decomposition of the *injection pattern*. For this purpose we decompose the injection pattern into balanced elementary patterns. Associated with the index α, an elementary injection pattern $P_n^{(\alpha)}$ with $\sum_n P_n^{(\alpha)} = 0$ leads to the partial flow pattern

$$F_l^{(\alpha)} = \sum_n H_{ln} P_n^{(\alpha)} \ . \tag{3.12}$$

We call a collection of elementary injection patterns $P_n^{(\alpha)}$ a decomposition of a given injection pattern P_n, if $\sum_\alpha P_n^{(\alpha)} = P_n$. The linearity of Eq. (3.4) then ensures that the superposition of all partial flows $F_l^{(\alpha)}$ gives the total flow on link l as $F_l = \sum_\alpha F_l^{(\alpha)}$. The input to this method is the PTDF matrix H_{ln} representing the solution of the linearised power flow equations for the network under consideration, and a collection of elementary injection patterns $P_n^{(\alpha)}$ which sum up to the given total injection pattern P_n. Equation (3.12) then yields as the output the corresponding partial power flows $F_l^{(\alpha)}$. Note that the use of the general index α allows arbitrary decompositions of the injection pattern, for instance according to individual contracts, or identifying the electricity mix (conventional, wind, solar,...) injected into the grid at a specific node or subset of nodes [44, 46].

For our investigation in this article we select a class of decompositions with an elementary injection pattern associated to every exporting or importing node.

At a specific instant in time, we partition the set of nodes $\mathcal{N}$ into the exporting nodes $\mathcal{N}^+$ with $P_n > 0$, and the set of importing nodes $\mathcal{N}^-$ with $P_n < 0$. If there is a transient node with $P_n = 0$ we add it to the set of exporting nodes. An export decomposition is given by the set of elementary injection patterns $\{P_n^{(s)}\}_{s\in\mathcal{N}^+}$ with

$$P_n^{(s)} = \begin{cases} P_s^+ \delta_{ns} & \text{if } n \in \mathcal{N}^+ \\ -P_{s\to n}^{\text{ex}} & \text{if } n \in \mathcal{N}^- \end{cases} . \tag{3.13}$$

The elementary injection pattern $P_n^{(s)}$ thus describes the total power P_s exported by node s through the network, with each sink $n \in \mathcal{N}^-$ covering the share $P_{s\to n}^{\text{ex}}$ of its respective deficit P_n^- by imports from node s. Given an injection pattern P_n, the components $P_{s\to n}^{\text{ex}}$ thus have to fulfill the conditions

$$\sum_{s\in\mathcal{N}^+} P_{s\to n}^{\text{ex}} = P_n^- , \tag{3.14}$$

$$\sum_{n\in\mathcal{N}^-} P_{s\to n}^{\text{ex}} = P_s^+ . \tag{3.15}$$

Analogously we define an import decomposition as the set of elementary injection patterns $\{P_n^{(b)}\}_{b\in\mathcal{N}^-}$ with

$$P_n^{(b)} = \begin{cases} -P_b^- \delta_{nb} & \text{if } n \in \mathcal{N}^- \\ P_{n\to b}^{\text{im}} & \text{if } n \in \mathcal{N}^+ \end{cases} . \tag{3.16}$$

In the following we will consider two specific implementations for export/import decompositions, which are each motivated by a different variant of electricity market trading. *Proportional decompositon* can be interpreted as a stylised model of a centralised market-clearing procedure, in which the participants interact via a central authority, which equates supply and demand based on the submitted bids. In the corresponding decomposition scheme the pooling nature of this market is represented by a homogeneous distribution of imports and exports in the system. In contrary, *random contract decomposition* serves as a coarse model of over-the-counter trading. In this interpretation, the participants engage directly in bilateral transactions without an intermediate central authority. The collection of all these contracts then determines the individual imports and exports. In the following we will consider these two schemes separately, but a mixture of both approaches would be a straightforward generalisation. Although for both implementations our general definition of import/export decompositions allows to define $P_{s\to b}^{\text{ex}} \neq P_{s\to b}^{\text{im}}$, the respective entries of the import and export decompositions coincide for a given injection pattern.

Proportional decomposition In this case the share $P^{\text{ex}}_{s\to n}$ of exports from node s to the importing node n is given by the share of this node's export with respect to all exports in the system:

$$P^{\text{ex}}_{s\to n} = \frac{P^+_s}{P^+} P^-_n \ , \tag{3.17}$$

with

$$P^+ = \sum_{s\in\mathcal{N}^+} P^+_s = P^- = \sum_{b\in\mathcal{N}^-} P^-_b \tag{3.18}$$

the total exports and imports for a balanced system. This elementary injection pattern corresponds to the situation that the exporting node s serves all sinks in the system, with their imports uniformly scaled down in such a way that the pattern is balanced. Analogously we define the import decomposition as

$$P^{\text{im}}_{n\to b} = \frac{P^-_b}{P^-} P^+_n \ . \tag{3.19}$$

With $P^+ = P^-$ it is easy to see that $P^{\text{ex}}_{s\to b} = P^{\text{im}}_{s\to b}$.

Random contract decomposition In this scenario we assume a situation where the import and export decompositions are based on randomly assigned contracts between importers and exporters. In order to ensure that the conditions Eq. (3.14) and Eq. (3.15) are fulfilled while circumventing any complications due to finite block sizes of these contracts, we implement the following random assignment algorithm. We start with the node which has the lowest value of imports or exports. For now we assume that this node is an importing node b. We randomly choose one exporter n, which by definition is able to completely cover the respective import of the node first chosen. This procedure defines a contract between this node n and the importing node b with size $c_{n\to b} = P^-_b$. We now remove the node b from the set of importing nodes $\mathcal{N}^-$, and update the export of node n as $P_n \to (P_n - c_{n\to b})$. Then we repeat this procedure until no node is left. If the node with the lowest import or export at some iteration of the algorithm is an exporter s, we randomly choose an importing node n and assume that all (remaining) exports from node s go to this importer n. Note that during this algorithm often contracts between smaller countries are selected initially, with the imports and exports of the larger countries covered among each other in the final iterations. This bias in the distribution is build in on purpose to obtain an import/export pattern which is statistically different from the proportional decomposition discussed above.

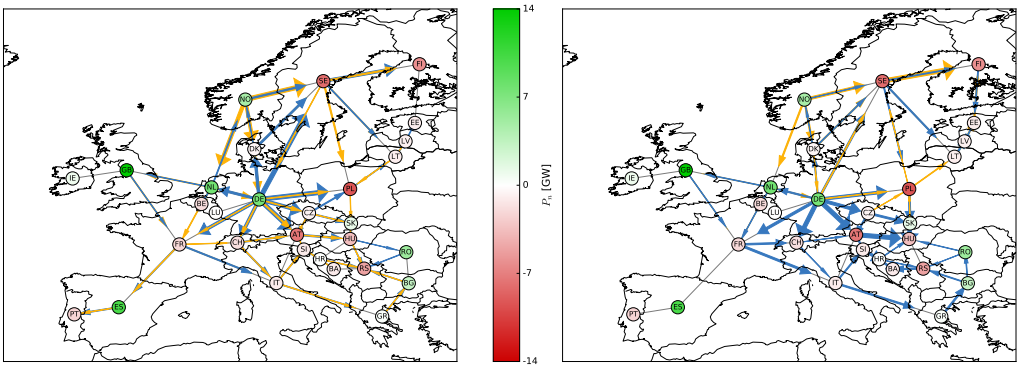

Figure 3.2: Decomposition of injection patterns: Illustration of the partial flows of Germany (DE) and Norway (NO) at an exemplary time step in a simplified model of the European electricity system (see the left part of Fig. 3.1 for the total power flow). The left figure shows the partial flows assigned to Germany (blue) and Norway (orange) according to the proportional decomposition scheme, whereas the right figure follows the random contract decomposition scheme. For the scaling of arrow sizes and the respective threshold see Fig. 3.1. To allow for a clearer visualisation, the partial flows associated with Spain are not shown in this figure.

After processing the algorithm, we define the import and export compositions based on this random assignment of contracts as follows:

$$P^{\mathrm{ex}}_{s\to b} = c_{s\to b} = P^{\mathrm{im}}_{s\to b} \,. \tag{3.20}$$

3.2.4 Flow tracing vs. decompositions of injection patterns

We want to emphasize some fundamental methodological differences between flow allocation techniques based on decompositions of injection patterns and the tracing based approach. In the former case one defines partial injection patterns and calculates partial flows via the linearised power flow equations. Both the amount of partial inflow at the net generators and outflow at the net loads are inputs to the calculation. In the latter case of flow tracing the inflow from the generators at the source nodes and the total power flow pattern are the inputs to the algorithm, which yields both the partial flows on the links and the corresponding shares of outflow at the sink nodes. Furthermore, since flow tracing dissects the total flow pattern into different strands from source nodes to sink nodes, the partial flows always follow the orientation of the total flow.

In contrast, the superposition of partial flow patterns under the decomposition method allows partial flows which are opposite to the total flow. These partial counter-flows mitigate the total power flow on a transmission line.

As an example, compare Fig. 3.2 to Fig. 3.1, that is the illustration of some partial flows for the simplified model of the European electricity system obtained via the method of flow tracing (Fig. 3.1) and based on proportional and random contract decomposition (Fig. 3.2). We observe that flow tracing leads to a decomposition of the import/export pattern based on geographically localised partial flows. The elementary injection patterns obtained from proportional decomposition on the contrary lead to partial flows spanning the whole system. For the random contract decomposition we observe a pattern with partial flows from Germany covering the south, whereas the partial flows from Norway are mostly restricted to the north. Note that for both implementations of decomposing injection patterns numerous counter-flows occur in the system.

3.3 POWER FLOW DECOMPOSITION IN A SIMPLIFIED MODEL OF A HIGHLY RENEWABLE EUROPEAN ELECTRICITY NETWORK

As a test case we apply the methods from the last section to a simplified model of a highly renewable European electricity system (see Appendix A for details about the model), and discuss the import/export transfer functions as well as the nodal usage of transmission link capacities. Five years of data from 2010 to 2014 with hourly resolution for the load and projected renewable generation are used, leading to 43822 different injection patterns $P_n(t)$ and resulting flow patterns $F_l(t)$.

3.3.1 Export and import transfer functions

Both methods, flow tracing and decomposition into elementary patterns, do not only lead to a decomposition of the power flow in the system, but also to a partition of the injection pattern which associates the exports from one country to the imports of another. Whereas for the decomposition method this partition is an input into the method which yields a decomposition of the flow pattern, for the method of flow tracing these import/export patterns are a result of the algorithm (see Sec. 3.2.4).

Given the whole time series, we quantify these import/export patterns using the

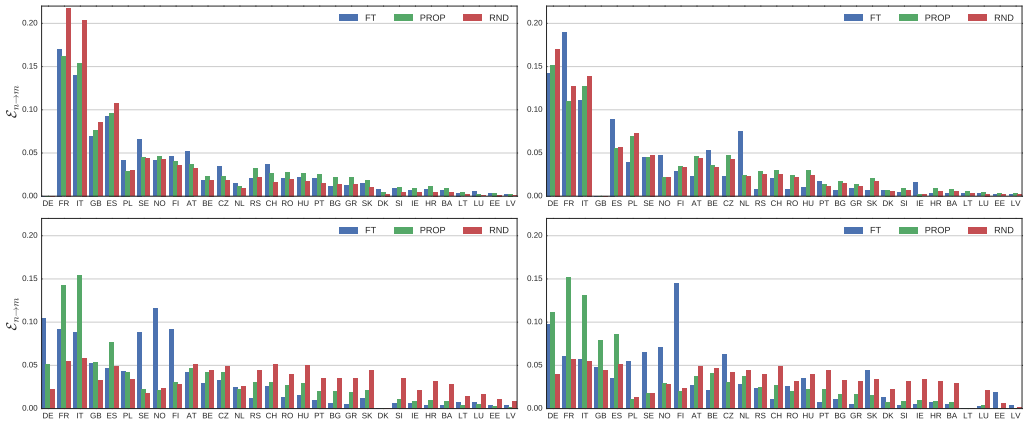

Figure 3.3: Export transfer function based on flow tracing (blue), proportional decomposition (green), and random contract decomposition (red). Top left: Germany (DE). Top right: Great Britain (GB). Bottom left: Denmark (DK). Bottom right: Lithuania (LT). The transfer functions resulting from the application of the flow tracing method emphasize transfers between geographically close countries, whereas the proportional decomposition yields a more homogeneous, delocalised distribution. The random contract decomposition scheme leads to transfer functions showing stronger exports among the larger countries as well as among the smaller countries, respectively, resulting from an implicit bias in the underlying contract algorithm.

following export transfer function [43]:

$$\mathcal{E}_{n\to m} = \frac{\langle q_m^{(n)} P_m^- \rangle}{\langle P_n^+ \rangle} \quad , \quad \mathcal{E}_{n\to m} = \frac{\langle P_{n\to m}^{\mathrm{ex}} \rangle}{\langle P_n^+ \rangle} \, . \tag{3.21}$$

Here the first definition refers to the method of flow tracing, whereas the second definition corresponds to the decomposition method. This export transfer function gives the share of the average exports of a country n which are associated with imports from a country m. An import transfer function can be defined analogously, but gives very similar results for the set-up chosen for our simplified system with $\langle P_n^+ \rangle = \langle P_n^- \rangle$ (see Appendix A).

In Fig. 3.3 we display the export transfer function based on flow tracing and the two injection pattern decomposition schemes for four selected countries: Germany (DE), Great Britain (GB), Denmark (DK), Lithuania (LT). We observe that, as expected, the method of flow tracing yields an export transfer function which emphasizes transfers between geographically close countries, see for instance exports from Denmark to Sweden (SE), Norway (NO) and Finland (FI),

or from Great Britain to France (FR). The corresponding localisation of the partial flows has already been illustrated in Fig. 3.1. The elementary injection patterns based on proportional decomposition yield a more homogeneous, delocalised distribution, which is mainly determined by the correlation between the imports and exports of the respective countries:

$$\mathcal{E}_{n\to m} = \frac{\langle P^{\mathrm{ex}}_{n\to m}\rangle}{\langle P^{+}_{n}\rangle} = \frac{\langle \frac{P^{+}_{n}P^{-}_{m}}{P^{+}}\rangle}{\langle P^{+}_{n}\rangle} \ . \tag{3.22}$$

The results for the random contract decomposition mirror the bias in the underlying contract algorithm: Germany as a country with a comparatively large load often exports to other large countries in the system, that is France, Italy (IT), or Great Britain, whereas Lithuania shows an export distribution characterised by exports to other smaller countries. Also consult Fig. 3.2 for exemplary partial power flow patterns which illustrate the import/export patterns obtained via proportional and random contract decomposition.

3.3.2 Usage of transmission capacity

The patterns of imports and exports discussed in the last section are associated with power flow patterns, which make use of the transmission capacity of the grid. Analogously to [43, 69] we define the transmission capacity $\mathcal{K}_l$ of a link l as the 99% quantile of the flow distribution $\mathcal{P}(f_l)$:

$$0.99 = \int_0^{\mathcal{K}_l} \mathcal{P}(f_l)\mathrm{d}f_l \ . \tag{3.23}$$

Here $f_l = |F_l|$ denotes the absolute flow on a link l. We want to compare methods of capacity allocation which assign a usage share $\mathcal{K}_l^{(n)}$ of the total link capacity to the different nodes n of the network. We use the usage measure introduced in [43], which is based on the ensemble of total and partial power flows $(F_l, F_l^{(n)})$:

$$\mathcal{K}_l^{(n)} = \int_0^{\mathcal{K}_l} \frac{d\mathcal{K}}{1-\mathcal{P}_l^{C}(\mathcal{K})} \int_{\mathcal{K}}^{\mathcal{K}_l} \mathcal{P}_l(f_l) \left\langle \frac{F_l^{(n)}}{F_l} | f_l \right\rangle \mathrm{d}f_l \ . \tag{3.24}$$

This measure incorporates correlations between the associated partial flows and the total power flows on a link and thus provides a fairer capacity allocation compared to simplified approaches using the average load, average import/-export or average partial flow [6, 43]. In Fig. 3.4 we illustrate the statistics of

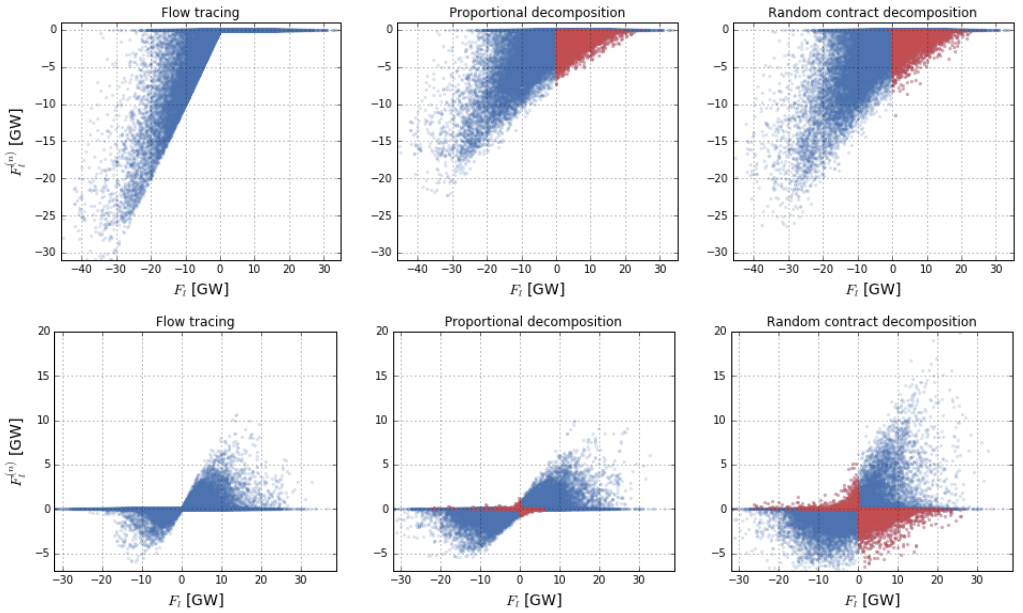

Figure 3.4: Statistics of total power flow and partial flow attributed to Germany for the link from France to Germany (top) and from France to Great Britain (bottom). The partial flows are obtained using the method of flow tracing (left) and the decomposition method with proportional decomposition (middle) and random contract decomposition (right). The method of flow tracing yields partial flows which are always oriented in the same direction as the total flow, whereas partial flows based on proportional or random contract decomposition can be oriented opposite to it. These counter flows are emphasised with red colour in the figure.

the total power and the partial power flow attributed to Germany for the link from France to Germany and from France to Great Britatin. The results are based on the different methods of flow decomposition discussed in the previous sections. For simplicity, here we only consider situations in which Germany is an exporter. Considering the flow tracing method, we observe that Germany only gets assigned partial flows in the direction towards France. This is due to the consideration of exports only, which will never be oriented in the opposite direction. In contrast, for the more remote link between France and Great Britain, Germany gets assigned partial flows in both directions. By definition, using the flow tracing method, we never observe counter flows, or partial flows larger than the total flow on a link. This is different for the partial flows based on the decomposition methods. Situations in which Germany is exporting power

to France despite a total power flow in the opposite direction are represented as partial counter flows in these schemes. We also observe partial power flows exceeding the total flow on the link. In this case, the partial flows associated with Germany are dominating the total power flow, which is reduced by opposing contributions from other countries. The same features are visible for the more remote link between France and Great Britain. With respect to the difference between the proportional and random decomposition scheme, we observe a more scattered distribution for the latter. These larger partial flows result from random contracts exceeding the respective proportional decompositions.

Based on the respective total and partial power flow statistics, in Fig. 3.5 we show the share of transmission capacity $K_l^{(n)}/K_l$ assigned to the different nodes for each link in the network, based on the different methods of flow decomposition discussed in the previous sections. For each method we calculate the usage measure according to imports and exports separately, and then display the average over both these results. Overall we observe that despite the significant differences in the underlying patterns at individual time steps, the statistical measure in Eq. (3.24) leads to similar results for the capacity allocation of the different links for the three methods. However, as for the import/export pattern the flow tracing based decomposition leads to more localised partial flows and thus a less distributed attribution of transmission usage. A noteworthy feature of the capacity allocation derived from the decomposition method is the occurrence of *negative* capacity allocations. This negative allocation results from a high share of counter-flows assigned to the respective countries, which lead to a reduction of the total power flow and thus savings in transmission capacity. These negative allocations are observed for both proportional and random contract decomposition, most prominently on the link between Norway (NO) and Denmark (DK). We finally compare the total transmission capacity costs allocated to the system nodes according to Eq. (3.24) for the different methods of flow allocation. We approximate the cost of a transmission line $l = m \to n$ as the transmission capacity K_l and the distance d_l between the capitals of the countries represented by node n and m. The total transmission cost in the network is then given by

$$M = \sum_l d_l K_l \ . \tag{3.25}$$

A share of this total transmission cost is associated with country n due the capacity allocation $K_l^{(n)}$:

$$M_n = \sum_l d_l K_l^{(n)} \ . \tag{3.26}$$

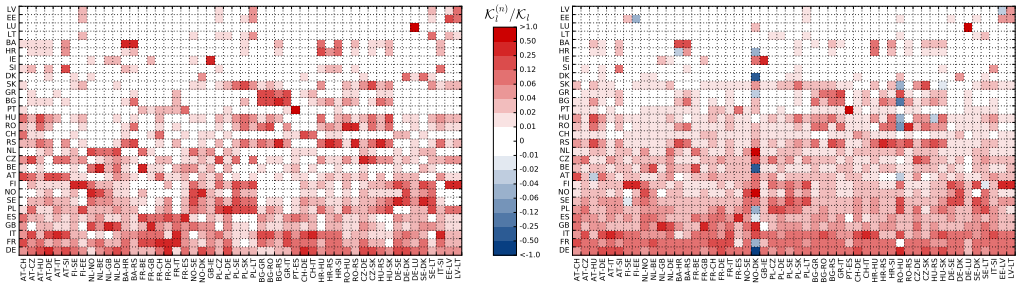

Figure 3.5: Partial transmission capacities $\mathcal{K}_l^{(n)}$ of all links in the simplified European electricity network assigned to the different countries according to the network usage measure defined in Eq. (3.24). The underlying partial flows $F_l^{(n)}$ have been obtained using the method of flow tracing (left) and proportional decomposition (right). The random contract decomposition leads to results which are very similar to the proportional decomposition and are not shown. The transmission capacities are less distributed for the flow tracing method due to a stronger localisation of the partial flows. The occurrence of counter flows leads to the allocation of some negative partial capacities under the proportional decomposition method, for instance on the link between Norway (NO) and Denmark (DK).

In Fig. 3.6 we compare the cost allocation M_n derived from the flow decomposition according to the three different methods presented in this article with a simplified allocation proportional to the average import/export of the individual nodes:

$$M_n = \frac{\langle\, |P_n| \,\rangle}{\sum_k \langle\, |P_k| \,\rangle} M \,. \tag{3.27}$$

We observe that these aggregated statistical measures of transmission capacity based on different flow allocation methods yield very similar results. This accordance contrasts with the significantly different partial flows according to the flow tracing method or decomposition method at individual time steps (see Figs. 3.1 and 3.2). After statistical aggregation over the whole time series and the whole network, for the considered methods the average import/export of a country is the most determining factor for the allocation of network usage. The variances visible in Fig. 3.6 due to the application of different decomposition methods depend on the geographical location of the respective country in the network, and in particular on the spatio-temporal correlations in the injection and resulting power flow patterns. While it is possible to trace back the influences underlying these differences by considering link specific partial and total power

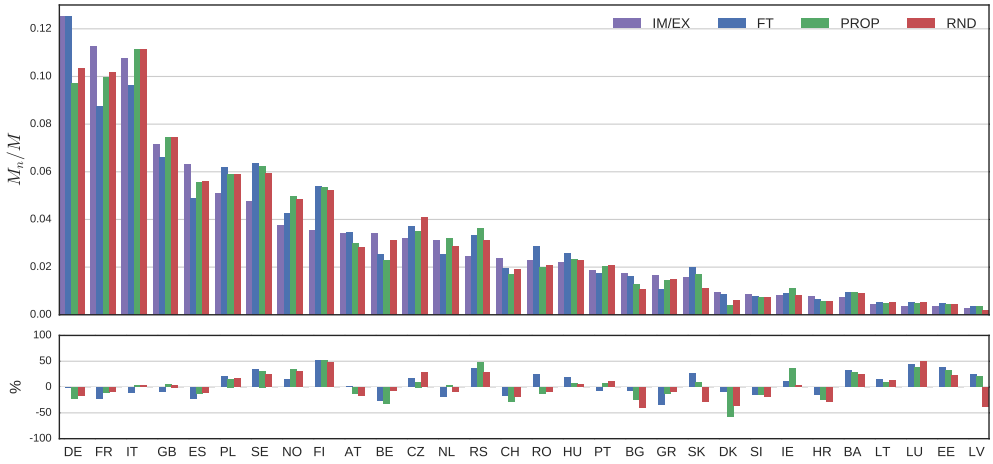

Figure 3.6: Top: Share of the total transmission system cost allocated to the different nodes of the network. The cost allocation is based on the usage measure in Eq. (3.24), with the partial flows determined either via flow tracing or the method of decomposing injection patterns (proportional and random contract decomposition). As a comparison, a simplified measure based on the average import/export of the respective nodes is also displayed. Bottom: This figure shows the same results as the top figure, but now as the relative difference compared to the simplified average import/export measure.

flow statistics (see Fig. 3.4) or individual system snapshots (see Figs. 3.1 and 3.2), it is difficult to deduce general trends for the aggregated usage measure. An exception is the localisation of partial flows for the flow tracing method as illustrated in Fig. 3.1, which benefits four of the five largest importers/exporters, while assigning a higher share of transmission capacity to smaller countries at the periphery like Finland (FI), Serbia (RS) or the baltic countries [43].

3.4 CONCLUSION

Flow tracing uses a directed diffusion process on the total flow graph to assign power flows to generators or loads in electricity networks [40, 41, 43]. Although the downstream dissection of the total flow into different strands emerging from the individual source nodes represents an intuitive technique for the flow allocation problem, this approach implies limitations for possible economic interpretations: The application to the total flow graph does not allow to associate power flows to individual trade contracts or other bilateral import/export patterns. In particular, partial power flows due to commercial exchanges which

are not aligned with the overall total power flow (as for example a possible contract between Germany and France in Fig. 3.1) cannot be represented by this method. In this contribution, we propose an alternative method of flow allocation, which decomposes the overall injection pattern into elementary injection patterns. These patterns can be associated with individual contracts or other commercial exchange patterns. Two different variants of this decomposition method are compared with the flow tracing technique by applying them to a simplified model of a highly renewable European electricity system. We observe that the respective partial flow patterns differ significantly for individual network flow events. These differences are still visible in the resulting partial flow statistics evaluated for a time series of fluctuating injection patterns. For the event-averaged import/export patterns and an aggregated statistical measure of total network capacity usage, the methods studied in this contribution yield similar results, which are mostly driven by the respective average imports and exports of the individual countries.

The decomposition method introduced in this contribution depends on the linearity of the equations describing the power flow in the network. Accordingly, for the application of this method, the accuracy of the DC approximation to the full AC power flow equations has to be assured. Whereas this usually is the case for the stable operation in high-voltage grids, for the power flow in distribution grids, in particular with infeed from renewable generation, one often has to consider voltage support or reactive power management not represented in the DC approximation [79]. On the other hand, the linear relationship between link flow and nodal injection is not exclusive to the DC power flow model, but also occurs for instance in models of network diffusion [76], hydraulic networks [74] or vascular networks [75]. Accordingly, the decomposition method can also be straightforwardly applied to such models, with a suitable choice of elementary injection patterns depending on the specifications of the system.

With respect to the application to electricity systems, it would be interesting to compare the decomposition method of injection patterns with further methods of flow allocation, for instance with marginal participation methods which also make use of the matrix of power transfer distribution factors [44, 80, 81]. The application to a more detailed model of the electricity system, in particular with a more realistic network representation and market-based dispatch schemes, could allow to learn more about the economical implications of the methods of flow allocation presented in this contribution. We emphasise that the analysis presented in this paper assumes an ex-post allocation of usage or costs to the users of the transmission system, that is the injection pattern itself is not

influenced by this allocation. For an efficient design of the electricity system, both the short-term operational and the long-term investment decisions of the system users should incorporate the resulting transmission costs. This feedback process proposes interesting research questions for simplified models of networked electricity systems, incorporating methods from game theory or control theory. We also expect that for such a feedback loop the influence of the specific choice of the allocation method increases significantly. If for example congestion-relieving counter-flows are rewarded, the network nodes are incentivised to cause flows opposite to the flows attributed to the remaining nodes. From the system perspective, this concept then shows some similarity to the principles found in minority games [82].

4

Flow-based nodal cost allocation in a heterogeneous highly renewable European electricity network

This chapter is published as "Flow-based nodal cost allocation in a heterogeneous highly renewable European electricity network" by Bo Tranberg, Leon J. Schwenk-Nebbe, Mirko Schäfer, Jonas Hörsch and Martin Greiner in Energy [2].

4.1 INTRODUCTION

A future sustainable electricity system will strongly depend on the large-scale integration of fluctuating renewable power generation from wind turbines and solar photovoltaics [14,22,83]. The weather-dependent resource quality and thus cost efficiency of these variable renewable energy sources (VRES) is unevenly distributed across the European continent. An efficient placement of generation capacity will thus result in a heterogeneous layout, in which locations with favorable conditions will be net exporters of electricity, whereas regions with less favorable conditions import electricity as power flows through the transmission grid [69,84–86]. Despite its efficiency in terms of reducing global system costs [7, 87], such a heterogeneous layout represents a political and economical challenge. Countries with favorable weather conditions will get assigned disproportionally high shares of generation capacity, which to a large degree will be exported and serve electricity consumption abroad. The associated investment costs thus must be incentivized by appropriate renumeration schemes, which in todays system are largely based on electricity markets complemented with different kinds of state-regulated support schemes [88–90]. Nevertheless, the increasing share of fluctuating renewable generation represents a challenge for the design of future market rules. A deeper understanding of the nodal structure of system costs might provide guidance to the development of a suitable regulatory framework,

which supports the transition towards an efficient sustainable system design by providing a fair allocation of costs and target-oriented incentives for investors.

Using a flow tracing technique based on average participation [40, 41] in this contribution, we derive nodal levelized costs of electricity (LCOE) which factor in the share of the system-wide operational and capital costs associated with the electricity consumption (load) of the individual nodes [42, 91]. We apply this formalism to a coarse-grained model of the European electricity system with a high share of renewable generation [7].

This paper is organized as follows: Section 4.2 describes the simplified model of the European electricity network and presents the respective infrastructure measures, cost modelling and heterogeneous renewable capacity layouts. Furthermore, the method of flow tracing is reviewed, which represents the cornerstone of the flow-based nodal cost allocation defined in Section 4.3. In Section 4.4 the application of this method is discussed for different renewable generation layouts and transmission cost allocation schemes. The paper is concluded with a discussion of the results and an outlook to future research.

4.2 MODELLING AND METHODS

4.2.1 The electricity network

In this study we use a simplified model of the European electricity network, shown in Figure 4.1. Each node represents an aggregated country and each link represents coarse-grained interconnector transmission capacity between the countries, distinguishing between AC lines and HVDC lines. The size of the nodes visualizes the average load. Wind and solar PV generation constitute the nodal VRES power generation:

$$G_n^R(t) = G_n^W(t) + G_n^S(t) \ . \tag{4.1}$$

As described in [7] the VRES generation is modeled using eight years of hourly weather data from 2000 to 2007 with a spatial resolution of $50 \times 50\text{km}^2$ [66, 92]. The weather data is converted into generation time series using country-specific capacity layouts from Eurostat [93, 94]. For simplicity this model focuses only on onshore wind and solar PV generation. We use two parameters to describe the renewable generation in Equation (4.1). The renewable penetration, which determines the amount of renewable generation relative to the load of a node

$$\langle G_n^R \rangle = \gamma_n \langle L_n \rangle \ , \tag{4.2}$$

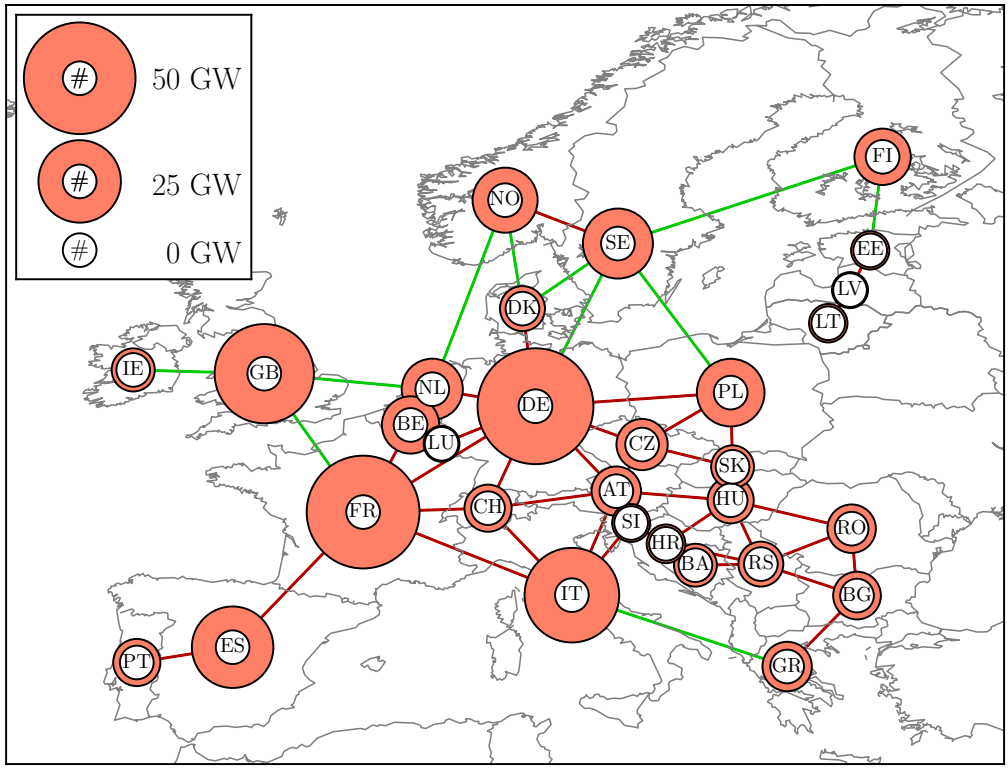

Figure 4.1: The simplified European electricity system. The size of the nodes shows the average load of the respective countries. AC lines are colored red and DC lines are colored green.

where the load time series $L_n(t)$ is based on historical data from ENTSO-E, and the mixing parameter α_n, which fixes the ratio between wind and solar generation

$$\langle G_n^W \rangle = \alpha_n \langle G_n^R \rangle \,, \tag{4.3}$$

$$\langle G_n^S \rangle = (1 - \alpha_n) \langle G_n^R \rangle \,. \tag{4.4}$$

Note the usage of averages which means that $\gamma_n = 1$ describes a country that on average covers its entire load by renewable generation. The hourly nodal mismatch between VRES generation and load

$$\Delta_n(t) = G_n^R(t) - L_n(t) \tag{4.5}$$

will be balanced by the dispatch of backup power generation, curtailment of excess generation, and power transmission between the countries. For simplicity,

storage is not considered. The resulting nodal balancing equation reads

$$G_n^R(t) - L_n(t) = \Delta_n(t) = B_n(t) + P_n(t) \ . \tag{4.6}$$

Here $B_n(t)$ represents the nodal balancing consisting of curtailment of excess power $C_n(t) = \max(B_n(t), 0)$ and the dispatch of backup generation $G_n^B(t) = -\min(B_n(t), 0)$, and $P_n(t)$ represents the power injected (ejected) to (from) the network. It is assumed that the model is balanced such that $\sum_n P_n(t) = 0$. We assumed that the dispatchable backup generation is realized by Combined Cycle Gas Turbines (CCGT). The dispatch of the nodal backup and curtailment is determined using the synchronized balancing scheme [28]:

$$B_n(t) = \frac{\langle L_n \rangle}{\sum_k \langle L_k \rangle} \sum_m \Delta_m(t) \ . \tag{4.7}$$

Combining Equation (4.6) and Equation (4.7) fixes the injection pattern $P_n(t)$. The injection pattern in turn determines the flows $F_l(t)$ on the links l:

$$F_l(t) = \sum_n H_{ln} P_n(t) \ . \tag{4.8}$$

Here we have used the DC approximation to the AC power flow equations [44,79], in which the entries H_{ln} of the matrix $\mathbf{H}$ are the power transfer distribution factors (PTDF) representing the influence of the line susceptances and network topology on the power flows. The PTDF matrix $\mathbf{H}$ can be calculated as

$$\mathbf{H} = \mathbf{\Omega} \mathbf{K}^T \mathbf{B}^\dagger \ , \tag{4.9}$$

where $\mathbf{B}^\dagger$ denotes the Moore-Penrose pseudo inverse of the nodal susceptance matrix $\mathbf{B}$ and the entries of the diagonal matrix $\mathbf{\Omega}$ are the line susceptances on the links l. The matrix $\mathbf{K}^T$ is the transposed incidence matrix with

$$K_{ln}^T = \begin{cases} 1 & \text{if link } l \text{ starts at node } n \ , \\ -1 & \text{if link } l \text{ ends at node } n \ , \\ 0 & \text{otherwise .} \end{cases} \tag{4.10}$$

For simplicity the susceptances are all chosen to be identical and $\mathbf{\Omega}$ is the identity matrix.

4.2.2 Infrastructure measures

The energy system cost is based on measures of the installed generation and transmission capacities as well as on the backup energy introduced in [87]. The nodal backup energy is given by the average backup power generation:

$$E_n^B = \left\langle G_n^B \right\rangle \ . \tag{4.11}$$

Excluding extreme events that are assumed to be covered by emergency equipment or flexible demand outside the model, the backup capacity is defined as the 99% quantile of the backup generation events:

$$0.99 = \int_0^{\mathcal{K}_n^B} dG_n^B p_n(G_n^B) \ . \tag{4.12}$$

The transmission capacity $\mathcal{K}_l^T$ is defined in a similar way as the 99% quantile of flow events,

$$0.99 = \int_{-\mathcal{K}_l^T}^{\mathcal{K}_l^T} dF_l p_l(F_l) \ , \tag{4.13}$$

assuming identical capacity in both directions. The total backup capacity is calculated by summing the nodal capacities $\mathcal{K}^B = \sum_n \mathcal{K}_n^B$. The total transmission capacity is calculated as the weighted sum

$$\mathcal{K}^T = \sum_l d_l \mathcal{K}_l^T \ , \tag{4.14}$$

taking into account the link length d_l approximated by the distance between the capitals of the countries. From the renewable penetration and the wind/solar mix we derive the capacities of wind and solar generation:

$$\mathcal{K}_n^W = \frac{\gamma_n \alpha_n \langle L_n \rangle}{\mathrm{CF}_n^W} \ , \tag{4.15}$$

$$\mathcal{K}_n^S = \frac{\gamma_n (1-\alpha_n) \langle L_n \rangle}{\mathrm{CF}_n^S} \ . \tag{4.16}$$

The capacity factors $\mathrm{CF}_n^{W/S}$ represent the average renewable generation as a fraction of the installed capacity. They are taken from [7] where they are based on data from [93, 94].

4.2.3 Cost modelling

We follow the cost modelling in [7]. The present value of investment V for each type of generation capacity is defined as

$$V = \mathrm{CapEx} + \sum_{t=1}^{T_{\mathrm{life}}} \frac{\mathrm{OpEx}_t}{(1+r)^t} \ , \tag{4.17}$$

where r, the rate of return, is assumed to be 4% per year. Cost assumptions for capital expenditures (CapEx) and operational expenditures (OpEx) are listed in Table 4.1.

Table 4.1: Cost assumptions separated into capital expenditures (CapEx) and fixed and variable operational expenditures (OpEx) as well as expected lifetimes.

Asset	**CapEx** [€/W]	**OpEx$_{\text{fixed}}$** [€/kW/y]	**OpEx$_{\text{variable}}$** [€/MWh]	**Lifetime** [years]
CCGT	0.90	4.5	56.0	30
Solar PV	0.75	8.5	0.0	25
Onshore wind	1.00	15.0	0.0	25

The present value of a transmission line is calculated as the cost of the line

$$V_l^T = \mathcal{K}_l^T d_l c_l, \tag{4.18}$$

where d_l is the line length and c_l is the specific transmission capacity cost:

$$c_l = \begin{cases} 400€/\text{km} & \text{(AC line)}, \\ 1500€/\text{km} & \text{(DC line)}. \end{cases} \tag{4.19}$$

The total present value of the transmission system is

$$V^T = \sum_l V_l^T + N_{\text{HVDC}} \cdot 150,000€. \tag{4.20}$$

The second term accounts for the cost of a pair of converter stations for each HVDC line [7,84,95]. The layout of AC and HVDC lines has been constructed in [69] based on the existing European network in the year 2011 [96] as well as new predicted lines until 2014 [97,98].

The system costs are measured using the Levelized Cost of Electricity (LCOE), which represents the average cost per consumed unit of energy during the system lifetime [99,100]:

$$\text{LCOE}_V = \frac{V}{\sum_{t=1}^{T_{\text{life}}} \frac{L_{EU,t}}{(1+r)^t}} \,. \tag{4.21}$$

The system LCOE is calculated by summation over the LCOEs for the system elements, which takes into account the different life times for solar PV, onshore wind, CCGT plants, and transmission infrastructure [7]. For $V \in \{V_W,\ W_S,\ V_B,\ V_T\}$:

$$\text{LCOE}_{\text{EU}} = \sum_V \text{LCOE}_V \,. \tag{4.22}$$

4.2.4 Optimal heterogeneity

All countries have a natural upper limit of the geographical potential for renewable generation capacity. A lower limit is set by the willingnesses of the countries to be dependent on imports from other countries. A stylized model of heterogeneity within these boundaries, which avoids specifying the exact renewable potentials in each country, is introduced by the heterogeneity parameter K:

$$\frac{1}{K} \leq \gamma_n \leq K \,. \tag{4.23}$$

The specific choice $K = 1$ results in a homogeneous layout, in which the average load $\langle L_n \rangle$ corresponds to the average renewable power generation $\langle G_n^R \rangle$ in each country. In [7] this condition was used to optimize the set of γ_n and α_n, a total of 60 variables, with the objective to minimize the system LCOE, and with the constraint that the renewable penetration of Europe is $\gamma_{\mathrm{EU}} = 1$. This was done using a Greedy Axial Search (GAS) algorithm [101]. The optimized layouts are refered to as GAS layouts. In the following, GAS $\rightarrow$ GAS* refers to an additional optimization, in which the transmission capacities have been uniformly scaled down from the definition in Equation (4.13), to yield a more cost effective constrained system despite a slightly higher cost for backup energy [7].

Figure 4.2 shows the sets γ_n and α_n of three optimized scenarios. The GASnoT layout in the top panel assumes a European system without transmission capacity between the individual countries. Setting the parameter $\gamma_n = 1$ for all nodes n, we assume that on average every country individually covers its load from renewable generation, with the instantaneous mismatch balanced by local backup power generation. This leaves the nodal mix between wind and solar α_n to be optimized by the GAS algorithm. For countries with strong wind resources like Denmark (DK) or Sweden (SE), a 100% wind layout is optimal, whereas southern countries like Italy (IT) or Greece (GR) introduce higher shares of solar power into the renewable energy mix. The middle panel represents a system allowing transmission between the nodes, allowing a more efficient placement of generation capacity and providing a spatial smoothing of fluctuations in the renewable generation. Whereas the GAS* (K=1) case still assumes a homogeneous parameter $\gamma_n = 1$ for all nodes, the optimized mix of renewable generation represented by the parameters α_n differs from the GASnoT scenario due to the possibility of power transmission. The GAS* (K=2) scenario describes a heterogenous system layout, in which also the parameters γ_n have been optimized under the condition Equation (4.23) with $K = 2$ and an overall VRES penetration of $\gamma_{EU} = 1$. The bottom part of Figure 4.2 illustrates this

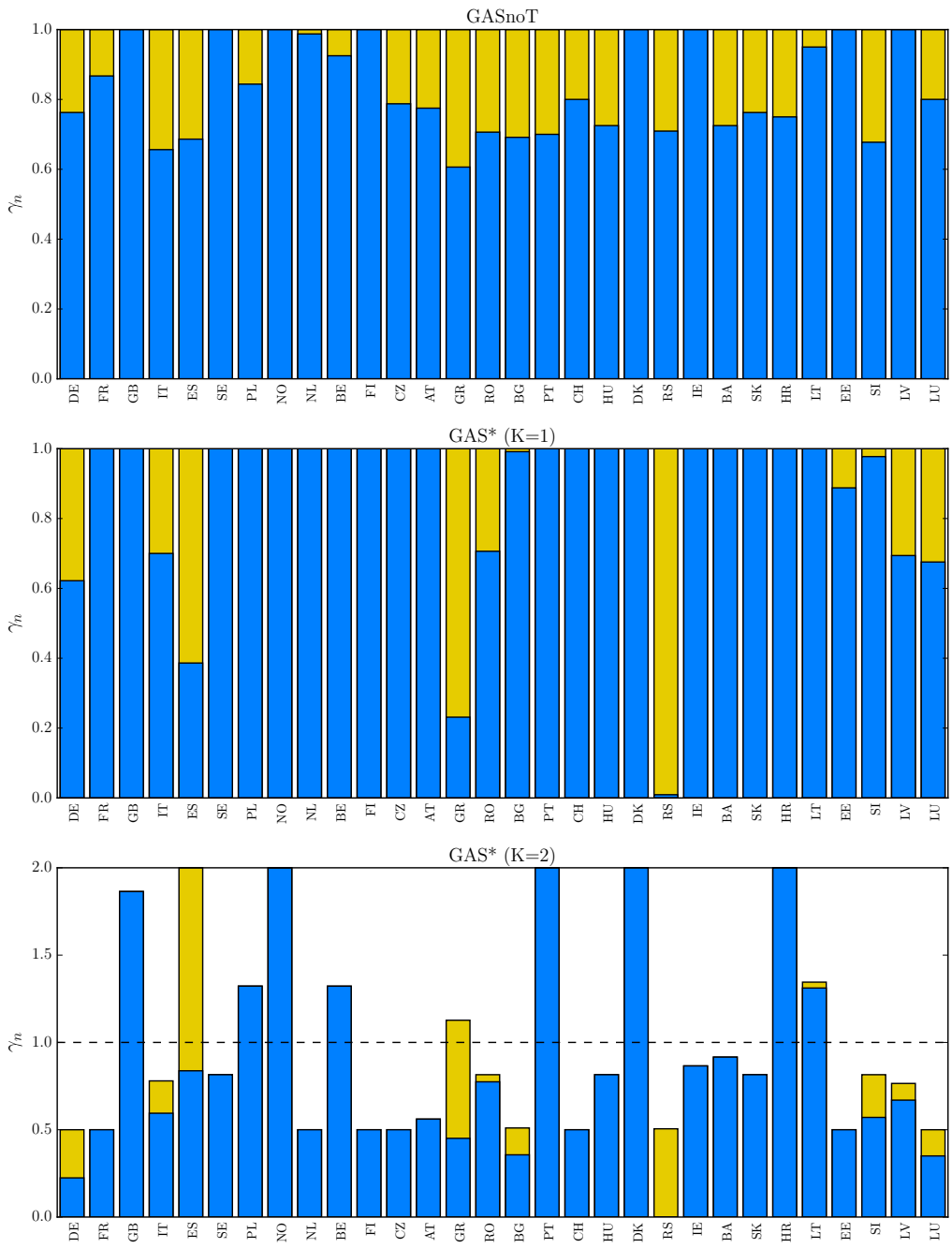

Figure 4.2: The renewable penetration parameter γ_n for GASnoT, GAS* K=1, and GAS* K=2 obtained in [7]. The mixing parameters α_n between wind (blue) and solar (yellow) power generation are also indicated.

heterogeneity: solar and wind generation capacity is concentrated at locations with favorable resource quality, leading to higher VRES penetration γ_n for these nodes. In this layout, nodes with $\gamma_n > 1$ are net exporters, whereas nodes with $\gamma_n < 1$ are net importers.

The overall system LCOE for the three layouts of Figure 4.2 are as follows. The GASnoT layout without transmission has the highest cost of 63 €/MWh. The more efficient placement of renewable capacity in the GAS* K=1 layout leads to a reduction of system LCOE to 56.6 €/MWh, just by introducing transmission. When introducing additional heterogeneity in the GAS* K=2 layout the resulting power flows in the system lead to higher transmission capacity costs. However, the total system LCOE can be further reduced to 53.8 €/MWh [7].

4.2.5 Flow tracing

The technique of flow tracing allows to follow the power flows from the exporting source nodes through the network to the importing sink nodes [40, 41]. This method has for instance been proposed as a flow allocation scheme in the context of the European inter transmission system operator compensation mechanism [51, 53], and has been used as an analytical tool for transmission capacity allocation in a simplified model of a highly renewable European electricity system [43]. Here we will follow the extended formulation as presented in [1, 46], using a decomposition of power flows across the network into strands associated with the injecting export node and the type of generation. For this purpose we define the in-partition $q^{\text{in}}_{(n,\mu)}$, which describes the share of the total power $P_n^+ := \max(P_n, 0)$ injected at node n associated with generation type $\mu \in \{W, S, B\}$ (wind, solar, backup power generation). This in-partition represents the input to the flow tracing algorithm, which then yields the following flow-partition and out-partition:

- The flow partition $\left\{q_{l,(n,\mu)}\right\}$ dissects the flow F_l on a link l into the components $F_{l,(n,\mu)} = q_{l,(n,\mu)} F_l$ that are attributed to the exporting node n and generation type μ.

- The out-partition $\left\{q^{\text{out}}_{n,(m,\mu)}\right\}$ describes the composition of power $P_n^- := -\min(P_n, 0)$ imported by node n. The respective share of this import P_n^- attributed to the exporting node m and generation type μ is given by $q^{\text{out}}_{n,(m,\mu)} P_n^-$.

The algorithm which determines this output from the in-partition is based on (m, μ)-flow conservation and the principle of proportional sharing [40, 41]:

$$\delta_{n,m} q^{\text{in}}_{(n,\mu)} P^+_n + \sum_k q_{k\to n,(m,\mu)} F_{k\to n} = q^{\text{out}}_{n,(m,\mu)} P^-_n + \sum_k q_{n\to k,(m,\mu)} F_{n\to k} \,, \quad (4.24)$$

with

$$q^{\text{out}}_{n,(m,\mu)} = q_{n\to k,(m,\mu)} \quad (4.25)$$

for the link $l = n \to k$ directed from node n to node k. The links are oriented along the total power flow F_l. We solve Equation (4.24) iteratively by starting at an exporting node without any inflow and following the power flow downstream. This is possible since the power flows on the network can be represented as a directed acyclic graph without loops [1].

The flow tracing algorithm has to be applied to every instantaneous injection pattern $P_n(t)$ and corresponding power flow pattern $F_l(t)$. The resulting out-partitions $q^{\text{out}}_{n,(m,\mu)}$ can be integrated into the following average export transfer function $\mathcal{E}^{\mu}_{m\to n}$:

$$\mathcal{E}^{\mu}_{m\to n} = \langle q^{\text{out}}_{n,(m,\mu)} P^-_n \rangle \,. \quad (4.26)$$

This measure describes the average amount of power injected at node m and resulting from generation type μ, which is exported through the network to the importing node n.

Prioritization of intrinsic renewable generation and decomposition of nodal exports We use a simplified model of the European electricity network, in which each country is represented by a single node. By disregarding the internal transmission networks, we aggregate over power generation and consumption on smaller scales, and determine the corresponding coarse-grained curtailment, backup power generation, imports, and exports on country scale. Nevertheless, since the flow tracing methodology considers the composition of the coarse-grained power flows and imports/exports, we have to introduce some additional rules on the nodal country level.

Recall that the total net injection $P_n(t)$ of node n is determined by the nodal balancing equation Equation (4.6):

$$P_n(t) = G^R_n(t) - L_n(t) + G^B_n(t) - C_n(t) \,. \quad (4.27)$$

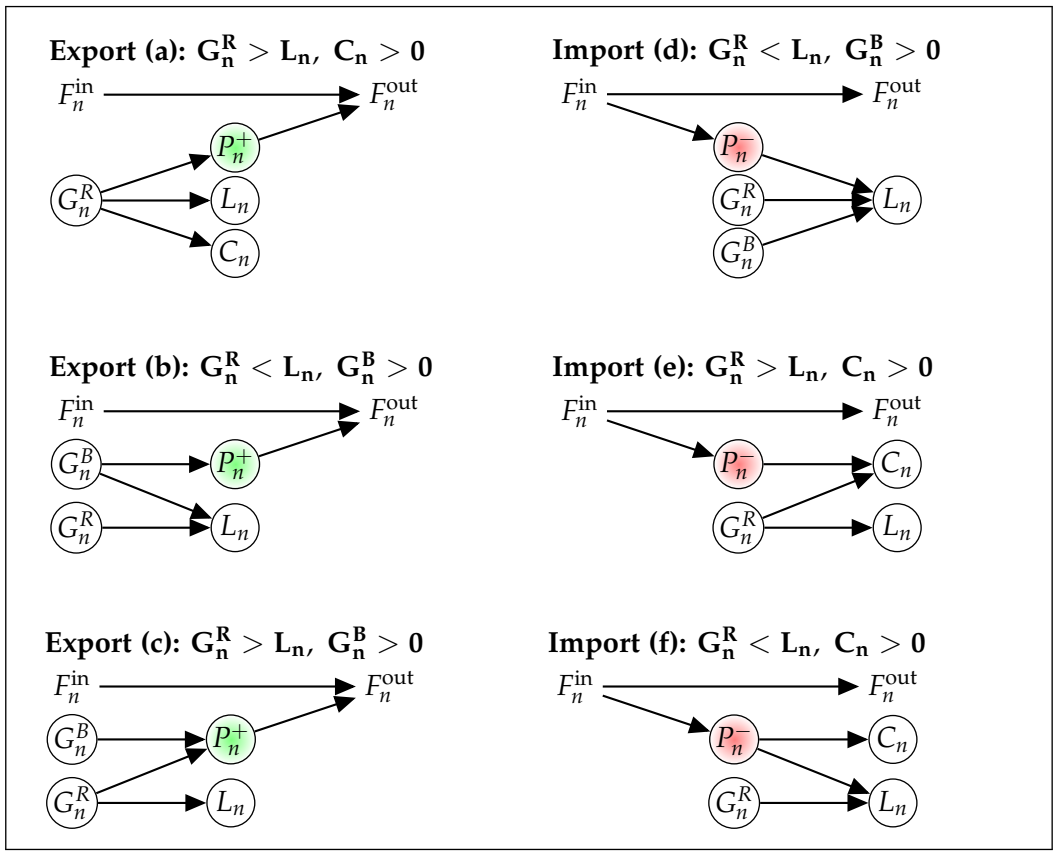

Figure 4.3: Nodal electricity partition cases. For every hour and every node one of these cases applies. Cases a-c all apply to nodal exports ($P_n^+ = P_n > 0$), while cases d-f all correspond to nodal imports ($P_n^- = -P_n > 0$).

Here we have written the balancing $B_n(t)$ in terms of backup power generation $G_n^B(t)$ and curtailment $C_n(t)$. Both the renewable generation $G_n^R(t)$ and nodal load $L_n(t)$ are given by the respective time series, whereas the balancing is determined from the heuristic scheme introduced in Equation (4.7). Although all terms in this equation are uniquely defined, the composition of exports P_n^+ or load $L_n(t)$ can be interpreted in different ways. Consider in particular an exporting node with $P_n > 0$, which besides renewable generation $G_n^R(t)$ provides backup power generation $G_n^B(t)$. In this case, which part of the renewable and backup power generation is assigned to the load $L_n(t)$ and which part to the net injection $P_n^+(t)$? In order to clarify this and related issues, in Figure 4.3 we distinguish between six different nodal electricity partition cases.

For the stated example, we apply a prioritization of intrinsic renewable gen-

eration, that is we assign as much intra-nodal renewable power generation as possible to the respective load, whereas a maximum of possible backup power generation is exported. Inside the boundaries of the simplified model considered here, this approach assumes that the individual countries use their generation capacity to their own benefit by exporting more expensive backup power generation from gas turbines, while using cheaper renewable generation for their own consumption. Note that the applied dispatch scheme distributes both backup power generation and curtailment to all countries relative to their average load.

The different nodal electricity partition cases illustrated in Figure 4.3 determine uniquely the in-partition $q_{(n,\mu)}$ for the flow tracing algorithm, and are consistent with a prioritization of intrinsic renewable generation:

Case (a):

$$q^{\text{in}}_{(n,\mu)}(t) = \begin{cases} \dfrac{G^W_n(t)}{G^R_n(t)} & \text{for } \mu = W \\ \dfrac{G^S_n(t)}{G^R_n(t)} & \text{for } \mu = S \\ 0 & \text{for } \mu = B \end{cases} . \tag{4.28a}$$

Case (b):

$$q^{\text{in}}_{(n,\mu)}(t) = \begin{cases} 0 & \text{for } \mu = W \\ 0 & \text{for } \mu = S \\ 1 & \text{for } \mu = B \end{cases} . \tag{4.28b}$$

Case (c):

$$q^{\text{in}}_{(n,\mu)}(t) = \begin{cases} \dfrac{G^W_n(t)}{G^R_n(t)} \dfrac{G^R_n(t) - L_n(t)}{G^B_n(t) + G^R_n(t) - L_n(t)} & \text{for } \mu = W \\ \dfrac{G^S_n(t)}{G^R_n(t)} \dfrac{G^R_n(t) - L_n(t)}{G^B_n(t) + G^R_n(t) - L_n(t)} & \text{for } \mu = S \\ \dfrac{G^B_n(t)}{G^B_n(t) + G^R_n(t) - L_n(t)} & \text{for } \mu = B \end{cases} . \tag{4.28c}$$

Cases (d), (e), (f):

$$q^{\text{in}}_{(n,\mu)}(t) = \begin{cases} 0 & \text{for } \mu = W \\ 0 & \text{for } \mu = S \\ 0 & \text{for } \mu = B \end{cases} . \tag{4.28d}$$

Here, (4.28a) refers to case (a) in Figure 4.3 and so forth. Note that only cases (a), (b), and (c) lead to a non-zero in-partition.

Transmission network usage measure The system participants make use of the transmission infrastructure through the power flows resulting from their imports and exports. The respective infrastructure costs thus have to be allocated to these users based on a suitable network usage measure. Although such a measure could be derived from nodal properties only, like average imports and exports (postage stamp method), this approach would ignore the role of the individual nodes in the fluctuating spatio-temporal flow pattern. In the following we apply a flow-based transmission capacity allocation measure, which has been introduced in [43]. Using the flow tracing method, this measure attributes the transmission capacity of a link $\mathcal{K}_l^T$, defined in Equation (4.13), to each country n based on the statistics of the corresponding partial flows $F_{l,n}(t) = q_{l,n}(t)F_l(t)$:

$$\mathcal{K}_{l,n}^T = \int_0^{\mathcal{K}_l^T} d\mathcal{K} \frac{1}{1 - P_l(\mathcal{K})} \int_{\mathcal{K}}^{\mathcal{K}_l^T} dF_l p_l(F_l) \langle q_{l,n} | F_l \rangle \,. \tag{4.29}$$

Here p_l is the probability distribution of the flow on the link l, P_l is the cumulative probability function, and $\langle q_{l,n}|F_l\rangle$ is the average fraction of the flow assigned to the source node n, given that the total flow is equal to F_l. Note that we here do not discriminate different generation technologies and thus omit the index μ. In [43] this measure is derived by virtually decomposing the total capacity $\mathcal{K}_{l,n}^T$ into infinitesimal increments $d\mathcal{K}$ for the whole time series. Each of these increments is then weighted according to the respective flow-based usage by the node n. The structure of the expression Equation (4.29) assures that the first increments of the total capacity are assigned to all users with partial flows on the respective link, whereas the last increments close to the total capacity are only assigned to those system participants which make use of the link in high-flow situations. For a further discussion of this approach we refer the reader to [1, 43, 46].

4.3 FLOW-BASED NODAL COST ALLOCATION

4.3.1 Nodal cost allocation

The system LCOE Equation (4.22) is an aggregated measure of the cost of electricity across all countries. Allocating costs for individual nodes requires a nodal LCOE measure. Here we introduce such a measure with the requirement that the weighted sum of nodal costs reproduces the aggregated system costs

$$\mathrm{LCOE}_{\mathrm{EU}} = \sum_n \frac{\langle L_n \rangle}{\langle L_{\mathrm{EU}} \rangle} \mathrm{LCOE}_n \,. \tag{4.30}$$

The costs related to the individual system components in Equation (4.17) and Equation (4.20), constituting the LCOE Equation (4.21), have to be allocated to the respective countries. This corresponds to the introduction of a node index on the set of present values:

$$\{V_W, V_S, V_B, V_T\} \Rightarrow \{V_{W,n}, V_{S,n}, V_{B,n}, V_{T,n}\}. \tag{4.31}$$

In the following we differentiate between generation capacity costs and transmission infrastructure costs. A straightforward method for the attribution of generation capacity costs would be according to their respective geographical location, that is for instance the cost of wind power generation capacity is assigned to the country in which the respective turbines are installed. Such an allocation ignores the fact that in an interconnected system with transmission a significant amount of generated power might be exported to and thus consumed in another country. In order to establish nodal LCOEs which take into account these import/export patterns, we thus have to connect the location of generation with the location of consumption. This connection is realized by the flow tracing method and expressed by the export transfer function $\mathcal{E}^{\mu}_{m\to n}$. Based on this function, we define the measure $\mathcal{K}^{\mu}_{m\to n}$, that describes the generation capacity of type $\mu \in \{W, S, B\}$ located at node m which is used by node n:

$$\mathcal{K}^{\mu}_{m\to n} = \begin{cases} \left[\frac{\mathcal{E}^{\mu}_{m\to n}}{\langle G^{\mu}_m\rangle - \langle C^{\mu}_m\rangle}\right] \mathcal{K}^{\mu}_m & \text{if } m \neq n \\ \mathcal{K}^{\mu}_m - \sum_{s\neq m} \mathcal{K}^{\mu}_{m\to s} & \text{if } m = n\ . \end{cases} \tag{4.32}$$

Here $\langle G^{\mu}_m\rangle$ and $\langle C^{\mu}_m\rangle$ denote the average generation and curtailment of generation type μ in node m, respectively. In the case $m \neq n$ this measure attributes a share $\mathcal{K}^{\mu}_m$ of the generation capacity of type μ in node m to an importing node n. The attribution is proportional to the respective export transfer function $\mathcal{E}^{\mu}_{m\to n}$ and the amount of power of type μ generated at node m that is not curtailed. The capacity that gets attributed to node m itself is the remaining capacity after the attribution to all importing nodes n. With this measure we can calculate the total share of system generation capacity of type μ which is attributed to node n:

$$\widetilde{\mathcal{K}}^{\mu}_n = \sum_m \mathcal{K}^{\mu}_{m\to n}\ . \tag{4.33}$$

In a similar way the share of the total system backup energy generation is attributed to a node n by:

$$\widetilde{E}^{B}_n = \langle G^{B}_n\rangle - \sum_{m\neq n} \mathcal{E}^{B}_{n\to m} + \sum_{m\neq n} \mathcal{E}^{B}_{m\to n} \tag{4.34}$$

$$= \sum_m \frac{\mathcal{K}^{B}_{m\to n}}{\mathcal{K}^{B}_m} \langle G^{B}_m\rangle\ . \tag{4.35}$$

Here we have used the definition in Equation (4.32) and $\langle C_m^B \rangle = 0$. Combining the nodal generation capacities Equation (4.33) and the nodal system backup energy usage Equation (4.34), the nodal LCOE is calculated as

$$\mathrm{LCOE}_n = \sum_\mu \frac{\widetilde{V}_n^\mu}{\sum_{t=1}^{T_{\mathrm{life}}^\mu} \frac{L_{n,t}}{(1+r)^t}} + \frac{V_n^T}{\sum_{t=1}^{T_{\mathrm{life}}^T} \frac{L_{n,t}}{(1+r)^t}} \,, \tag{4.36}$$

where the nodal present values of investment $\widetilde{V}_n^\mu$ are now based on $\widetilde{\mathcal{K}}_n^\mu$ and $\widetilde{E}_n^B$ where applicable. For the allocation of transmission capacity costs V_n^T in the nodal LCOEs we consider different schemes. A simple realization based on nodal properties only is an assignment according to the average load of a country:

$$V_n^T = \frac{\langle L_n \rangle}{\langle L_{\mathrm{EU}} \rangle} V^T \,. \tag{4.37}$$

An alternative flow-based transmission infrastructure cost allocation makes use of the capacity usage measure $\mathcal{K}_{l,n}^T$ in Equation (4.29):

$$V_n^T = \sum_l \mathcal{K}_{l,n}^T d_l c_l \,. \tag{4.38}$$

Here we assume that the cost for the DC converter stations are allocated following the assignment of the corresponding HVDC lines. Note that $\mathcal{K}_{l,n}^T$ can be either based on exports or imports, depending on how the flow tracing algorithm is applied.

4.3.2 Variation of nodal costs

Our primary goal with the introduction of heterogeneity is to reduce the overall system costs. As a side effect, the introduced heterogeneity of the renewable generation capacities might lead to a change in the variation of the individual nodal costs. To measure this change, we use the weighted standard deviation (WSD) of the nodal LCOEs:

$$\mathrm{WSD} = \sqrt{\sum_{n=1}^{N} \frac{\langle L_n \rangle}{\langle L_{\mathrm{EU}} \rangle} \left(\mathrm{LCOE}_n - \mathrm{LCOE}_{\mathrm{EU}}\right)^2} \,. \tag{4.39}$$

4.4 RESULTS

4.4.1 Patterns of imports and exports

We now look at the patterns of imports and exports for the GAS* K=2 layout. In the top panel of Figure 4.4 we show the six largest average exports for six

countries, which are all, except for Serbia (RS), net exporters with $\gamma_n > 1$; see Figure 4.2 for reference. The average exports are calculated using the export transfer function Equation (4.26) and displayed in terms of the mean load of the country of interest. The percentage in parenthesis denotes the amount of the country's total average export accounted for by the sum of the six bars. Similarly, the bottom panel shows the six largest average imports for six countries, all net importers with $\gamma_n < 1$.

The leftmost part of the top panel displays the top six countries that Great Britain is exporting to (normalized to the mean load of Great Britain). It shows that 79% of the average exports of Great Britain are accounted for by only six countries. Similarly, the leftmost part of the bottom panel shows the top six countries contributing to the imports of Germany (normalized to the mean load of Germany). In both panels the six countries of interest are sorted by descending mean load.

The mix between wind and solar, which is shown in Figure 4.2, is visible in the export components in the top panel, with GB and DK having only wind and ES having a solar dominated mix.

All net importers in the bottom panel are importing from GB, and almost all are importing from ES as well. This holds even for countries far away in the network, such as FI, BG, RS, see Figure 4.1 for reference. GB and ES have considerable mean load and γ_n close or equal to 2, which is why their exports are ubiquitous in the network. Note that the renewable mix of Spain is solar dominated while GB is purely wind.

Serbia is included in both panels of Figure 4.4. It is a net importer with $\gamma_n = 0.5$. We see that even net importers will be exporting during some hours. Since for Serbia $\alpha_n = 0$, solar and backup power generation accounts for the entire export. The imports of Serbia are almost entirely wind, which is due to the dominance of wind power generation in the net exporting neighboring countries.

4.4.2 Nodal cost of electricity

We apply the method of flow-based nodal LCOEs as defined by Equation (4.36) to the two GAS* optimized scenarios with transmission and heterogeneity limits K=1 and K=2 (see Section 4.2). For the heterogeneity constraint of K=1 the results are shown in the top part of Figure 4.5, whereas the bottom part shows the results for the more heterogeneous layout for K=2. In these figures, the transmission capacity costs are attributed equally to the countries based on

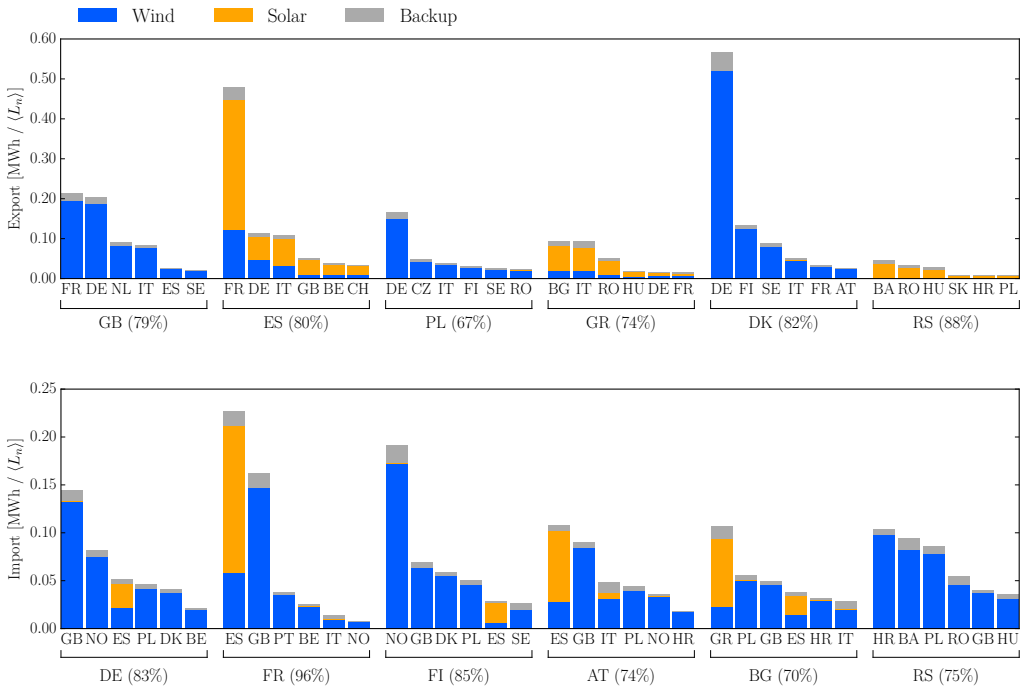

Figure 4.4: Average exports (top) and imports (bottom) for selected countries in the GAS* K=2 layout. Results are calculated using the export Equation (4.26) transfer function. The percentage in parenthesis denotes the amount of the country's total average export (top) or import (bottom) accounted for by the sum of the six bars.

their respective mean load according to Equation (4.37). We observe that the external capacity and backup energy costs allocated using the flow tracing method represent a significant part of the nodal LCOE. This becomes particularly apparent for Serbia, which is assigned almost none local wind power capacity (see Figure 4.2), but uses a substantial amount of external wind power generation to cover its electricity demand; see also Figure 4.4. Similarly, for both layouts with transmission France has no local solar generation capacity, but to some extent imports such solar power generation through the transmission grid. The usage of backup power capacity and backup energy is relatively homogeneously distributed for most nodes, which has its origin in the synchronized balancing scheme (recall the definition in Equation (4.7)).

In [7] it was shown that power transmission between the European countries and a higher degree of heterogeneity lowers the total system LCOE from 63€/MWh

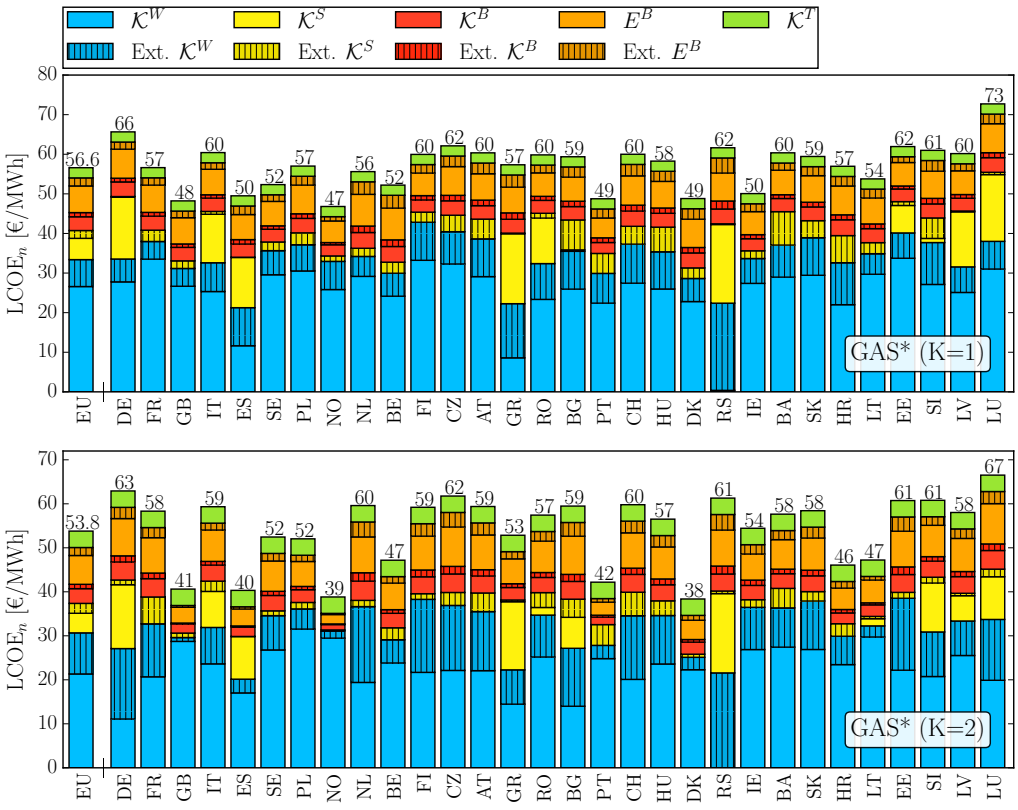

Figure 4.5: Nodal component-wise LCOE for the GAS* K=1 (top) and the GAS* K=2 (bottom) layout. The components are split into their local and external parts. In both cases the transmission cost component of the LCOE is distributed according to the average load of the individual countries as defined in Equation (4.37).

to 53.8€/MWh. This is shown in the leftmost bar of Figure 4.6. How does this cost reduction translate to the nodal LCOEs associated with the individual countries? Remarkably, the transition from the GAS K=1 layout without transmission to the GAS* K=1 layout with transmission leads to reduced nodal LCOE for every single country; see Figure 4.6. This shows that under a flow-based cost allocation mechanism, cooperation in a European electricity system through power transmissions does not only lead to a global, but also to a system-wide local cost reduction. Allowing a more heterogeneous GAS* K=2 layout decreases the system LCOE further from 56.6€/MWh to 53.8€/MWh. Apart from a few exceptions (France, Sweden, Netherlands, Bulgaria, Ireland) this global cost reduction is again related with reduced or unchanged LCOEs on the nodal level.

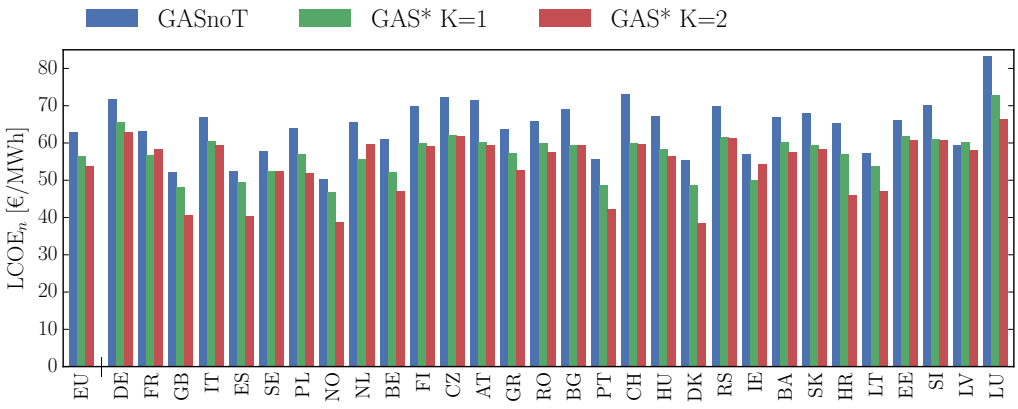

Figure 4.6: Comparison of nodal LCOEs for GASnoT (blue), GAS* K=1 (green), and GAS* K=2 (red). Allowing transmission reduces the system LCOE and all nodal LCOEs. Increasing the heterogeneity from K=1 to K=2 leads to a decrease of the system LCOE and all nodal LCOEs except small increases for FR, SE, NL, BG and IE.

Compared with the system layout without transmission, we observe the largest drop in nodal LCOEs for Denmark (DK) and Luxembourg (LU), with a nodal cost reduction of 17€/MWh and 16€/MWh, respectively, compared to an overall cost reduction of 9.2€/MWh. In the case of Luxembourg this cost reduction is due to its low capacity factor for local wind energy [7], whereas for Denmark the cost reduction can be explained in an efficient usage of abroad generation capacity combined with a high local capacity factor for wind energy.

In both panels of Figure 4.5, we see fluctuations in nodal LCOEs around the EU average shown on the left. In Table 4.2 we display the WSD as defined in Equation (4.39) as a measure of the heterogeneity of nodal LCOEs for the scenario without transmission and for the scenarios with transmission (heterogeneity parameter K=1 and K=2). We observe that K=1 the incorporation of power transmission reduces the WSD from 7.27 €/MWh to 5.38 €/MWh. This shows that the spread in nodal LCOEs is at first reduced by cooperation between the European countries, which can be explained by the partial smoothing out of the heterogeneity in the renewable generation resources and the accompanying generation costs. For increasing heterogeneity K=2 we then observe an increasing WSD from 5.38 €/MWh to 8.54 €/MWh. This shows that even under the flow based nodal cost allocation scheme the system-wide cost reduction due to higher heterogeneity is unequally distributed among the different countries. In

particular, net exporting countries with $\gamma_n > 1$ are the main beneficiaries of the transition from the K=1 to the K=2 scenario (see Figure 4.6). These countries are able to consume higher shares of renewable generation, therefore saving costs in backup power generation, while exporting the involved surplus and the related capacity costs. However, this benefit from heterogeneity goes along with a disproportional usage of the transmission grid, which is not represented in the transmission cost allocation based on average loads applied so far. In the next section we explore how a respective flow based allocation affects the spread in the nodal LCOEs.

4.4.3 Transmission cost allocations

Besides a transmission cost allocation according to the average load of a country, in the following we consider three variants of the flow based cost assignment in Equation (4.38): 1) the importer alone pays for transmission, 2) the transmission expenses are shared equally between both importer and exporter, and 3) the exporter alone pays for the transmission. The respective underlying network usage measure $\mathcal{K}_{l,n}$ in Equation (4.29) in general is used to allocate transmission capacity to exporters by tracing the exported power flows. This is the export picture, which is described in Section 4.2.5 and is used for case 3). To allocate transmission capacity to importers we swconsentec2006h to the import picture, that is $P_n(t) \to -P_n(t)$ and $F_l(t) \to -F_l(t)$, and apply Equation (4.29) to trace the imported power flows for case 1) [43]. Case 2) is an average of the import and export picture. These three cases of flow based transmission cost allocation are compared with the one based on average loads in Figure 4.7. The nodal LCOEs values are, except for the transmission component, equal to the results shown in Figure 4.5. For this reason we highlight the transmission cost component of the nodal LCOEs in Figure 4.7, leaving the other components grey. The four green bars shown for each country represent from left to right the four cases described above.

The top panel of Figure 4.7 shows results for the homogeneous GAS* K=1 layout with $\gamma_n = 1$, while the bottom panel shows results for the more heterogeneous GAS* K=2 layout with $0.5 \leq \gamma_n \leq 2$. For the K=1 layout for all node there are only minor differences between the three cases of transmission cost allocation. This is due to the fact that, on average, each country serves its own load by its own renewable generation, and only the fluctuating surpluses are subject to power transmission. In the more heterogeneous case of K=2, however, we see significant differences between the three transmission cost allocations. In this scenario the occurrence of net importers and net exporters lead to a more

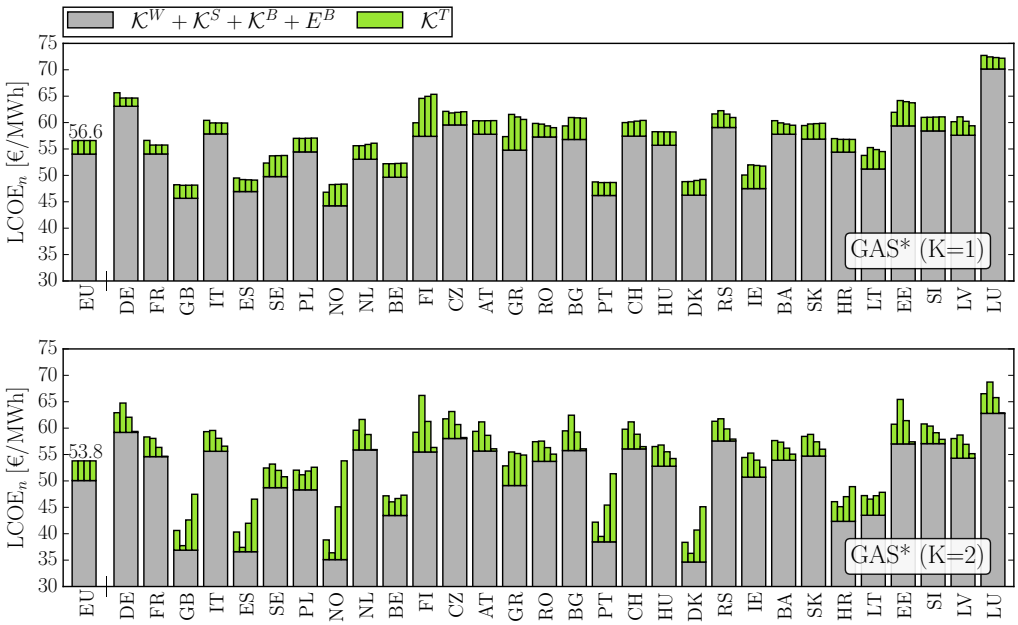

Figure 4.7: Comparison of four transmission cost allocations. Leftmost of the green bars: assignment proportional to average loads. Then from left to right: importing countries alone pay for the transmission line costs, equal sharing of expenses between both importer and exporter, and transmission cost allocated to exporting countries. Note that all transmission cost allocations will always result in the same weighted average value of the total European LCOE.

disproportionate usage of the transmission grid. As discussed in the previous section, the transition from the K=1 to the K=2 scenario mainly benefits the net exporting countries. Accordingly we observe in Table 4.2 an increasing WSD if we allocate transmission costs using the flow based methodology based on imports. The equal partition between exports and imports then reduces the WSD compared to the case of a transmission cost assignment based on average loads due to its incorporation of some of the exporters significant transmission usage. Although such an allocation scheme could be considered as most fair by representing the individual countries role in the overall flow pattern, it does not balance the benefit of higher heterogeneity in terms of nodal LCOEs for net exporters. Accordingly, the WSD in Table 4.2 as expected adopts its lowest value in the case of a purely export based transmission cost allocation. Such an attribution mainly affects the six countries with γ_n close or equal to 2, which incur the strongest benefit from the increasing heterogeneity in the system. The

Table 4.2: The weighted standard deviation (WSD) of the fully usage-based nodal LCOE for different shares of the transmission cost between the importing and exporting countries. Results are shown for different values of the constraint parameter K and different flow allocation schemes. The LCOE_{EU} values are shown for reference. All results are obtained for the GAS* layouts and all values are expressed in units of €/MWh.

Heterogeneity constraint	**LCOE_{EU}**	**WSD**	**WSD for import/export:**		
			100/0	**50/50**	**0/100**
$K = 1$ (no trans.)	63.0	7.27			
$K = 1$	56.6	5.38	5.28	5.22	5.17
$K = 2$	53.8	8.54	10.22	6.72	3.83

respective countries are Great Britain, Spain, Norway, Portugal, Denmark and Croatia (see Figure 4.2 for reference), which as shown in Figure 4.7 display disproportionally large allocations of transmission infrastructure costs.

4.5 CONCLUSION AND OUTLOOK

In this contribution we study flow-based nodal levelized costs of electricity (LCOEs) in the framework of a simplified model of a highly renewable European electricity network with countries as aggregated network nodes. As shown in [7], an optimal heterogeneous placement of renewable generation capacity reduces the system-wide LCOE in this model. In order to be able to investigate LCOEs on a nodal level, we use a flow tracing technique to connect the location of power generation with the respective location of consumption. This method allows to assign shares of capital and operational costs associated with imported power from generation capacities abroad, and to allocate transmission capacity costs based on the countries role in the fluctuating spatio-temporal power flow patterns. We observe that for the model of the European system, both cooperation between the countries by importing and exporting excess generation, and a more efficient heterogeneous capacity placement not only lead to a reduction of the system LCOE, but also to a reduction of the nodal LCOE for all countries compared to the case without transmission. It is shown that net exporters are the main beneficiaries of a heterogeneous system layout, with an export flow-based attribution of transmission infrastructure cost reducing the related spread of nodal LCOEs.

Methodologically it would be interesting to use other flow allocation measures

for the transmission cost allocation, for instance methods based on the PTDF matrix [1, 44], and compare the resulting influence on the nodal LCOEs. Also the allocation of backup power capital costs as used in this contribution could be expanded to include correlations to the injection and flow pattern, similar to the approach used for the network usage measure in [43].

For the investigation in the present contribution we have used a coarse-grained model where the heterogeneity has been limited to country aggregates. However, the capacity factors vary within each country, which can be exploited by using a model with higher spatial resolution. A recent paper has shown that the cost of renewable generation capacity in a heterogeneous system is up to 10% lower for a high resolution network of 362 nodes when compared to a 37 node network with one node per country [30]. It would be interesting to apply the concept of nodal LCOEs and understand the distribution of costs in such a more detailed model.

The method of flow-based nodal LCOEs first and foremost serves as an analytical tool to investigate the system costs of an interconnected electricity system on a nodal level. By definition, it does not take into account the role of markets as the prevalent way to allocate costs and remunerate investors in todays electricity system. Nevertheless, comparing a statistical measure of market prices with the nodal LCOEs could point towards how additional capacity pricing mechanisms could lead to a fair distribution of the respective costs in a cost-efficient heterogeneous highly renewable energy system.

5

Flow-based analysis of storage usage in a low-carbon European electricity scenario

This chapter is published as "Flow-Based Analysis of Storage Usage in a Low-Carbon European Electricity Scenario" by Bo Tranberg, Mirko Schäfer, Tom Brown and Jonas Hörsch and Martin Greiner in the proceedings of the 15th International Conference on the European Energy Market (EEM) [3].

5.1 INTRODUCTION

The European Union has set a target to reduce CO_2 emissions by 80-95% in 2050 compared to 1990 levels [14]. Most scenarios for reaching this target rely on the large-scale integration of intermittent wind and solar power generation, which requires future investments in transmission and storage capacity to smooth the variable generation over large spatial distances and appropriate time scales. The seeming dichotomy of these two flexibility sources emphasises the need to understand their actual interplay in cost-efficient scenarios of a future low-carbon electricity system.

Energy system models often employ a global optimisation approach to derive cost optimal scenarios [102]. Even when all input data and modelling details are available, the complexities and interdependencies inherent to such models tend to impede a deeper understanding of the mechanisms at play in an optimal combination of resources and technologies. This in particular applies to the role of the electricity grid, given that the pooling nature of power transmission in general disguises the influence of individual nodes on the global flow pattern. In this context, the method of flow tracing has been shown to yield important insights. By following the path of partial power flows through the transmission network, this technique allows to connect the location of consumption with the location of generation, and to allocate power flows on transmission lines

to exporters and importers [40, 41, 46]. It has been proposed for instance as a flow allocation method as part of the inter transmission system operator compensation (ITC) mechanism [51], or as the basis of a demand-side-oriented carbon emission allocation method [103]. In the context of the system analysis of highly renewable electricity scenarios, flow tracing has been applied to allocate transmission capacities [6, 43], or as a technique to introduce flow-based nodal systems costs [2, 8]. In this contribution we introduce an extended application of the generalised flow tracing method, which traces flows in and out of storage and is able to keep track of the originating source of generation. We apply this method to a low-carbon future European electricity scenario first presented in [30].

This article is organised as follows: Section 5.2 introduces the modelling of dispatch and investments in generation capacities of a low-carbon European electricity scenario. Section 5.3 reviews the flow tracing methodology and introduces the formulation for including storage facilities. Results are presented and discussed in Section 5.4, and Section 5.5 presents the conclusions.

5.2 POWER SYSTEM MODELLING

The input data for the system model is based on PyPSA-Eur, a dataset of the European electricity system containing spatially detailed information about the transmission network topology, conventional generators, hydro power, and time series for wind and solar power potential and demand, compiled from various sources [29, 104]. The 5612 transmission lines and 4653 substations within the dataset are merged using the k-means clustering algorithm to 64 nodes and 132 transmission lines covering 33 countries, see Figure 5.1. The distribution of generation capacities as well as generation and load time series are also aggregated to yield corresponding nodal representations. We choose a spatial resolution of 64 nodes for the European system in order to work on a coarse-grained level while still being able to capture patterns on regional scale within larger countries. See [30] for further details on the underlying data set, and in particular for a discussion of network aggregation methods and the role of spatial scale for electricity system modelling.

The model uses a techno-economic optimisation minimising total annual system costs:

$$\min_{\substack{G_n^\alpha, F_l, \\ g_n^\alpha(t), f_l(t)}} \left[\sum_{n,\alpha} c_n^\alpha G_n^\alpha + \sum_l c_l F_l + w_t \sum_{n,\alpha,t} o_{n\mathcal{g}}^\alpha g_n^\alpha(t) \right] . \tag{5.1}$$

Here G_n^α are the capacities of generation and storage technologies α at node n and their associated fixed costs c_n^α, $g_n^\alpha(t)$ is the nodal dispatch during hour t and the associated operating cost o_n^α, and F_l are the line capacities and their associated fixed costs c_l. The model is run using weather and demand data for a representative year chosen to be 2012. To keep computation time reasonable the model is run for every third hour of the representative year leading to the weighting $w_t = 3$ in the objective function and following constraints. As fossil fuel generators we assume open cycle gas turbines, which are more flexible but less efficient than combined cycle gas turbines. Renewable generators include solar PV, onshore wind and offshore wind. Batteries and hydrogen storage are used as extendable storage options, whereas hydroelectricity capacities (run-of-river, reservoirs and pumped storage) are fixed to today's level. All cost assumptions are given in [30].

For every (weighted) hour, the demand at each node $d_n(t)$ must be met by local generation and storage discharge or by imported power flows $f_l(t)$ on transmission line l,

$$\sum_\alpha g_n^\alpha(t) - d_n(t) = \sum_l K_{n,l} f_l(t) \ , \tag{5.2}$$

where $K_{n,l}$ is the incidence matrix representing Kirchhoff's Current Law. For the HVAC part of the network also Kirchhoff's Voltage Law is enforced by demanding that the voltage differences around any closed cycle must sum to zero [30, 105].

The dispatch $g_n^\alpha(t)$ of conventional generators is constrained by their capacity, expressed by the condition $0 \leq g_n^\alpha(t) \leq G_n^\alpha$. Similarly, the dispatch of renewable generators is constrained by their capacity, $0 \leq g_n^\alpha(t) \leq \bar{g}_n^\alpha(t) G_n^\alpha$, where $\bar{g}_n^\alpha(t)$ is the fraction of capacity available depending on the weather conditions obtained from historical reanalysis weather data. When the generation is less than the available energy the remainder is curtailed.

The state-of-charge of all storage facilities must be consistent across all hours:

$$\begin{aligned} \mathrm{soc}_n^\alpha(t) = \mathrm{soc}_n^\alpha(t-1) &+ w_t g_{n,\mathrm{inflow}}^\alpha(t) - w_t g_{n,\mathrm{spillage}}^\alpha(t) \\ &\pm \begin{cases} w_t \eta_1 g_n^\alpha(t), & \text{charging} \\ w_t \eta_2^{-1} g_n^\alpha(t), & \text{discharging} \end{cases} . \end{aligned} \tag{5.3}$$

Here η_1 and η_2 are the charging and discharging efficiencies, respectively. These efficiencies ensure that the storage facilities are only charged when there is an oversupply of power, and discharged only when generators and imports are not able to fully serve the demand. The state of charge is limited by the storage

energy capacity, $0 \leq \mathrm{soc}_n^\alpha(t) \leq E_n^\alpha$, which is defined by the nominal power G_n^α through

$$E_n^\alpha = h_{\max}^\alpha G_n^\alpha \,. \tag{5.4}$$

Here $h_{\max}^\alpha$ is the maximum number of hours that a storage facility can charge or discharge at the full nominal power. We set $h_{\max}^\alpha = 6\text{h}$ for battery storage and pumped hydro, and $h_{\max}^\alpha = 168\text{h}$ for hydrogen storage [86]. This constraint implies that there is no separate optimisation of storage power and energy capacity.

The power flow on the transmission lines is constrained by the transmission capacities, $|f_l(t)| \leq F_l$. The sum of the product of transmission capacities and transmission line lengths are constrained by an overall maximum capacity

$$\sum_l l_l F_l \leq \mathrm{CAP}_{\mathrm{trans}}, \tag{5.5}$$

which is fixed to a moderate expansion corresponding to 150% of the current transmission capacities

$$\mathrm{CAP}_{\mathrm{trans}} = 1.5 \cdot \sum_l l_l F_l^{\mathrm{today}}. \tag{5.6}$$

CO_2 emissions are limited by a global constraint $\mathrm{CAP}_{\mathrm{CO}_2}$, defined by specific emissions e_α in CO_2-tonne-per-MWh of the fuel α and the efficiency η_α of the generator

$$\sum_{n,\alpha,t} \frac{1}{\eta_\alpha} w_t g_n^\alpha(t) e_\alpha \leq \mathrm{CAP}_{\mathrm{CO}_2} \,. \tag{5.7}$$

This constraint is set to a reduction of emissions of 95% compared to 1990 levels. Since the only fossil fuel generators in the model are open cycle gas turbines, the constraint Equation (5.7) directly translates into the amount of fuel burned by these generators, and thus into the amount of power generated from this source [86, 106].

5.3 FLOW TRACING

For clarity we omit in this section the time index t and decompose the generation term in the hourly nodal power balance Equation (5.2) into generators (conventional and renewable) g_n^α, storage discharging $s_n^{\alpha,+}$, and storage charging $s_n^{\alpha,-}$. We define the net nodal inflow into the network and the net nodal outflow

from the network as

$$P_n^{\text{in}} = \max\left(\sum_\alpha \left[g_n^\alpha + s_n^{\alpha,+} - s_n^{\alpha,-}\right] - d_n, 0\right) , \tag{5.8}$$

$$P_n^{\text{out}} = \max\left(d_n - \sum_\alpha \left[g_n^\alpha + s_n^{\alpha,+} - s_n^{\alpha,-}\right], 0\right) . \tag{5.9}$$

We rewrite Equation (5.2) as

$$P_n^{in} + \sum_k f_{k\to n} = P_n^{\text{out}} + \sum_k f_{n\to k} , \tag{5.10}$$

where the incidence matrix has been replaced with the sums of inflows and outflows. Assuming perfect mixing of the various flow components, the method of flow tracing follows the different nodal inflows P_m^{in} downstream through the network. The share $q_{n,m}$ of outflow from node n (both through the network and into node n), which has been an inflow at node m has to fulfil the following partial flow conservation:

$$\delta_{n,m} P_n^{\text{in}} + \sum_k q_{k,m} f_{k\to n} = q_{n,m} P_n^{\text{out}} + \sum_k q_{n,m} f_{n\to k} . \tag{5.11}$$

Rearranging this equation yields the matrix equation formulation of flow tracing

$$\delta_{n,m} P_n^{\text{in}} = \sum_k \left[\delta_{n,k}\left(P_n^{\text{out}} + \sum_{k'} f_{n\to k'}\right) - f_{k\to n}\right] q_{k,m} \tag{5.12}$$

which can be inverted to calculate the nodal mixes $q_{n,m}$ [46]. We can now derive the fraction of load d_n or storage charging $s_n^{\beta,-}$ associated with nodal inflow from generation technology α at node m. For this purpose we first define the internal mix for net exporters with $P_n^{\text{in}} > 0$:

$$r_{n,\alpha}^{\text{in}} = \frac{g_n^\alpha + s_n^{\alpha,+}}{\sum_\alpha \left(g_n^\alpha + s_n^{\alpha,+}\right)} . \tag{5.13}$$

This internal mix is then attached to the nodal inflow from node n and followed through the network, leading to the internal mix for net importers n with $P_n^{\text{out}} > 0$:

$$r_{n,(m,\alpha)}^{\text{out}} = \frac{\delta_{m,n}\left(g_n^\alpha + s_n^{\alpha,+}\right) + q_{n,m} r_{m,\alpha}^{\text{in}} P_n^{\text{out}}}{\sum_\alpha \left(g_n^\alpha + s_n^{\alpha,+}\right) + P_n^{\text{out}}} . \tag{5.14}$$

The share of load and storage charging at node n associated with generation or storage discharging from technology type α at node m is then

$$d_n(m,\alpha) = \delta_{n,m} r_{n,\alpha}^{\text{in}} d_n , \quad s_n^{\beta,-}(m,\alpha) = \delta_{n,m} r_{n,\alpha}^{\text{in}} s_n^{\beta,-} \tag{5.15}$$

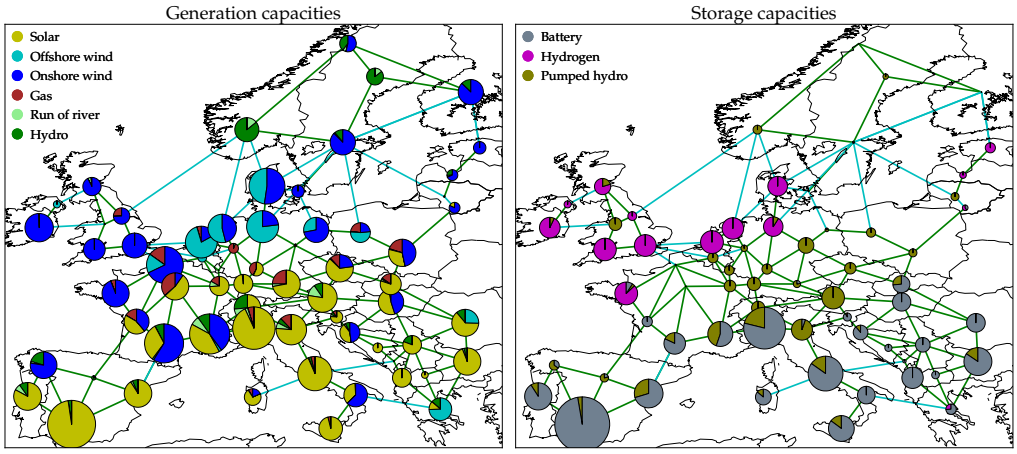

Figure 5.1: Optimised generation layout (left) and storage layout (right) resulting from the optimisation Equation (5.1). AC lines in green and DC lines in blue.

for net exporters, and

$$d_n(m,\alpha) = r^{\text{out}}_{n,(m,\alpha)} d_n\,, \quad s_n^{\beta,-}(m,\alpha) = r^{\text{out}}_{n,(m,\alpha)} s_n^{\beta,-} \tag{5.16}$$

for net importers. The scheme applied here assumes that first all inflow and outflow inside a node is aggregated, and then this aggregated flow is coupled to the network. This description is suitable for a coarse-grained system representation as used for this contribution. For a spatially more detailed representation, alternatively all inflows and outflows could be directly coupled to the network. The influence of choosing either approach on the flow tracing results will be studied in a forthcoming publication.

5.4 RESULTS

The distribution of generation capacities in the scenario resulting from the system optimisation Equation (5.1) is shown in the left panel of Figure 5.1. This layout is sensitive to the input parameters and optimisation constraints, in particular to the cap on the total transmission capacities and CO_2 emissions in Equation (5.5) and Equation (5.7) [106]. The figure shows that solar generation capacities are predominantly located in the southern half of the system, in line with the favourable solar radiation conditions in the southern countries. Offshore wind is located mainly at the North Sea and Baltic Sea along with minor capacities in the Black Sea and the Mediterranean Sea. Onshore wind is spread more evenly throughout the northern and western countries.

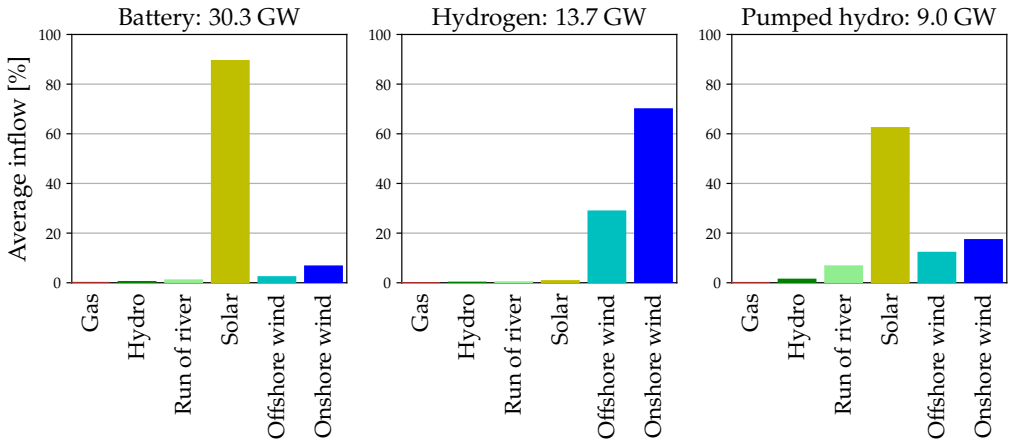

Figure 5.2: Average hourly inflow per storage technology decomposed into the six generation technologies. The total average inflow is denoted in the title.

The right panel of Figure 5.1 displays the distribution of the optimised nominal power for storage technologies G_n^α in Equation (5.4). This corresponds to the ability of the storage facilities to balance hourly fluctuations in electricity production and demand. The total energy capacity can be calculated from Equation (5.4). Scaling the nominal power with $h_{\max}^\alpha$ shows that the energy capacity is largest for hydrogen storage followed by battery storage and last pumped hydro storage.

The spatial distribution of the generation and storage capacities proposes that the short term battery storage is paired with solar generation capacity to balance the strong diurnal pattern of solar power generation, whereas the long term hydrogen storage is associated with wind power generation capacity to balance weekly and seasonal weather patterns.

This intuition is confirmed by tracing the composition of power inflow for the charging of the different storage technologies. Figure 5.2 shows aggregated average hourly inflows $\langle \sum_{n,m} s_n^{\beta,-}(m,\alpha) \rangle$ for the three storage technologies for each of the six generation technologies. Corresponding with the spatial distribution shown in Figure 5.1, hydrogen storage is mainly utilised for wind power generation, whereas battery storage mostly receives inflow from solar power generation. The pumped hydro storage capacities are fixed to today's layout, leading to a mixed utilisation of different generation technologies, but dominated by solar.

Tracing the power flow originating from generation and storage technologies

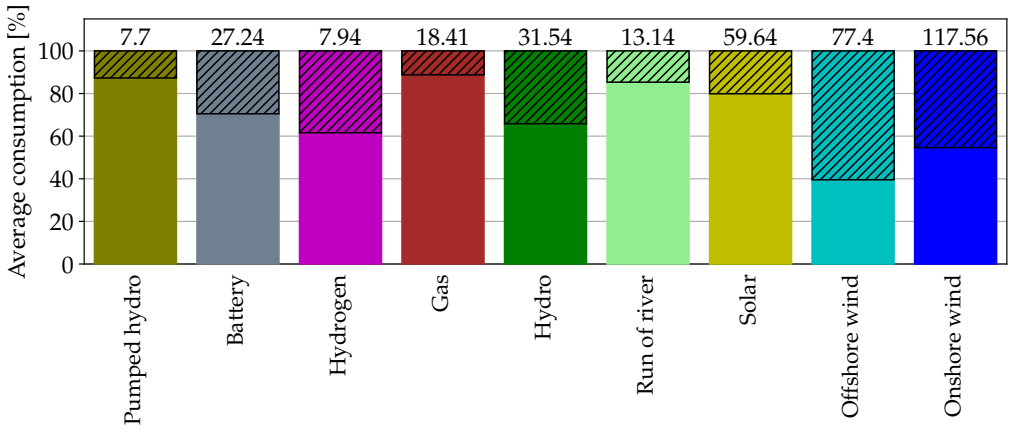

Figure 5.3: Average local vs. non-local consumption per technology split between the source node and externally (shaded area). The absolute average consumption for each technology is written in GW above each bar.

allows to assess how locally this power is consumed. Figure 5.3 shows how much of the average generation or storage discharging is consumed inside the same node, or alternatively is transmitted as a power flow over the network for consumption in another node (shaded area). Using the expressions in Equation (5.15) and Equation (5.16) this can be expressed as $\langle \delta_{n,m} d_n(m,\alpha) \rangle$ and $\langle \sum_{m \neq n} d_n(m,\alpha) \rangle$, respectively. The absolute average consumption associated with each generation or storage discharge is noted in GW above each bar. Note that due to the efficiencies in Equation (5.3) the total storage discharging is lower than the total storage charging as given in Figure 5.2.

We observe that pumped hydro discharging, gas and run of river power generation is predominantly consumed locally (87%, 89% and 85%, respectively). While the placement of pumped hydro and run-of-river capacities is not optimised in the system, the cost structure of open cycle gas turbines (low capital costs, high marginal costs) proposes that this technology is locally deployed for peak demand covering when other flexibility options are not cost optimal. Solar and hydro power generation are also mostly consumed locally (80% and 66%, respectively), since they represent the predominant local generation capacities when they are installed in a node. Nevertheless, for battery and hydrogen storage the 30% to 38% of non-local usage show that the system uses these storage technologies as a system-wide backup. Wind power generation is consumed locally up to 55% (onshore) and 40% (offshore), but due to its massive deployment in the system it is also to a comparatively higher share transmitted

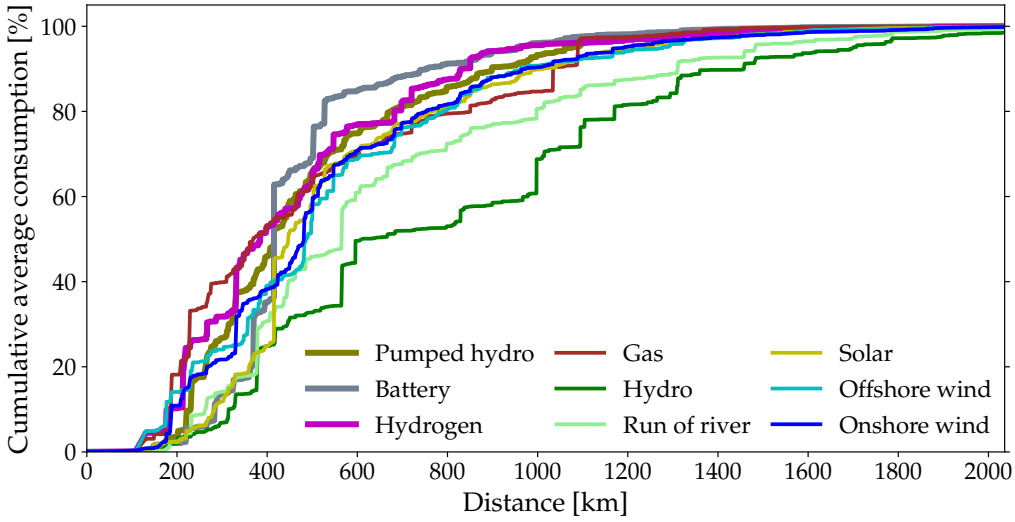

Figure 5.4: Cumulative average consumption as a function of distance. Only exported power is included hence the starting point at zero. The lines in this figure correspond to the shaded areas in Figure 5.3.

over the network for consumption at other nodes. These results also reflect the spatial distribution of renewable generation resources for wind and solar power PV: whereas favourable wind power conditions occur in general only distant from load centres, solar PV is less locationally sensitive within each country and can be built close to the loads. Note that for simplicity we do not use the ability to inter-temporarily trace power flow through the storage and discard the information of the original source of the storage outflow.

Figure 5.4 shows the cumulative average consumption per technology as a function of the spatial distance between the exporting and consuming node. The figure is cut off at 2036km at which point all technologies have reached 99%. For reference, the largest distance between two nodes in the network is 3455km. The lines in this figure correspond to the shaded areas in Figure 5.3. The three storage technologies (highlighted with thicker lines) have a tendency to be consumed more locally than the generation technologies. Most of the generation and storage technologies follow a similar pattern, except reservoir hydro, and, to a lesser extent, run of river, which are both being exported over large distances in the network. The results in this figure emphasize the importance of transmission capacity for the system. Although the power from most generation and storage technologies on average is consumed predominantly locally, in case of exports it

is often distributed over wide parts of the system.

5.5 DISCUSSION & CONCLUSIONS

In this article we have extended the application of flow tracing to power flows associated with charging and discharging of storage capacities in a low-carbon scenario of a future European electricity system first presented in [30]. Using this tracing approach we are able to determine the composition of storage inflow with respect to the different generation technologies present in the system. We observe that short-term battery storage is predominantly used by solar power generation, whereas longer-term hydrogen storage is almost completely charged with power from onshore and offshore wind power generation. This flow-based result quantitatively confirms the intuition gained from the spatial distribution of generation and storage capacities. Bearing in mind the limits of the spatial resolution of 64 nodes for the European electricity system we furthermore determine how much of power generation or storage outflow is consumed in the same node or alternatively distributed over the transmission network to loads at other nodes in the system. It is shown that storage outflow is mostly consumed locally inside the same node. This is similar for the usage of hydro or solar PV power generation, with the local usage even more pronounced for power from open cycle gas turbines. In contrast, power generation from onshore wind is less locally consumed, and offshore wind power is predominantly exported to other nodes in the network. Whereas these findings propose an interpretation of a generally more local usage of storage technologies, the analysis of the exported power flows show that these often stretch across large parts of the system. For all generation and storage technologies around 20% of the average exported power flow is consumed at nodes which are more than 1000 km away from the location of network inflow. Our flow-based analysis thus suggests a local-but-global usage of storage capacities – whereas on average these capacities are deployed locally, if needed their flexibility is used also by distant nodes connected through sufficient transmission capacities of the power grid.

The study presented in this contribution calls for an extension in several directions. Increasing the spatial resolution of the system representation and considering different levels of transmission expansion allows a more detailed investigation of the local-but-global usage of storage capacities in a low-carbon European electricity system. Analysing the time-series of corresponding flow patterns will further shed light on the system conditions which correspond to either a local or global impact of different generation and storage technologies.

Combining this information with a flow-based nodal cost allocation mechanism could inspire new economic contract concepts for future electricity markets with a high share of renewable generation. Equally important, by revealing the details of the system benefit of power transmission, the flow-based system analysis as advocated in the presented analysis is a valuable contribution in the context of public discussions on transmission expansion.

6

Real-Time Carbon Accounting Method for the European Electricity Markets

This chapter has been submitted as "Real-time carbon accounting method for the European electricity markets" by Bo Tranberg, Olivier Corradi, Bruno Lajoie, Thomas Gibon, Iain Staffell and Gorm Bruun Andresen to Energy Strategy Reviews [4].

6.1 INTRODUCTION

For several decades, more than 80% of the global electricity generation originates from fossil fuel [17]. As a result, electricity and heat production account for 25% of global greenhouse gas (GHG) emissions [18]. Furthermore, electricity demand is widely expected to rise because of electrification of vehicles [107]. These facts highlight the importance of an accurate and transparent carbon emission accounting system for electricity.

Reducing emissions related to electricity consumption requires accurate measurements readily available to consumers, regulators and investors [108]. In the GHG protocol [109], "Scope 2 denotes the point-of-generation emissions from purchased electricity (or other forms of energy)" [108]. A major challenge regarding Scope 2 emissions is the fact that it is not possible to trace electricity from a specific generator to a specific consumer [110, 111]. This has lead to the use of two different accounting methods: the of *grid average* emission factors or the *market based* method [108, 111]. Grid average factors are averaged over time and therefore not specific to the time of consumption due to limited availability of emission factors with high temporal resolution. The market based method entails purchasing contractual emission factors in the form of different types of certificates, which do not affect the amount of renewable electricity being

generated, and therefore fail to provide accurate information in GHG reports. For a detailed criticism of both approaches, see [108].

In this case study, we propose a new method for real-time carbon accounting based on flow tracing techniques. This method is applied to hourly market data for 28 areas within Europe. We use this method to introduce a new consumption-based accounting method that represents the underlying physics of the electricity system in contrast to the traditional input-output models of carbon accounting [112–114]. The approach advances beyond [103], where a similar flow tracing methodology is used to create a consumption-based carbon allocation between six Chinese regions. However, the data for that study was limited to annual aggregates and different generation technologies were also aggregated. We apply the method to real-time system data, including the possibility of distinguishing between different generation technologies, providing real-time signals for all actors involved. This increases the overall transparency and credibility of emission accounting related to electricity consumption, which is of high importance [115]. To investigate the impact of the new consumption-based accounting method we compare it with the straightforward production-based method (i.e. looking at the real-time generation mix within each area). For discussions on the shift from production-based to consumption-based accounting and the idea of sharing the responsibility between producer and consumer, we refer to [116, 117].

6.2 METHODS

6.2.1 Data

The method is applied to data from the electricityMap database [118], which collects real-time data from electricity generation and imports/exports around the world. The European dataset, consisting of 28 areas, is used with hourly resolution for the year 2017. Data sources for each individual area can be found on the project's webpage [119]. Figure 6.1 shows the 28 areas and the 47 interconnectors considered. Power flows to and from neighboring areas, e.g. Switzerland, are included when available. The black arrows show a snapshot of hourly power flows between the areas. In the results, we aggregate the two price areas of Denmark and, thus, compare 27 countries.

The top panel of Figure 6.2 shows stacked daily-average production for each technology for Austria. The bottom panel shows daily-average exports and imports. The black line represents the sum of the hourly exports and imports

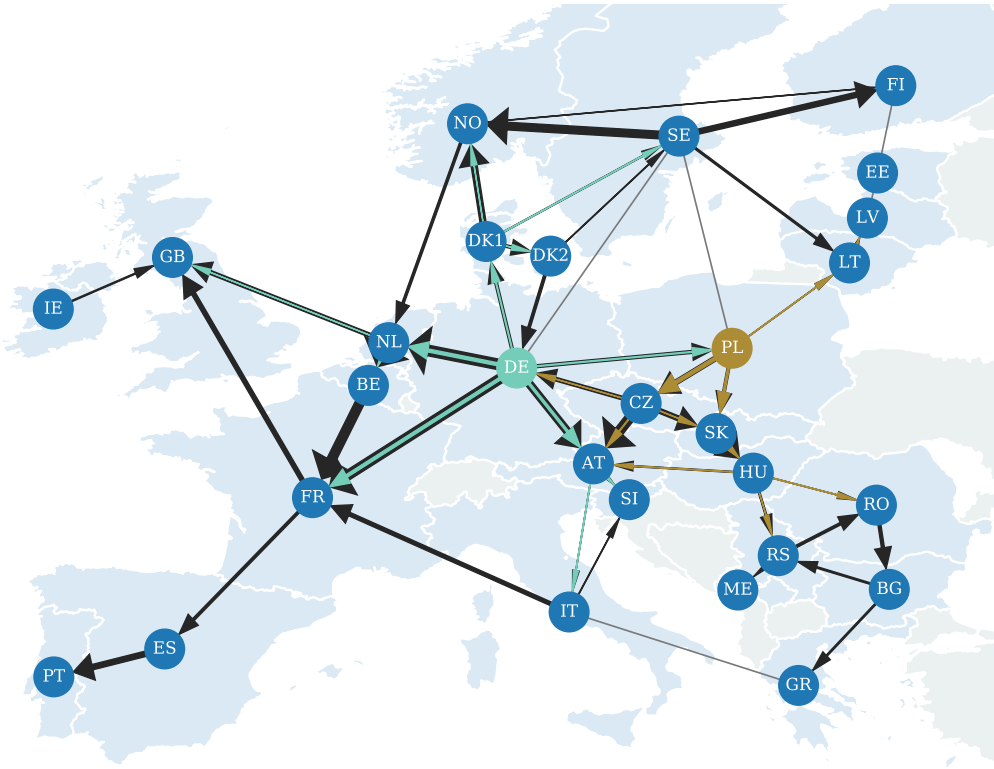

Figure 6.1: The 28 areas considered in this case study, and the power flows between them for the first hour of January 1, 2017. The width of the arrows is proportional to the magnitude of the flow on each line. Power flows to and from neighboring countries, e.g. Switzerland, are included when available, and these areas are shown in gray. The cascade of power flows from German wind and Polish coal are highlighted with blue and brown arrows, respectively.

showing Austria's net import/export position. The daily averages in this figure are based on the full 8760 hours in the dataset representing the full year 2017.

Carbon emission intensities are derived from the ecoinvent 3.4 database to construct an accurate average intensity per generation technology per country decomposed in lifecycle, infrastructure and operations [120]. The operations intensities are used for the production and consumption-based carbon allocation in this study. Operational emissions include all emissions occurring over the fuel chain (from extraction to supply at plant) as well as direct emissions on site. For fossil fuels, operational emissions are therefore higher than only direct combustion emissions. For solar, geothermal and wind, the emissions are strictly

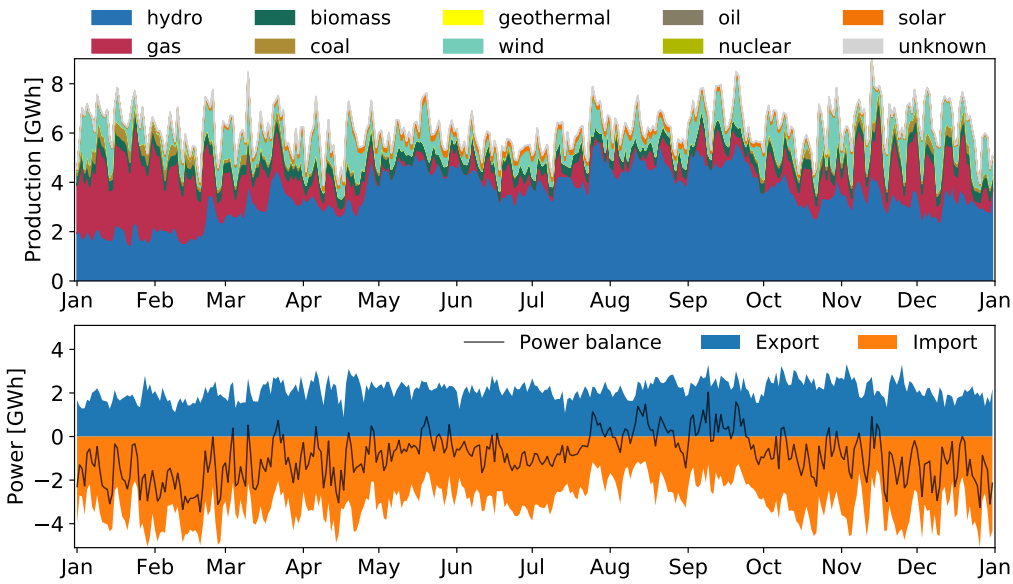

Figure 6.2: Daily-average stacked power production for each technology for Austria during 2017 (top) as well as exports, imports and power balance (bottom).

from maintenance operations.

The operations intensity per technology averaged over all countries is summarized in Table 6.1. The dashed line indicates the split between non-fossil and fossil technologies. For details on country-specific values, see Table 1–3 in the supplementary material.

6.2.2 Carbon emission allocation

The consumption-based accounting method proposed in this case study builds on flow tracing techniques. Flow tracing was originally introduced as a method for transmission loss allocation and grid usage fees [40, 41]. It follows power flows on the transmission network mapping the paths between the location of generation and the location of consumption. It works in such a way that each technology for each country is assigned a unique color mathematically. This is a mathematical abstraction since it is not physically possible to color power flows. For each hour local production and imported flows are assumed to mix evenly at each node in the transmission network (see Figure 6.1) and determine the color mix of the power serving the demand and the exported flows. As an example, the colored arrows in Figure 6.1 show the cascade of power flows resulting from

Table 6.1: CO_2 equivalent operation intensity per technology averaged across countries. The dashed line indicates the split between non-fossil and fossil technologies. For details, see Table 1–3 in the supplementary material.

Technology	Intensity [$kgCO_2eq/MWh$]
solar	0.00410
geothermal	0.00664
wind	0.141
nuclear	10.3
hydro	16.2
biomass	50.9
gas	583
unknown	927
oil	1033
coal	1167

flow tracing of German wind power (light blue) and Polish coal power (brown) for the first hour of January 1st, 2017. The size of the colored arrows shows how much of the total power flow (in black) is accounted for. A threshold has been applied such that the technology specific flows are only shown if they account for at least 2% of the total power flow for each interconnector.

Flow tracing has been proposed as the method for flow allocation in the Inter-Transmission System Operator Compensation mechanism for transit flows [51,53]. Recently, the method has been applied to various aspects of power system models to allocate transmission network usage [6, 43], a generalization that allows associating power flows on the grid to specific regions or generation technologies [46], creating a flow-based nodal levelized cost of electricity [2], and analyzing the usage of different storage technologies [3].

The challenge of cross-border power flows in relation to carbon emission accounting has previously been studied in [103,110]. Both studies simplify nodes as being either net importers or net exporters and neither are able to distinguish between different generation technologies. Those simplifications are not necessary in our approach as we can deal with both imports, exports, consumption and generation simultaneously at every node while also distinguishing between different generation technologies. Additionally, Figure 6.1 exhibits loop flows. However, these do not affect the validity of the flow tracing methodology [103], and no effort has been made to eliminate them as they occur naturally in the transmission system at the area level [121].

Flow tracing methods are almost unanimously applied to simulation data – typically with high shares of renewable energy. In this case study, we apply the flow tracing method to hourly time series from the electricityMap [119]. From this we are able to map the power flows between exporting and importing countries for each type of generation technology for every hour of the time series. Applying country-specific average carbon emission intensity per generation technology to this mapping, we construct a consumption-based carbon accounting method. For details on the mathematical definitions, see Section B in the supplementary material.

The production-based accounting method used for comparison, is calculated as the carbon intensity from local generation within each country.

6.3 RESULTS

Figure 6.3 shows a comparison of average production and consumption intensity as a function of the share of non-fossil generation in each country's generation mix. The consumption intensity is calculated using flow tracing. The size of the circles is proportional to the average hourly generation and consumption in MWh, respectively. A vertical gray line connects the production and consumption intensity corresponding to the same country. We see a decline in intensity with increasing share of non-fossil generation. For high shares of non-fossil generation, the consumption intensity tends to be higher than the production intensity due to imports from countries with higher production intensity. The pattern is reversed for low shares of non-fossil generation. The values plotted in this figure are shown in Table 4 in the supplementary material.

Some countries exhibit a huge difference between production and consumption intensity. An example of this is Slovakia (SK), which has a high share of nuclear power and Austria (AT), which has a high share of hydro power, but both rely heavily on imports of large amounts of coal power especially from Poland (PL) and Czech Republic (CZ). Denmark (DK) is an extreme example of the opposite case, having a high share of coal and gas power and importing large amounts of hydro and nuclear power from Norway (NO) and Sweden (SE).

While this figure only shows average values, Figure 7 in the supplementary material highlights the interval of hourly variation of production and consumption intensity per country. This interval is high for all countries except the ones with very high non-fossil share (FR, SE, NO).

From a national perspective, it is important to know the source electricity that is

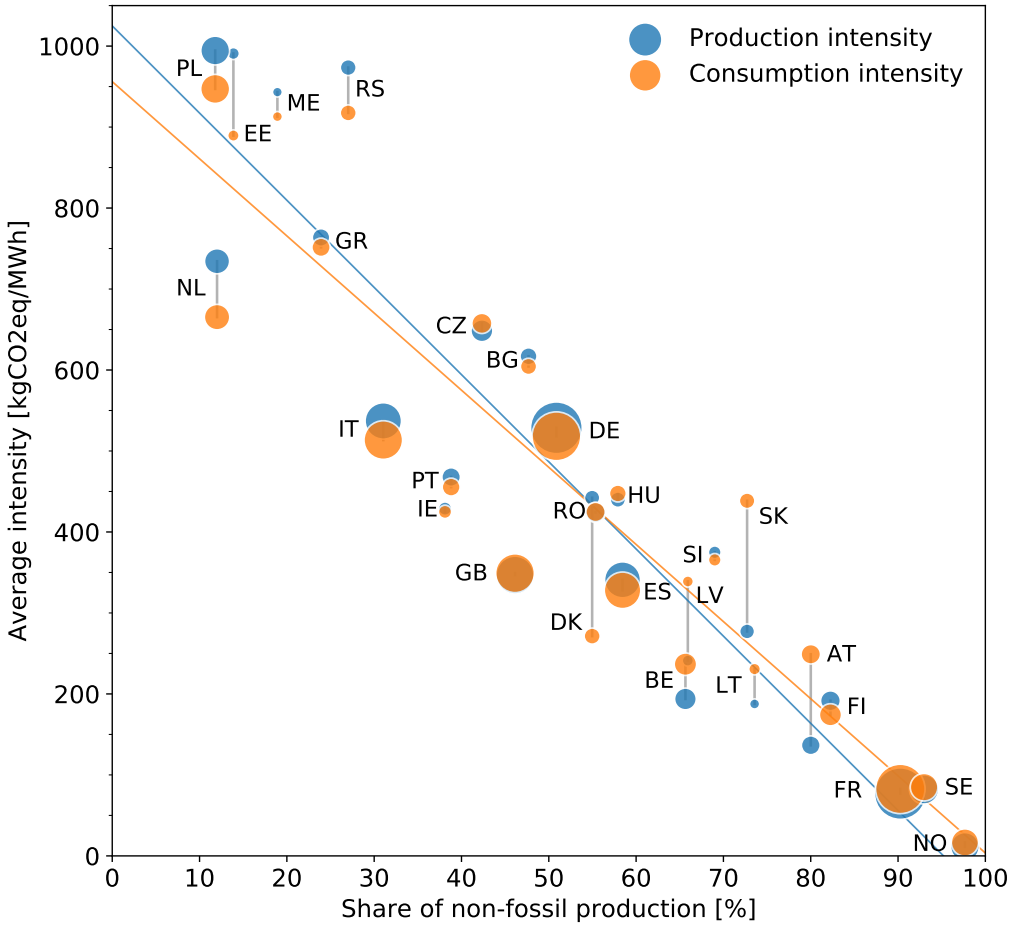

Figure 6.3: Comparison of average hourly production and consumption intensity as a function of the share of non-fossil generation in the country's generation mix. Size of circles are proportional to mean generation and mean consumption for each country.

being imported, and whether it increases a country's reliance on high-carbon, insecure, or otherwise undesirable sources of generation.

Figure 6.4 shows the consumption-based intensity per country. The height of each bar corresponds to the consumption intensity for each country shown in Figure 6.3. This figure decomposes the consumption intensity for each country and shows how much of a particular country's consumption intensity is caused by the local generation mix compared with the generation mix of imported

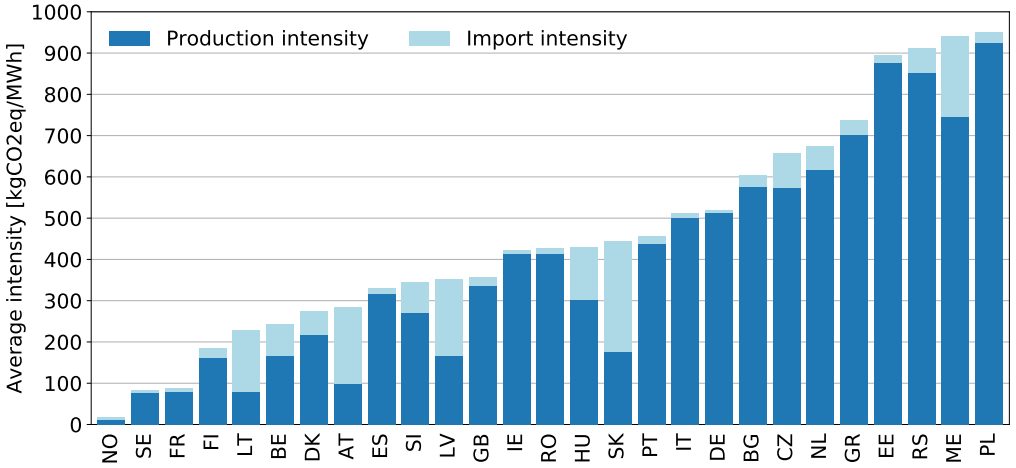

Figure 6.4: Average hourly consumption intensity per consumed MWh per country (stacked bar) split in contributions from local generation and imports. The countries are sorted by average consumption intensity.

power. We see that for many countries it is important to be able to distinguish between local generation and imports since the imports make a substantial contribution to the country's consumption-based emission. In cases with a large difference between the intensity of local power production and the imported power, imports have a high impact. As mentioned in an earlier example, this is the case for both Austria and Slovakia. For details on the average intensity of imports and exports between the countries, see Figure 9 and Table 5 in the supplementary material.

6.4 CONCLUSION

In this study we have introduced a new method for consumption-based carbon emission allocation based on flow tracing applied to a historical sample of real-time system data from the electricityMap.

With this method we have found substantial differences between production and consumption intensities for each country considered, which follow a trend proportional to the share of non-fossil generation technologies.

The difference between production and consumption intensities and the associated impact of imports on average consumption intensity emphasize the importance of including cross-border flows for increased transparency regarding

carbon emission accounting of electricity. While there are limitations to the accuracy of this method due to data availability and the approximation of flow tracing, we believe that this method provides the first step in a new direction for carbon emission accounting of electricity.

This case study focuses on the European electricity system. When additional sources of live system data become available this approach could be extended to cover a wider geographical area or a higher spatial resolution. Another interesting application of this method would be to include additional sectors such as heating, since these are coupled through technologies like heat pumps, resistive heaters, and power plants with cogeneration. This could lead to real-time carbon emission signals for the entire energy system.

Part II

Managing wind risk

7

Introduction

7.1 MOTIVATION

For more than a decade, the installed capacity of wind power has been increasing rapidly [122], with expectations of continued future increases [123]. See Figure 7.1 for historical and expected capacities for EU. In 2017, the total EU capacity reached 168.7 GW of which 15.6 GW was installed in 2017. The country shares of new wind capacity installed in 2017 is shown in Figure 7.2.

Price setting in the day-ahead (spot) electricity market is based on matching bids of supply and demand. For an introduction to price setting in electricity markets with nodal as well as zonal pricing, see [124]. The supply curves are constructed according to increasing marginal prices, the so-called merit order principle. The marginal cost of production are close to zero for wind power resulting in wind power constituting the left-most part of the supply curve. Wind is a variable natural phenomenon hence wind power production is variable. In situations of high (low) wind production, the supply curve is shifted to the right (left) leading to low (high) market clearing prices. This negative dependence has been found in several studies [125–128]. The variable nature of wind power production combined with this negative dependence is referred to as wind risk and is strengthened by the fact that electricity in contrast to traditional commodities cannot (yet) be stored in large quantities over long periods of time and, thus, must be consumed simultaneously with production.

I consider the perspective of a energy trading company entering into long-term power purchase agreements (PPAs), in which fluctuating wind power is bought from a producer at a fixed price. The increasing wind power capacity in turn increases the effect of wind on the electricity price in the day-ahead market. This is of high importance for energy trading companies in relation to pricing, hedging, and risk management of PPAs.

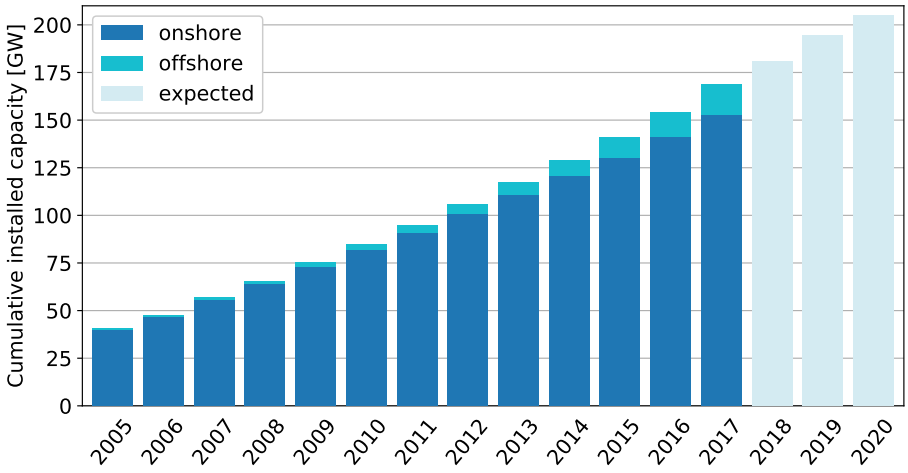

Figure 7.1: Cumulative installations onshore and offshore in the EU [122]. Expected future capacities from [123].

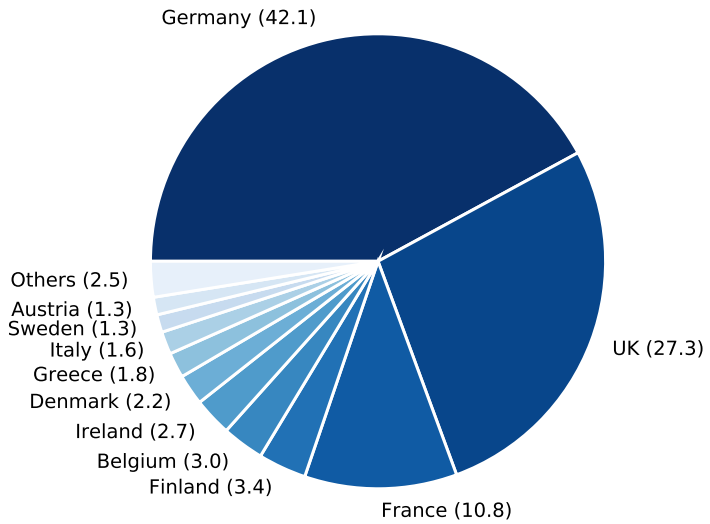

Figure 7.2: EU country shares of new wind capacity installed during 2017 [122]. Numbers in parentheses indicate percentages. The total capacity is 15.6 GW.

The main research questions regarding risk management of long-term PPAs are:

1. What is the financial risk associated with a long-term PPA?
2. What is the appropriate method of modeling this risk?
3. To what extent can the risk be mitigated using a hedge?

In the following, I decompose the general wind risk into price risk and volumetric risk. These risks are assessed by a joint model of wind power production and electricity spot prices using copulas, with the goal of improving risk management of long-term PPAs for energy trading companies.

7.2 METHODS

The methodology is split in two parts. First, I perform model selection and parameter estimation. Second, I apply the model to risk management of long-term PPAs.

The area of interest is the West Denmark price area (DK1). I use publicly available data on hourly wind power production and electricity spot price, as well as daily installed wind power capacity. The data exhibits a strong negative correlation between wind production and spot price. Because of this, I use copulas to create a joint model of the two variables, which is able to model the correlation.

A copula is a multivariate cumulative distribution function (CDF) whose univariate marginal distributions are all uniform [129]. In this case, the marginals are the wind power production and electricity spot price, which I seek to model jointly. I need to uniformly transform the marginals to use copulas to model the dependence between them. An example is shown in Figure 7.3. The left panel shows the joint distribution of two Gaussian random variables (the marginals) with a correlation of -0.5. Applying the probability integral transform (PIT) to each marginal variable result in the uniform variables u_1 and u_2 with joint distribution shown in the right panel. The procedure is then to fit a copula to this joint distribution, jointly simulate the two univariate variables from the fitted copula and lastly inverse transform them to the distribution of the original variables Z_1 and Z_2. This is the principle of the joint model of wind power production and electricity spot price in the following chapter.

Copulas are sensitive to the fits of the marginal models. I use an ARMA-GARCH model for the wind marginal, which includes terms describing autoregression,

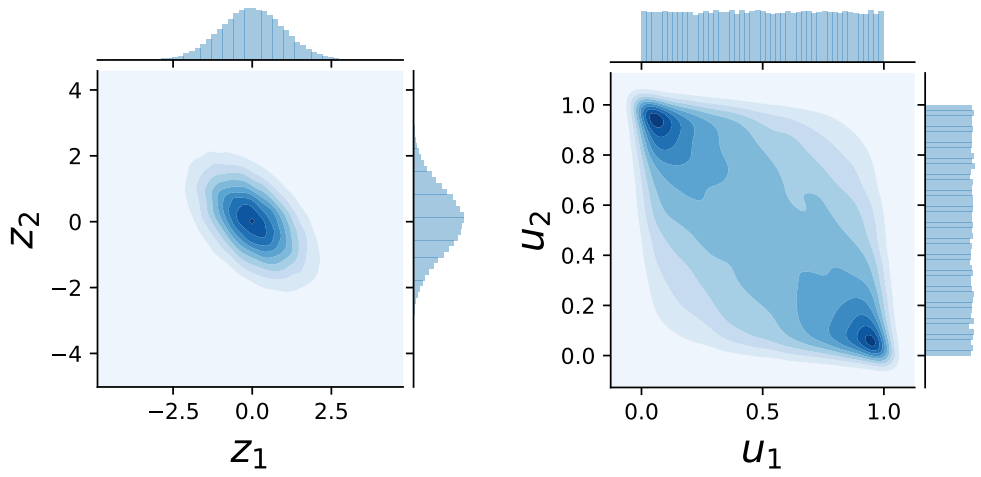

Figure 7.3: Joint distribution of two Gaussian random variables with a negative correlation of -0.5 (left). Joint distribution of the probability integral transforms of Z_1 and Z_2 (right).

moving average and stochastic volatility of a stationary time series. This choice is in accordance with [130]. The electricity spot price exhibits both long memory and a non-negligible number of extreme values. Hence, I propose using a score-driven model, specifically multiple-components models, which are able to handle long memory and are more robust to extreme events compared to ARMA-GARCH models.

The joint model for wind power production and electricity spot price is used to simulate profits of long-term power purchase agreements. From these simulations, I estimate the profit distribution and Value-at-Risk (VaR) as well as determine the fair price of the contract and the optimal hedging volume. When a hedge volume H^* is performed, the profit of a PPA during a time interval from t_1 to t_2 is given by

$$\pi^H = \sum_{t=t_1}^{t_2} Q_t \left(S_t - (F - c)\right) + H^* \left(F - \bar{S}\right), \tag{7.1}$$

where Q_t is the hourly wind power production, S_t is the hourly electricity spot price, F is the forward price, and c is the price of correlation risk. The latter two constitute the fair contract price

$$R = F - c, \tag{7.2}$$

which is offered to the owner of the wind farm. The price of correlation risk is calculated as

$$c = F - \frac{\mathbb{E}_{t_0}^{\mathbb{Q}}\left(\sum_{t=t_1}^{t_2} Q_t S_t\right)}{\mathbb{E}_{t_0}^{\mathbb{Q}}\left(\sum_{t=t_1}^{t_2} Q_t\right)}, \tag{7.3}$$

where the latter term is the wind-weighted spot price.

7.3 MAIN FINDINGS

The findings are based on benchmarks against a previously published model using constant and time-varying copulas with ARMA-GARCH marginals [130].

In the benchmark, I find that using a score-driven model as marginal model for the spot price is superior to marginal models of the ARMA-GARCH type.

When the dependence between wind power production and electricity spot price is ignored the VaR is underestimated by 7.7%, which shows the importance of using copulas to model the dependence structure.

I confirm the results in [130] that time-varying copulas outperform constant copulas, since the negative dependence between wind power production and electricity spot price is observed to vary with time.

The best-performing model is found to be a time-varying Gaussian copula with an ARMA(3,1)-GARCH(1,1) for the wind power production marginal and a two-component score-driven model for the electricity spot price marginal. In the benchmark, this model results in lower VaR and most importantly higher accuracy in predicting the VaR. The improvement of predictive accuracy is found to be statistically significant.

8

Managing volumetric risk of long-term power purchase agreements

This chapter has been submitted as "Managing Volumetric Risk of Long-term Power Purchase Agreements" by Bo Tranberg, Rasmus Thrane Hansen and Leopoldo Catania to Energy Economics [5].

8.1 INTRODUCTION

The last decade has seen a huge increase in renewable power generation capacity all over the world. In this period the installed capacity has doubled in Denmark which is the focus of this study. In 2016 wind power alone accounted for 44.4% of the total power generation in Denmark, with all renewable sources combined reaching 52% [131]. In the same year 33.4% of the electricity consumption in the ENTSO-E area[1] was covered by renewable generation of which wind power accounted for 12.2 percentage points [131]. These numbers are set to increase over the coming decades as the [14] has set a target to reduce CO_2 emissions by 80-95% in 2050 compared to 1990 levels.

The increasing share of variable, non-dispatchable renewable power generation is a structural change to the electricity system and markets compared with the traditional thermal power sources where production can be planned if necessary.

In a study of the German electricity market [125] found that the spot price decreases with increasing shares of wind and solar power. This was named the merit order effect as these technologies have very low marginal costs leading to a shift of the supply curve, which, in combination with the demand for electricity being inelastic in the short-run, causes lower average spot prices. The same effect

[1] Currently covering 36 countries: `https://www.entsoe.eu/about/inside-entsoe/members/`.

has been found for Germany [126], Denmark [127], and California [128]. This is evidence of a negative dependence between wind power generation and power spot price.

Another study of the German electricity market found that variable wind power not only decreases the wholesale electricity price but also increases its volatility [132]. A robust result that holds for various specifications of GARCH models. A similar effect was found for the Australian electricity market in [133].

A particular feature of electricity markets is the occurrence of negative prices. A new phenomenon, which started in 2009 on the Nord Pool exchange [134]. Negative prices might occur in periods of high supply from non-dispatchable renewable sources combined with low demand, which pose a substantial challenge in energy risk management [134].

The variable nature of renewable power generation exposes investors to two forms of risk: price risk in the spot market and volumetric risk in the produced power. Both of these risks were assessed using a joint model of wind power production and power spot price in [130] using copulas to model the negative dependence. Copulas are a flexible tool for describing dependence between a number of random variables while allowing for arbitrary marginal models. Copulas have been widely applied to financial time series [135]. Recent applications of copulas in relation to electricity markets include modeling dark/spark spreads [136] and forecasting portfolio Value-at-Risk (VaR) [137].

The importance of hedging for risk management under joint price and volumetric risk in the electricity market has been studied for the demand-side in [138–140]. Recently, similar challenges for the production side have been studied based on copula models in [130, 141].

In this study we follow the approach of [130] using time–varying copulas to create a joint model of the wind power production and power spot price for the western Denmark price area (DK1). Copula estimation is sensitive to the fit of the marginal models [142]. We show that the spot price time series exhibits both long memory and a non-negligible number of extreme values. This argues against using a simple ARMA-GARCH marginal model as in [130]. Instead, we propose to use score-driven models, in particular multiple-components models [143, 144], which are able to handle long memory and are more robust to extreme events compared to ARMA-GARCH models [144, 145].

We present a simulation study with applications to risk management of long-term power purchase agreements (PPAs) for wind power production in DK1. In

such a contract a buyer guarantees a fixed price per unit of energy produced regardless of the price in the market at time of production and the volume produced. This means the buyer takes on both price and volumetric risk from the owner of the power generating asset. We use the model of [130] as benchmark. Performance of the models is measured by the resulting profit and VaR as well as a statistical test of the ability to predict the VaR, which is fundamental for traders and financial institutions when designing portfolio risk management strategies [146].

This paper is structured as follows: Section 8.2 introduces the methods used for estimating marginal models and combining these with copulas to create a joint model. In Section 8.3 we estimate and compare models for the western Denmark price area. Section 8.4 presents a simulation study with applications to risk management in which we compare the performance of the introduced score-driven model with a previously published model. In Section 8.5 we conclude on this study.

8.2 MODELING FRAMEWORK

We use copulas to model the dependence between power spot prices and wind power production and thereby creating a joint forecast. Copulas are a flexible tool for studying the dependence between random variables and have been proved useful in many fields of research like finance, economics, and engineering, see [147] for a textbook treatment of copulas. Let $\mathcal{F}_{i,t} = \sigma(Y_{i,s}, s \leq t)$ be the filtration generated by the stochastic process $\{Y_{i,t}\}$ up to time t, for $i \in \{1,2\}$ where $i = 1$ and $i = 2$ are referred to the power spot price and wind power production series, respectively. Let $h(y_{1,t}, y_{2,t}|\mathcal{F}_{t-1})$ be the joint density function of $(Y_{1,t}, Y_{2,t})$ conditional on $\mathcal{F}_{t-1} = \{\mathcal{F}_{1,t-1}, \mathcal{F}_{2,t-1}\}$. By exploiting the [148]'s theorem and its extension to conditional copulas discussed in [149], we factorize the joint density as:

$$h(y_{1,t}, y_{2,t}|\mathcal{F}_{t-1}) = c_t(u_{1,t}, u_{2,t}|\mathcal{F}_{t-1}) p_{1,t}(y_{1,t}|\mathcal{F}_{1,t-1}) p_{2,t}(y_{2,t}|\mathcal{F}_{2,t-1}), \tag{8.1}$$

where $u_{i,t} = P_{i,t}(y_{i,t}|\mathcal{F}_{i,t-1})$ is the probability integral transform (PIT) of $y_{i,t}$ according to its cumulative distribution $P_{i,t}(y_{i,t}|\mathcal{F}_{i,t-1}) = \int_{-\infty}^{y_{i,t}} p_{i,t}(x|\mathcal{F}_{i,t-1})dx$.[2] From now on we assume that $p_{i,t}(\cdot|\mathcal{F}_{i,t-1}) = p_i(\cdot|\mathcal{F}_{i,t-1}; f_{i,t}, \psi_i)$ where $f_{i,t}$ is a set of time–varying $\mathcal{F}_{i,t-1}$–measurable parameters describing the dynamic features of $Y_{i,t}$, and ψ_i is a set of constant parameters for $i = 1, 2$. Similarly, we

[2]Note that we have assumed that $p_{i,t}(y_{i,t}|\mathcal{F}_{t-1}) = p_{i,t}(y_{i,t}|\mathcal{F}_{i,t-1})$.

assume that $c_t(\cdot,\cdot|\mathcal{F}_{t-1}) = c(\cdot,\cdot|\mathcal{F}_{t-1}; f_{c,t}, \psi_c)$, where $f_{c,t}$ is a set of time–varying $\mathcal{F}_{t-1}$–measurable parameters describing the dependence between $Y_{1,t}$ and $Y_{2,t}$, given $\mathcal{F}_{t-1}$ and ψ_c is a set of constant copula parameters. Note that, in this paper we might use the following notation to improve readability $p_i(y_{i,t}|\mathcal{F}_{i,t-1})$ instead of $p_i(y_{i,t}|\mathcal{F}_{i,t-1}; f_{i,t}, \psi_i)$ for $i = 1, 2$, and similarly $c(u_{1,t}, u_{2,t}|\mathcal{F}_{t-1})$ instead of $c(u_{1,t}, u_{2,t}|\mathcal{F}_{t-1}; f_{c,t}, \psi_c)$.

8.2.1 Time-varying parameters

We now detail how we model the time–varying parameters $f_{1,t}$, $f_{2,t}$, and $f_{c,t}$. Within the time series literature the ARMA-GARCH framework has been widely employed to model time variation in the conditional mean and variance. Specifically, in the ARMA(p,q)-GARCH(l,m) model we set $f_{i,t} = (\mu_{i,t}, \sigma^2_{i,t})$, where $\mu_{i,t} = E[Y_{i,t}|\mathcal{F}_{i,t-1}]$ and $\sigma^2_{i,t} = Var[Y_{i,t}|\mathcal{F}_{i,t-1}]$ and specify:

$$\mu_{i,t} = \zeta + \sum_{r=1}^{p} \phi_r y_{t-r} + \sum_{j=1}^{q} \theta_j \varepsilon_{t-j}$$

$$\sigma^2_{i,t} = \omega + \sum_{i=1}^{l} \alpha_i \varepsilon^2_{t-i} + \sum_{g=1}^{m} \beta_g \sigma^2_{t-g},$$

where $\varepsilon_{i,t} = y_{i,t} - \mu_{i,t}$ and ζ, ω, ϕ_r, θ_j, α_i, β_g for $r = 1, \ldots, p$, $j = 1, \ldots, q$, $i = 1, \ldots, l$, and $g = 1, \ldots, m$ need to be estimated by numerical maximization of the likelihood function subject to constraints that ensure the weekly stationarity of the process and positivity of the conditional variance at each point in time. The ARMA-GARCH framework is widely used in time series analysis due to its easy estimation and interpretation. However, we note two important features that characterize the behaviour of $\mu_{i,t}$ and $\sigma^2_{i,t}$: i) $\mu_{i,t}$ responds linearly to the past observations $y_{i,t-s}, s > 0$, and ii) $\sigma^2_{i,t}$ responds quadratically to past residuals $\varepsilon_{i,t-s}, s > 0$. It follows that, whenever $|y_{i,t}|$ is "big" the response of $\mu_{i,t}$ and $\sigma^2_{i,t}$ is "large". This feature, which is intrinsic in the ARMA–GARCH framework, can have dramatic impacts in the filtering procedure of $\mu_{i,t}$ and $\sigma^2_{i,t}$ as well as in the estimation of the model parameters, see for example [150], [151], and [152]. We also note that energy time series, like the spot price of wind, usually exhibits a large number of observations that can be considered outliers according to a reference Gaussian distribution (so called "spikes") as for example reported in Figure 8.2. It is thus of great importance to model energy time series relying on a modeling framework which is robust to these events. It is also worth to be mentioned that the ARMA-GARCH modeling framework does not offer any

guidance to the modeling of $f_{c,t}$, i.e. the time–varying copula parameters. In this paper we model the joint dynamics of the spot price and the wind production using a different modeling framework recently developed by [153] and [144] called score-driven framework. The ARMA-GARCH model is then used as a benchmark.

Score-driven modeling framework

Score-driven models differ from ARMA-GARCH models in the way observations drive the time variation in the dynamic parameters. Indeed, the goal of this class of models is to take into account the whole shape of the conditional distribution of the data in order to update the time–varying parameters of the model. For instance, if the conditional distribution of the data is fat-tailed, we expect that an extreme observation (a spike) should not affect the conditional mean and conditional variance too much, since extreme observations are likely to be observed from such a distribution. Score-driven models naturally introduce this mechanism by exploiting the information contained in the score of the conditional distribution of the data to update a set of time–varying parameters. Furthermore, this modeling framework is general in the sense that it can be used to induce time variation in any parameter of the conditional distribution, and not only in the conditional mean and variance. For instance, in our case we can model the marginal parameters, $f_{1,t}$ and $f_{2,t}$, as well as the copula parameter $f_{c,t}$, using the same methodology. Indeed, let $f_t \in \Omega \subset \Re^d$ be a generic vector of time–varying parameters, and let $\tilde{f}_t \in \Re^d$ be a reparameterized version of f_t, such that $f_t = \Lambda(\tilde{f}_t)$ for a $\mathcal{F}_{t-1}$ measurable mapping function $\Lambda : \Re^d \to \Omega$. For example, if $f_t = f_{i,t}$ and $f_{i,t} = (\mu_{i,t}, \sigma_{i,t})$ then $\Omega = \Re \times \Re_+$ and $d = 2$ such that Λ can be set to:

$$\Lambda(\tilde{f}_{i,t}) : \begin{cases} \tilde{\mu}_{i,t} & = \mu_{i,t} \\ \exp(\tilde{\sigma}_{i,t}) & = \sigma_{i,t} \end{cases},$$

where $\tilde{f}_{i,t} = (\tilde{\mu}_{i,t}, \tilde{\sigma}_{i,t})$. The updating equation for $f_{i,t}$ is then defined as:

$$
\begin{aligned}
f_{i,t+1} &= \Lambda(\tilde{f}_{i,t+1}) \\
\tilde{f}_{i,t+1} &= \kappa_i + A_i s_{i,t} + B_i \tilde{f}_{i,t} \\
s_{i,t} &= S_i\left(\tilde{f}_{i,t}\right) \nabla_i\left(y_{i,t}, \tilde{f}_{i,t}\right) \\
\nabla_i\left(y_{i,t}, \tilde{f}_{i,t}\right) &= \frac{\partial \log p_i\left(y_{i,t} \mid \mathcal{F}_{i,t}\right)}{\partial \tilde{f}_{i,t}},
\end{aligned}
\tag{8.2}
$$

where κ_i is a 2–dimensional vector of intercepts, $A_i = diag(\alpha_{i,1}, \alpha_{i,2})$ and $B_i = diag(\beta_{i,1}, \beta_{i,2})$ are two 2×2 diagonal matrices collecting parameters that control for the evolution of $\tilde{f}_{i,t}$. In equation Equation (8.2) the forcing variable of $\tilde{f}_{i,t}$ is defined as the product of two quantities: $\nabla_i\left(y_{i,t}, \tilde{f}_{i,t}\right)$ and $S_i\left(\tilde{f}_{i,t}\right)$ representing the score of the conditional distribution with respect to $\tilde{f}_{i,t}$ evaluated in $y_{i,t}$ and a 2×2 positive defined scaling matrix, respectively. Following [153] we set $S_i\left(\tilde{f}_{i,t}\right) = \mathcal{I}(\tilde{f}_{i,t})^{-c}$, where $\mathcal{I}(\tilde{f}_{i,t}) = E[\nabla_i\left(y_{i,t}, \tilde{f}_{i,t}\right) \nabla_i\left(y_{i,t}, \tilde{f}_{i,t}\right)' | \mathcal{F}_{i,t-1}]$ is the Fisher information matrix of $\tilde{f}_{i,t}$ and $c \in \{0, 1/2, 1\}$ is a parameter chosen by the econometrician.[3] We denote $c = 0$ as identity scaling, $c = 1/2$ as inverse square root scaling and $c = 1$ as inverse scaling.

The updating equation Equation (8.2) can be modified to include additional lags of $\tilde{f}_{i,t}$ and $s_{i,t}$ as well as to introduce other dynamic features such as long memory for some of the model parameters as detailed in [154] and [143]. We follow this latter approach and introduce long memory via a set of K auxiliary processes as follows:

$$
\begin{aligned}
\tilde{f}_{i,t+1} &= \kappa_i + \sum_{k=1}^{K} \tilde{f}^{\dagger}_{i,k,t+1} \\
\tilde{f}^{\dagger}_{i,k,t+1} &= A_{i,k} s_{i,t} + B_{i,k} \tilde{f}^{\dagger}_{i,k,t},
\end{aligned}
$$

where $A_{i,k}$ and $B_{i,k}$ are diagonal matrices to be estimated for all $k = 1, \ldots, K$, and K is selected using information criteria, see [154] and [143] for additional details.

In the case of f_t being a copula parameter $f_t = f_{c,t}$, say the correlation parameter of a Gaussian copula, the updating equation remains the same and the score is evaluated according to the copula density with respect to the reparametrized copula parameter $\tilde{f}_{c,t}$:

[3] The choice of c can be based on BIC. We choose $c = 0$ even though BIC chooses $c = 1/2$ since $c = 1/2$ resulted in exploding forecasts. Further analysis about the implications of the scaling mechanism for this class of models are considered for future research.

$$\nabla_i \left(u_{1,t}, u_{2,t}, \tilde{f}_{c,t} \right) = \frac{\partial \log c(u_{1,t}, u_{2,t} | \mathcal{F}_{t-1})}{\partial \tilde{f}_{c,t}}.$$

Score-driven models are also called Dynamic Conditional Score (DCS) in [144] and Generalized Autoregressive Score (GAS) in [153]. In this paper we follow the latter nomenclature and define the model reported in equation Equation (8.2) GAS(1,1), while its extension with multiple component as "multiple component GAS(1,1)".

8.2.2 Distributional assumptions

Having specified the updating equation driving the dynamic parameters we close the model's specification by defining the parametric formulation of $p_i(\cdot|\mathcal{F}_{i,t-1})$ for $i = 1, 2$ and $c(\cdot, \cdot|\mathcal{F}_{t-1})$. In our empirical analysis we consider several distributional assumptions for the marginal and copula specifications. Regarding the marginals specification we consider the Gaussian and Student's t distributions as well as their skewed version constructed according to the [155] methodology. We also consider the asymmetric Student's t with asymmetric tail decays introduced by [156] in order to capture the possible different behavior in the left and right tail of the spot price's distribution. Regarding the copula specification, we consider four parametric copulas namely the Gaussian copula, the Student's t copula, the Clayton copula and the Gumbel copula. The Gaussian and Student's t copula are both symmetric but the latter exhibits tail dependence. The Clayton copula and the Gumbel copula are asymmetric and exhibit lower and upper tail dependence, respectively. The characteristics are summarized in Table 8.1. Expressions for the score and the information matrices of the copulas here considered are reported in Appendix B.

Copula	Parameter	Ind.	Pos./Neg. Dep.	ρ_S	ρ_τ	λ_l	λ_u	MoM
Gaussian	$\rho \in (-1,1)$	$\rho = 0$	Yes	$\frac{6}{\pi} \arcsin \frac{\rho}{2}$	$\frac{2}{\pi} \arcsin \rho$	0	0	$\hat{\rho}$
Student's t	$\rho \in (-1,1)$ $\nu \in (2,\infty)$	$\rho = 0$ $\nu = \infty$	Yes	n.a.	$\frac{2}{\pi} \arcsin \rho$	$g(\rho,\nu) = 2t_{\nu+1}\left(-\sqrt{\frac{(\nu+1)(1-\rho)}{1+\rho}}\right)$	$g(\rho,\nu)$	$\hat{\rho}$ n.a.
Gumbel	$\theta \in (1,\infty)$	$\theta = 1$	Positive	n.a.	$\frac{\theta-1}{\theta}$	0	$2 - 2^{1/\theta}$	$(1-\hat{\rho}_\tau)^{-1}$
Clayton	$\theta \in (0,\infty)$	$\theta = 0$	Positive	n.a.	$\frac{\theta}{\theta+2}$	$2^{-1/\theta}$	0	$2\hat{\rho}_\tau / (1-\hat{\rho}_\tau)$

Table 8.1: Copula characteristics for the copulas used in the application. Adapted from [157].

8.2.3 Model estimation and selection

We estimate model parameters by the two steps maximum-likelihood (ML) estimation for conditional copulas detailed in [149]. Specifically, let $\theta_i = (\psi_i, \kappa_i, A_{i,k}, B_{i,k}, k = 1, \dots, K)$ for $i = 1, 2$ and $\theta_c = (\psi_c, \kappa_c, A_c, B_c)$ be vectors of static marginals and copula parameters. Assuming to observe a sequence of T observations for the spot price and wind production collected in the vector $y_{1:T}$, the joint likelihood can be written as:

$$\begin{aligned}\mathcal{L}(\theta|y_{1:T}) &= \sum_{t=1}^{T} \log h_t\left(y_{1,t}, y_{2,t}; \theta\right) \\ &= \sum_{t=1}^{T}\sum_{i=1}^{2} \log p_i(y_{i,t}|\mathcal{F}_{i,t-1}; f_{i,t}(\theta_i)) + \\ &\quad \sum_{t=1}^{T} \log c(u_{1,t}, u_{2,t}|\mathcal{F}_{t-1}; f_{c,t}(\theta_c)),\end{aligned}$$

where $\theta = (\theta_1, \theta_2, \theta_c)$ and we have emphasized that $f_{c,t}$ and $f_{i,t}$ depend from θ_c and θ_i, for $i = 1, 2$, respectively. In copula estimation it is common to split the estimation procedure in two steps, the so-called Inference For Margins (IFM) procedure, see e.g. [158]. In IFM the marginal distributions are estimated and then the copula is fitted to the PIT. This two steps estimation procedure leads to an efficiency loss when compared to standard maximum likelihood, however, it greatly simplifies the estimation procedure, see [149]. Our estimation step is thus composed of three parts:

$$\begin{aligned}\hat{\theta}_i &= \arg\max_{\theta_i} \sum_{t=1}^{T} \log p_i(y_{i,t}|\mathcal{F}_{i,t-1}; f_{i,t}(\theta_i)), \quad i = 1, 2, \\ \hat{\theta}_c &= \arg\max_{\theta_c} \sum_{t=1}^{T} \log c(\hat{u}_{1,t}, \hat{u}_{2,t}|\mathcal{F}_{t-1}; f_{c,t}(\theta_c)),\end{aligned}$$

where $\hat{u}_{i,t} = P_i(y_{i,t}|\mathcal{F}_{i,t-1}; f_{i,t}(\hat{\theta}_i))$. It should be noted that copula estimation is sensitive to the fit of the marginal models [142]. When the IFM approach is used the standard errors obtained by inverting the Hessian does not account for the variance from the estimation of the marginal models and therefore the estimated standard errors are too small relative to the correct ones [157]. The stationary bootstrap of [159] can be used to obtain more reliable standard errors [157].

In this study we use an in-sample and out-of-sample (OOS) comparison of the copula fits. The in-sample comparison based on the method of [160]. This test allows for both nested and non-nested models and additionally it allows for both marginal models to be misspecified. The test can also be used to compare constant and time–varying copulas [130]. The null hypothesis is equal performance of the competing copula models:

$$H_0 := \mathbb{E}\left(L_{1t}\left(\theta_{1t}\right) - L_{2t}\left(\theta_{2t}\right)\right) = 0, \tag{8.3}$$

where L_{1t} and L_{2t} are the likelihood of the two competing models. The null is tested against the alternative of one of the model fits being superior i.e.:

$$H_A := \mathbb{E}\left(L_{1t}\left(\theta_{1t}\right) - L_{1t}\left(\theta_{2t}\right)\right) \neq 0, \tag{8.4}$$

where the sign of $\mathbb{E}\left(L_{1t}\left(\theta_{1t}\right) - L_{1t}\left(\theta_{2t}\right)\right)$ determines the preferred model. [160] show that under H_0 a simple t-statistic on the difference between the sample averages of the log-likelihood is asymptotically standard normal [157]:

$$\frac{\sqrt{T}\left(\bar{L}^1 - \bar{L}^2\right)}{\hat{\sigma}} \xrightarrow{d} N\left(0,1\right) \tag{8.5}$$

where $\bar{L}^i = \frac{1}{T}\sum_{t=1}^{T} L_{it}\left(\theta_{it}\right)$ is the sample average of the log-likelihood and $\hat{\sigma}^2$ is a consistent estimator of the variance of $\sqrt{T}\left(\bar{L}^1 - \bar{L}^2\right)$. We follow [157] and use the HAC-estimator for $\hat{\sigma}^2$. We note that when the marginal models are the same for the competing models, we only need to consider the copula log-likelihoods.

When considering OOS comparison, the data is divided into an in-sample period of length ($R < T$) and an OOS period of length $T - R$. The OOS comparison test of [161] is based on a comparison of the log-likelihood of the OOS forecasts. It requires that a rolling window of fixed size is used to reestimate the model for each forecast. Specifically the estimated joint distribution model is used to compute the log-likelihood of the OOS data. The null, alternative hypothesis, and the test-statistic are equivalent to the in-sample comparison of [160] and as before only the copula likelihood is required when the marginal models are kept fixed. Additionally, the limiting distribution is also standard normal [130].

A preliminary analysis in this study comparing the performance of the GAS(1,1) model with the multi components model found the multiple components model to be superior for the marginal distributions, hence in this paper we limit the discussion of modeling marginal distributions to the multiple components model and use the ARMA-GARCH model from [130] as benchmark. The GAS(1,1) model is used to model time–varying dependence between the marginals.

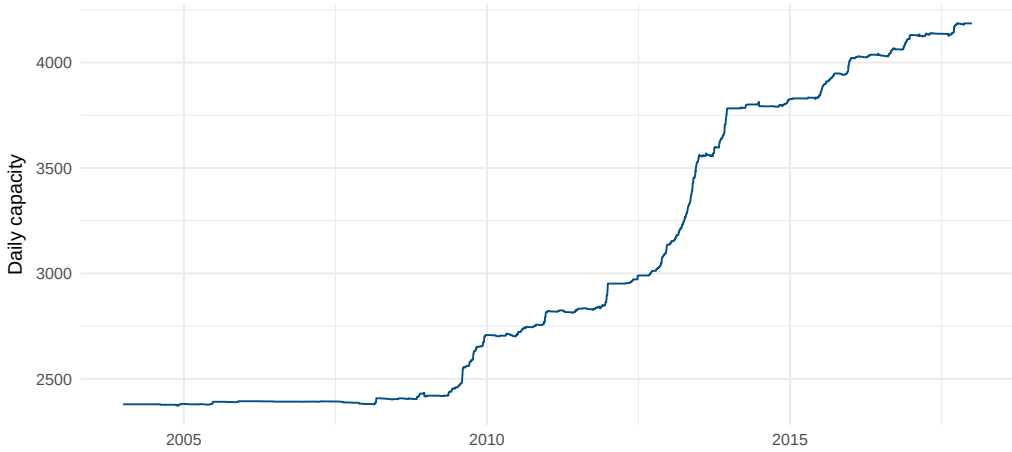

Figure 8.1: Daily installed capacity in MW in DK1. Data is publicly available from the Danish Energy Agency: https://ens.dk/service/statistik-data-noegletal-og-kort.

8.3 MODELING POWER SPOT PRICE AND WIND POWER PRODUCTION

The high share of wind generation in Denmark of 44.4% of total power generation [131] together with the rapidly increasing installed capacity (see Figure 8.1) emphasizes the importance of risk management regarding long-term PPAs for wind production. Studying the DK1 area can provide future guidance for other price areas as wind power capacity is expected to grow in all of Europe to reduce CO2 emission [14, 123].

8.3.1 Data

In this study we consider the Western Denmark pricing zone (DK1). The analysis is based on historical data for daily averaged wind production and spot price as well as the daily installed capacity.[4] The dataset is from January 1st 2004 to December 31st 2017. It is split into in-sample (2004-2015) and out-of-sample (2016-2017).

The daily averaged load factor is shown in the top panel of Figure 8.2 and is

[4] All data is publicly available at `https://www.energidataservice.dk`, `https://www.nordpoolgroup.com` and `https://ens.dk/service/statistik-data-noegletal-og-kort`, respectively.

calculated as:

$$L = \frac{\text{Total daily power production [MWh]}}{\text{Daily installed capacity [MWh]} \cdot 24}. \tag{8.6}$$

The daily install capacity is shown in Figure 8.1 and shows a steep increase since 2009. The load factor is a relative measure in the interval [0, 1]. This is problematic when fitting a marginal model to the data as we need to constrain the fitted values. We therefore apply a logit transformation to the load factor such that the transformed load factor takes values on the entire real line, allowing the marginal model to be unrestricted. The transformed load factor is given by:

$$\tilde{L} = \log\left(\frac{1}{L^{-1} - 1}\right) \tag{8.7}$$

The spot price series is shown in the bottom panel of Figure 8.2. The plot indicates that the average spot price has changed over the sample. If we assume that prices are realizations of some stochastic process, it would be reasonable to believe that the location and possibly the scale parameter are time–varying. This justifies the use of the ARMA-GARCH model in [130] and the score-driven model used in this study. We note that extreme observations of both positive and negative signs are observed over the sample, which might harm the fit of a ARMA-GARCH model, and is the main argument for considering a score-driven marginal model [151].

It is worth noting that the spot price can be negative. Negative prices are not usually observed for commodities but since electricity cannot be stored on a large scale the price setting works different than in other markets. Negative prices can arise when wind power production is very high, while at the same time it is difficult to export energy to other price areas [134]. It might be difficult to understand why producers do not turn of wind power production when they are paying customers for buying the produced energy. One of the reasons is that wind power production is subsidized and therefore producers can make a positive profit when prices are negative.

There is a negative dependence between the wind power production and prices due to the low marginal cost of wind power production [125–128]. Table 8.2 presents different measures of correlation between the transformed load factor and the spot price. As expected the two series are negatively dependent i.e. scenarios of high prices and low wind power production and vice versa are more likely than the opposite.[5]

[5]We note that the logit transformation does not affect this dependence as Kendall's tau and Spearman's rho are invariant to strictly increasing transformations.

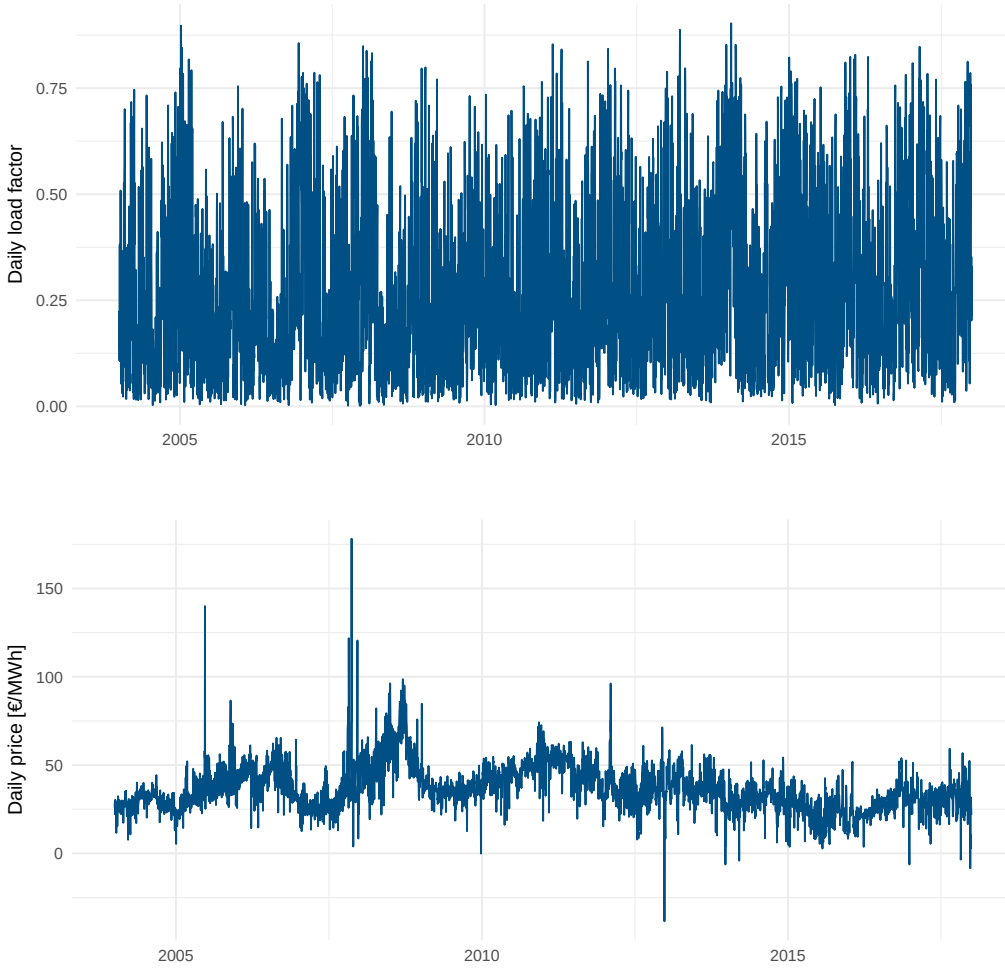

Figure 8.2: Daily averaged load factor and spot price from 2004 to 2017.

To investigate how the dependence has changed over time we compute rolling Spearman's rho with a window size of 60 days and confidence intervals obtained by *i.i.d.*. bootstrap shown in Figure 8.3. The figure suggests that the dependence between the two series is time–varying and therefore we expect a time–varying copula to outperform the constant copulas. Comparing Figure 8.3 with Figure 8.1 it seems that the negative dependence between wind power production and spot price has grown stronger with the steeply increasing generation capacity since 2009.

	Kendalls τ	Spearmans ρ	Linear correlation
Correlation	-0.25	-0.37	-0.35
Sd	0.03	0.04	0.04

Table 8.2: Measures of dependence. Standard errors are obtained by $B = 1000$ bootstraps using the stationary block bootstrap of [159].

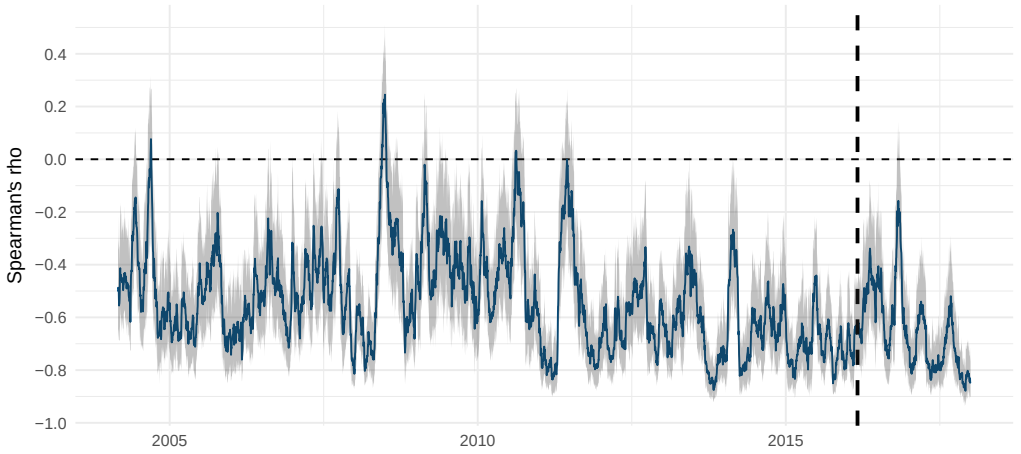

Figure 8.3: 60-days rolling Spearman's rho for the transformed load factor and spot price with 95% confidence interval. The confidence interval has been smoothed using an EWMA with $\lambda = 0.95$. The vertical dashed line separates the in-sample and out-of-sample period.

We divide the data into an in-sample period and an out-of-sample period. The last $H = 731$ observations covering the period from 1/1/2016 to 12/31/2017 are considered as out-of-sample and used for evaluation of the OOS forecasts. This is in line with [130] where two years of OOS data is used.

We use a dataset of forward prices for the DK1 price area[6] to evaluate the performance of the estimated models. Forwards are only available for the overall system area supplemented by CFDs[7] between the system area and each pricing zone, hence we construct synthetic forward prices for the DK1 by combining the system forward price and the CFD price for each day, delivery code and

[6] Available at `https://www.nordpoolgroup.com`.

[7] A CFD on Nord Pool is named Electricity Price Area Difference (EPAD).

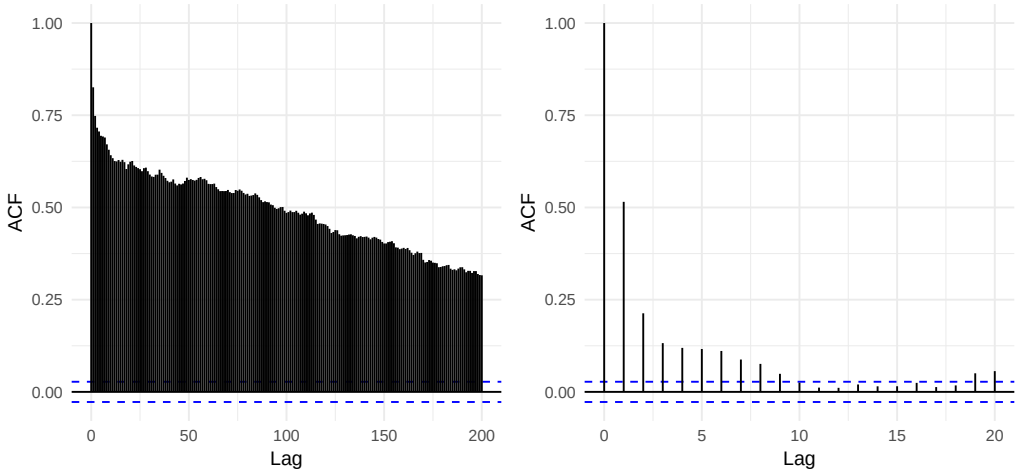

Figure 8.4: ACF of the deseasonalized spot price (left) and the deseasonalized transformed load factor (right).

load profile. The load profile can either be base or peak whether the seller of the forward agrees to deliver the agreed quantity each hour of the day or only in the peak hours (8am-8pm). We consider only monthly forwards and base load. The dataset consists of data from 7/1/2007-12/29/2017 and therefore it does not cover the whole in-sample data as CFDs were not available for the DK1 area before the 7/1/2007. However, as the forward data is only used to evaluate the OOS performance of the models it does not cause any problems.

8.3.2 Marginal model for wind power production

The stylized facts for the transformed load factor and spot price series are filtered by demeaning followed by deseasonalizing by linear regression. For the transformed load factor we consider month-in-year as dummy variable and for the price series we consider both month-in-year and day-in-week.

Having deseasonalized the data we plot the autocorrelation function (ACF) in Figure 8.4 for visual inspection before deciding on an appropriate marginal model for each series. The ACF of the transformed load factor decays fast and therefore the use of an ARMA-GARCH model seems appropriate.

The slowly decaying autocorrelation function for spot prices might be caused by a unit root or long memory [144]. In order to ensure that the series does not exhibit a unit root we employ the augmented Dickey-Fuller test [162]. This test

results in $DF = -4.97$ with p-value < 0.01 and therefore a rejection of the null hypothesis of a unit root, hence there is evidence that the price series exhibits long memory since the ACF decays in a hyperbolic way. Due to long memory of the spot price time series, the choice of an ARMA-GARCH model is not obvious as it is probably better described by a long memory type model e.g. a multiple components model or a fractionally integrated model.

As marginal model for the transformed load factor we follow [130] and consider an ARMA(p,q)-GARCH(l,m) model. The plot of the transformed load factor shown in Figure 8.2 and the ACF in Figure 8.4 justify the use of an ARMA-GARCH model as we observe no extreme observations, a time–varying variance and an exponential decaying ACF. We consider a range of different specification of p,q,l and m and a set of different error distributions. Specifically we consider $p,q \in \{0,1,\ldots,7\}$, $l,m \in \{1,2\}$ and for the error distributions we examine: Normal, Skew Normal, Student's t, Skew Student's t, Generalized Error and skewed Generalized Error. To choose among the different specifications we use the Bayesian Information Criterion (BIC). We find the preferred model to be ARMA$(2,2)$-GARCH$(1,1)$ with a Skew Normal as error distribution. The estimated parameters are shown in Table 8.3. This differs from [130], where an ARMA(1,3)-GARCH(1,1) Skew Generalized Error distribution is found to be best. We find close to zero difference between the two model specifications in terms of BIC and therefore we do not expect this to influence the conclusions.

	Estimate	Std. Error	t value	Pr(> |t|)
ϕ_1	1.2755	0.0145	87.8671	< 0.0001
ϕ_2	-0.2893	0.0143	-20.2614	< 0.0001
θ_1	-0.7587	0.0012	-642.1598	< 0.0001
θ_2	-0.1926	0.0023	-83.5237	< 0.0001
ω	0.0217	0.0034	6.4514	< 0.0001
α_1	0.0093	0.0029	3.2385	0.0012
β_1	0.9713	0.0013	763.2778	< 0.0001
Skewness	0.7911	0.0201	39.4182	< 0.0001

Table 8.3: Parameter estimates of ARMA$(2,2)$-GARCH$(1,1)$ model for daily wind power production series with Skew Normal as conditional distribution.

8.3.3 Marginal model for power spot price

We estimate the multiple components model for various numbers of components $(K = 2,3,4)$ on the in-sample deseasonalized spot price series. We consider

time–varying location and scale. Specifically: identity, inverse and inverse square root scaling mixed with different conditional distributions. Specifically the following conditional distributions have been considered: Normal, Skew Normal, Student's t, Skew Student's t, Asymmetric Student's t with two tail decay parameters and Asymmetric Student's t with one tail decay parameter. We also investigate whether the additional flexibility of the multiple components model makes the changing scale unnecessary. Considering only a time–varying location has the advantage of reducing the number of estimated parameters and therefore it might give a better penalized likelihood criterion. Therefore we consider both the multiple components model with only time–varying location and the multiple components model where we have both time–varying location and scale. The total number of models considered adds up to $2 \cdot 3 \cdot 18 = 108$. We find that the Normal distribution fails to handle the fat tails of the empirical distribution properly. The results show that according to BIC the inclusion of a time–varying scale is valuable for all conditional distributions. We find that the best model according to the selection process is a two-components model with Student's t distribution as conditional distribution and identity scaling. The estimated parameters for the two-components model are shown in Table 8.4.

	Estimate	Std. Error	t value	Pr($>\|$t$\|$)
κ_1	-10.6901	3.1828	-3.3587	0.0004
κ_2	3.0836	0.0534	57.7909	< 0.0001
κ_3	-2.9607	0.2024	-14.6297	< 0.0001
α_{11}	4.7486	0.4508	10.5335	< 0.0001
α_{21}	0.0888	0.0200	4.4519	< 0.0001
α_{12}	7.9605	0.6098	13.0544	< 0.0001
α_{22}	0.3772	0.0441	8.5623	< 0.0001
β_{11}	0.9988	0.0009	1157.0327	< 0.0001
β_{21}	0.9654	0.0109	88.3452	< 0.0001
β_{12}	0.4843	0.0592	8.1760	< 0.0001
β_{22}	0.2327	0.0952	2.4449	0.0072

Table 8.4: Parameter estimates of two-components model with Student's t as conditional distribution and scalingtype identity for daily spot price series.

Additionally, we estimate the ARMA$(3,1)$-GARCH$(1,1)$ model with a Skew Student's t distribution from [130] and use it as a benchmark for the multiple components model. The estimated parameters are seen in Table 8.5. We note that there are no larger deviations between the estimated parameters in Table 8.5

and [130]. This is not surprising considering the large sample sizes used in both estimations. We do also note that the estimated values for the ARMA(3,1) model indicate that the model is at the borderline between stationarity and non-stationarity. We find the root of the lag polynomial to be ≈ 1.005 and hence the model is close to non-stationarity [163]. However, we note that when considering the ACF of the residuals we see almost no autocorrelation indicating a good model fit, which is also found in [130].

	Estimate	Std. Error	t value	Pr(> |t|)
ϕ_1	1.4377	0.0043	337.3660	< 0.0001
ϕ_2	-0.5074	0.0113	-44.8908	< 0.0001
ϕ_3	0.0665	0.0176	3.7836	0.0002
θ_1	-0.8543	0.0075	-114.0857	< 0.0001
ω	2.4342	0.5106	4.7677	< 0.0001
α_1	0.1520	0.0213	7.1341	< 0.0001
β_1	0.7882	0.0289	27.2284	< 0.0001
Skewness	0.9633	0.0194	49.6600	< 0.0001
Shape	5.1558	0.3689	13.9773	< 0.0001

Table 8.5: Parameter estimates of the ARMA$(3,1)$-GARCH$(1,1)$ model from [130] with Skew Student's t as conditional distribution.

8.3.4 Goodness-of-fit test for marginal models

To investigate the fit of the two-components model and the ARMA-GARCH model we perform the test of the probability integral transform (PIT) used in [164]. Under correct model specification the PIT should be *i.i.d.* $U(0,1)$. The validity of this is assessed through a graphical test which provides information on where possible misspecifications occur. [130] assess the model fit through the Kolmogorov–Smirnov (KS) and the Cramér–von Mises (CvM) goodness-of-fit tests. The drawback of the KS and CvM tests is that if we reject the null hypothesis of the PIT being *i.i.d.* $U(0,1)$ using these tests, we have no guidance on which part of the distribution is wrongly specified. Therefore we prefer the approach of [164] where two graphical tools are used. Namely one for the test of $u_{it} \sim U(0,1)$ i.e. the uniformness of the PIT and one for the independence assumption. The uniformity is assessed through simple histograms with the confidence intervals from the $U(0,1)$ null distribution. The independence assumption is assessed through correlograms and a more formal test where the dependence between the PIT is assessed through a simple

regression [164]. To reveal whether a possible dependence arises from the conditional first, second, third or forth moments we plot the correlogram of $(\hat{u}_{i,t} - \bar{\hat{u}}_i)$, $(\hat{u}_{i,t} - \bar{\hat{u}}_i)^2$, $(\hat{u}_{i,t} - \bar{\hat{u}}_i)^3$, $(\hat{u}_{i,t} - \bar{\hat{u}}_i)^4$, where $\hat{u}_{i,t}$ is the estimated PIT and $\bar{\hat{u}}_i$ is the average PIT.

The density plots of the PIT are seen in Figure 8.5. In general the plots indicate that the PITs are $U(0,1)$ of both marginal models for spot prices. We see some deviations in the $0.75 - 0.85$ percentile indicating that too many observations lie in this area compared to the $U(0,1)$ distribution. But as the models are qualitatively the same, this does not provide a case to differ between them. The PIT from the ARMA-GARCH model fitted to the transformed load factor seems to be $U(0,1)$ according to Figure 8.5.

In general we find that all moments of the PIT for both marginal models for the spot price are correlated cf. Figure 8.6 and Figure 8.7. We notice that for both models the autocorrelation is high at lag 7 and 14 indicating that the deseasonalization of the data has not been done properly. However, we do not address this issue further in this study. For the transformed load factor the PIT seems to be *i.i.d.*. cf. Figure 8.8.

A more formal test of the *i.i.d.*. assumption is done by running the regression:

$$(\hat{u}_{i,t} - \bar{\hat{u}}_i)^k = \zeta + \sum_{n=1}^{20} \gamma_n \left(\hat{u}_{i,t-n} - \bar{\hat{u}}_i\right)^k + \xi_t \tag{8.8}$$

and testing for the joint significance of the coefficients $\gamma_1, \ldots, \gamma_{20}$. We consider demeaned PITs up to fourth power i.e. $k = 1, \ldots, 4$. The results indicate that both marginal models for spot prices fail to capture the dynamics for all four moments of the PIT as we reject the null of independence for all powers. Considering the PIT obtained from the marginal model for the transformed load factor we cannot reject the PIT being *i.i.d.*. at a 1% level.

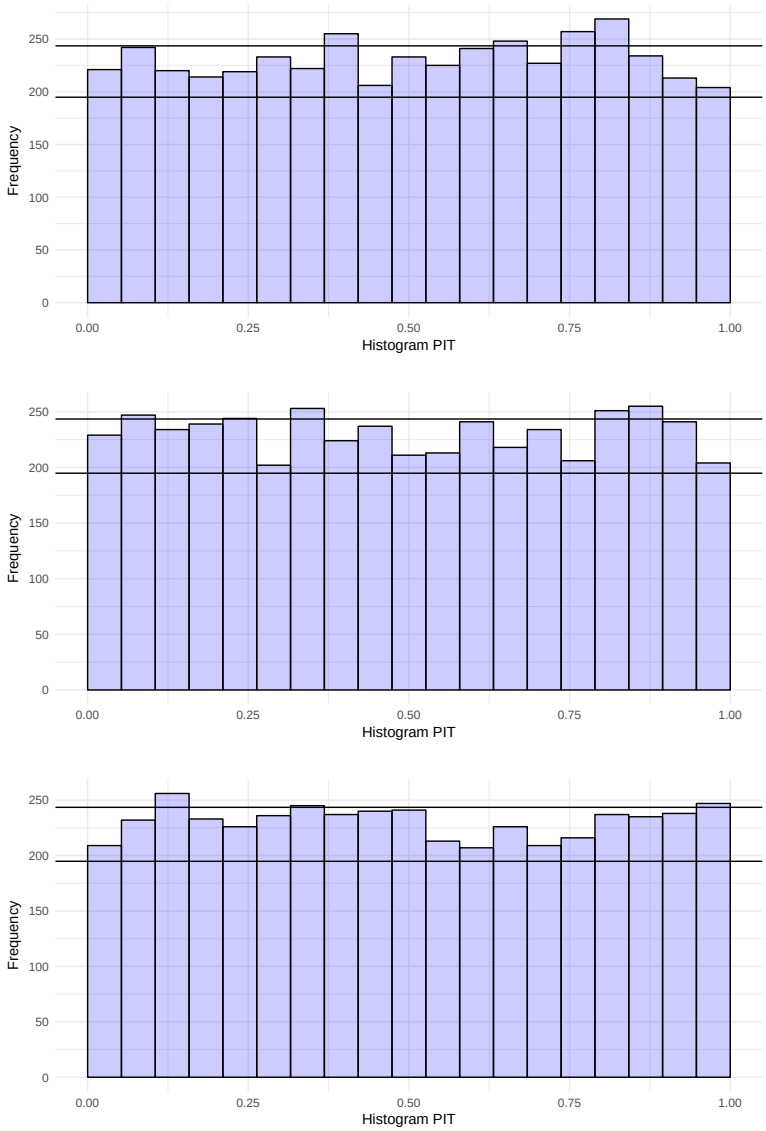

Figure 8.5: From top to bottom the panels show the test of PIT is uniform(0,1) for the multiple components model, the ARMA-GARCH model from [130], and the ARMA-GARCH for the transformed load factor. The horizontal lines are the confidence intervals.

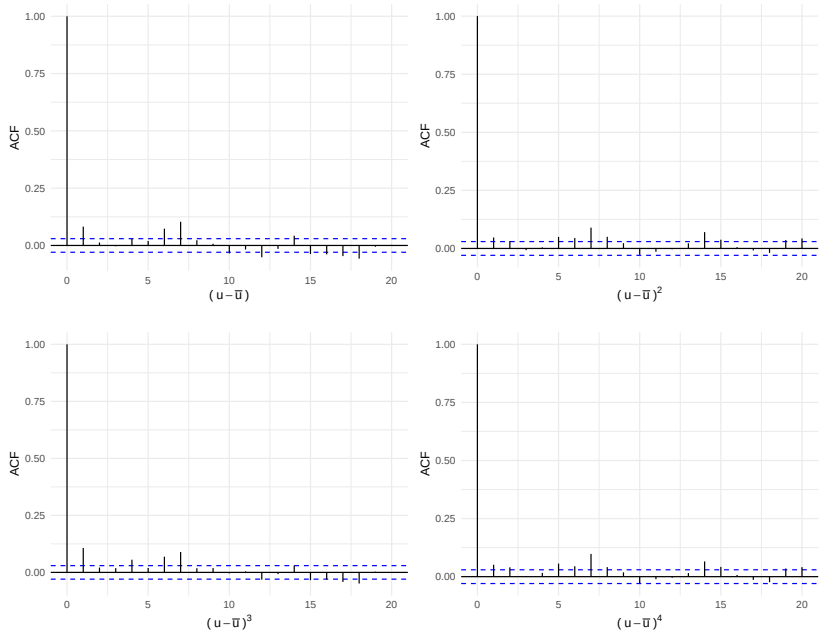

Figure 8.6: ACF PIT, multiple components model for $k = \{1, 2, 3, 4\}$.

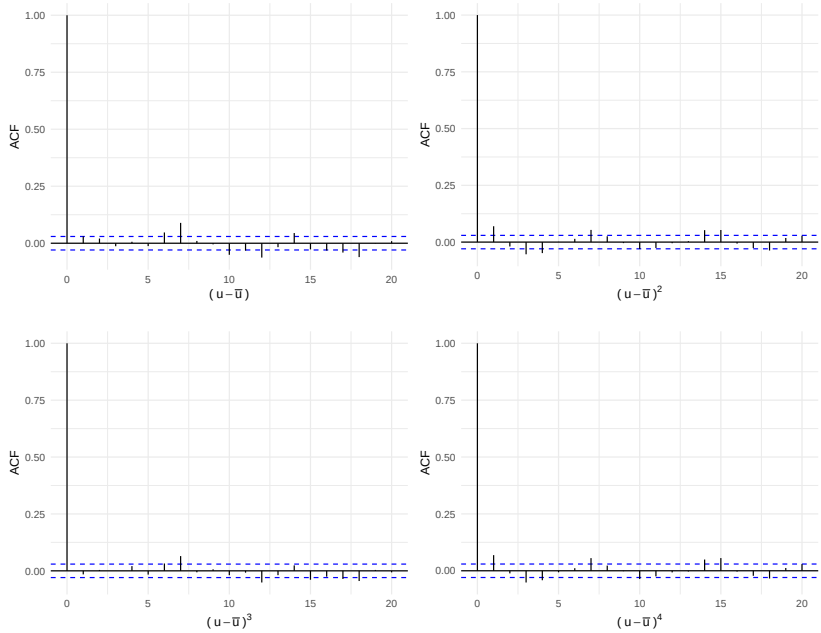

Figure 8.7: ACF PIT, ARMA(3,1)-GARCH(1,1) model from [130].

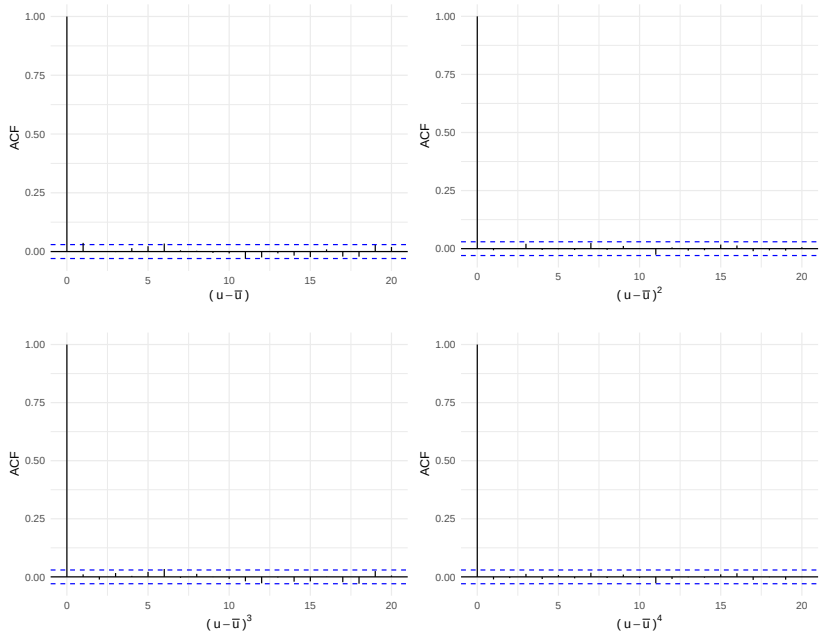

Figure 8.8: ACF PIT, ARMA-GARCH model for the transformed load factor.

8.3.5 Estimation of copula models

Following [157] we begin our dependence analysis by applying the ARCH-LM test of [165] and test for autocorrelation in the product of the PITs. Specifically, we consider the following regression:

$$u_{1t}u_{2t} = \omega_0 + \sum_{i=1}^{p} \omega_i u_{1,t-i}u_{2,t-i} + \varepsilon_t. \tag{8.9}$$

Under the null of a constant conditional copula we have $\omega_i = 0$ for $i = 1, \ldots, p$. This is tested using a standard LM-test. Critical values are found by bootstrap as detailed in [157]. We test for autocorrelation in lag $1, 5, 7$ and 10. The results for both models are seen in Table 8.6. According to the test we clearly reject the null of constant dependence between the PITs for all models. The results indicate that we can expect the time–varying copulas to outperform the constant copulas.

We now combine the PIT from the marginal models using a copula which results in a joint distribution of the transformed load factor and the spot price. For all copulas we consider both time–varying dependence i.e. a score-driven model for the dependence parameter and a constant version of the copula to investigate

	AR(1)	AR(5)	AR(7)	AR(10)
Multiple Components	<0.001	<0.001	<0.001	<0.001
ARMA(3,1)-GARCH(1,1)	<0.001	<0.001	<0.001	<0.001

Table 8.6: p-values for the ARCH-LM test of no serial correlation in the PIT for both marginal models for spot prices.

how changing dependence affects the results. We estimate all copulas for the two marginal models considered for spot prices.

For the score-driven copulas we fit all copula models with different types of scaling for each combination of marginal models as the PITs are different. The scalingtype minimizing BIC is preferred.

For each marginal model specification the score-driven copulas have been estimated using the scalingtype minimizing BIC.

Before considering the estimated copula models in more details, we address the goodness-of-fit for all estimated copulas using the AD-test i.e. we test whether the estimated copulas resemble the true but unknown copula:

$$H_0 : C_i\left(\hat{u}_{1,t}, \hat{u}_{2,t}, f_{c,t}(\hat{\theta}_c)\right) = C_0\left(u_{1,t}, u_{2,t}, f_{c,t}(\theta_c^0)\right). \tag{8.10}$$

According to the test we cannot reject that all of the estimated copulas resemble the true copula on a 1% significance level except for the Gaussian copula for the ARMA-GARCH model where we reject. Thus generally we cannot reject that the true copula has been constant through the sample for any of the two marginal models.

We note that the dependence parameters in the time–varying copulas are quite persistent for all models.

8.3.6 Comparison of estimated copulas

We compare the copulas for each marginal model for prices. Comparing the different copulas using BIC for each marginal specification for spot prices we see that the time–varying Gaussian copula is preferred for both models.

However, we do also perform a pairwise comparison of the estimated copulas using the in-sample test by [160] and the OOS test by [161] and test if the estimated copulas are statistically different. For the OOS test we follow [130] and estimate the marginal models only on the in-sample data and hence we do

not use a rolling estimation window of fixed size as the theory requires [161]. However, due to the long in-sample data this is not expected to affect the validity of the asymptotic distribution. The estimated marginal models and the copula are used to forecast the OOS values for the model and the likelihood of the observed data is evaluated according to these parameters.

The results for the two-components model are seen in Table 8.7 and Table 8.8 for the in-sample and out-of-sample comparison, respectively. The results are not very different from what is found when comparing BIC. Generally the Gaussian GAS and Student's t GAS copulas are preferred to all other copulas in both the in-sample and out-of-sample test suggesting that the dependence between the PIT is symmetric and time–varying. The two copulas are not significantly different for any of the models according to the in-sample and out-of-sample comparison and hence we cannot differ between them. This is much in line with the results from [130] where the Gaussian GAS copula performs well in the OOS[8] comparison. Additionally we note that the Clayton GAS and Gumbel GAS copulas are not always superior to the constant copulas.

	Gaussian	Clayton	Gumbel	Student's t	Gaussian*	Clayton*	Gumbel*
Clayton	1.32						
Gumbel	-7.1^a	-7.74^a					
Student's t	-3.55^a	-4.33^a	10.44^a				
Gaussian*	3.76^a	3.23^a	9.03^a	5.78^a			
Clayton*	-5.69^a	-6.21^a	2.95^a	-6.4^a	-8.02^a		
Gumbel*	-1.72	-2.2^a	10.56^a	3.51^a	-4.36^a	10.74^a	
Student's t*	3.93^a	3.85^a	9.33^a	6.34^a	0.58	8.44^a	5.03^a

Table 8.7: In-sample comparison of the estimated copulas where a multiple components marginal model for the spot prices is used. A positive value indicates that the model to the left is better than the model above, a negative value indicate the opposite. '*' indicates GAS copulas. 'a' indicates that the copulas are significantly different at a 5% significance level. Comparison of Student's t and the Gaussian copula has been done using a t-test with $H_0 : \nu^{-1} = 0$. The limiting distribution is not $N(0,1)$ for this test However, the right-tail critical value of 1.96 is still valid [157]. The Standard error for ν^{-1} has been obtained using the stationary bootstrap of [159].

[8] [130] do not consider a Student's t GAS copula but instead they estimate a Joe-Frank GAS copula which also performs well.

	Gaussian	Clayton	Gumbel	Student's t	Gaussian*	Clayton*	Gumbel*
Clayton	-0.26						
Gumbel	-5.67^a	-5.89^a					
Student's t	-3.67^a	-3.97^a	6.98^a				
Gaussian*	2.53^a	2.88^a	6.04^a	4.5^a			
Clayton*	-5.37^a	-5.59^a	-0.86	-6.16^a	-5.89^a		
Gumbel*	-3.23^a	-3.48^a	4.93^a	-0.18	-4.27^a	6.12^a	
Student's t*	1.53	1.85	5.96^a	4.53^a	-0.74	5.98^a	4.52^a

Table 8.8: Out-of-sample comparison of the estimated copulas where a multiple components marginal model for the spot prices is used. A positive value indicates that the model to the left is better than the model above, a negative value indicates the opposite. '*' indicates GAS copulas. 'a' indicates that the copulas are significantly different at a 5% significance level.

8.4 APPLICATION TO RISK MANAGEMENT

We reconstruct the simulation study considered in [130] and use their model as benchmark for the score-driven model introduced in this study.

8.4.1 Simulated profit distributions

With copulas it is straightforward to simulate from the estimated joint distributions using the following steps:

1. Using the dependence parameter ρ_t we simulate (u_{1t}, u_{2t}) from the copula.

2. u_{1t} and u_{2t} are inverted using the quantile function for the given marginal models. We distinguish between the cases where a marginal score-driven model and a marginal ARMA-GARCH model is used:

   When the marginal model is score-driven we get $\tilde{Y}_{1t} = F_1^{-1}(u_{1t}; f_t)$, where $\tilde{Y}_{1t}$ is the simulated deseasonalized price.[9]

   When the marginal model is of the ARMA-GARCH type, we have $\eta_{it} = F_i^{-1}(u_{it}; \theta)$,[10] where $i = 1, 2$ or $i = 2$ depending on which model we consider.[11] η_{it} is the standardized residuals from the ARMA-GARCH model. Inserting η_{it} into the ARMA-GARCH filter together with either past

[9] f_t is the time–varying parameters of the conditional distribution.

[10] θ denotes the parameters of the error distribution.

[11] When both marginal models are of the ARMA-GARCH type, $i = 1, 2$ and when a score-driven marginal model for the price series is used, $i = 2$.

observed or simulated values of $\tilde{Y}_{i,t-j}$ and $\sigma_{i,t-k}$ yields the deseasonalized value $\tilde{Y}_{it}$ and the conditional volatility $\sigma_{i,t}$.

3. When the marginal model is score-driven, the deseasonalized price $\tilde{Y}_{1t}$ is used to update the parameters of the conditional distribution f_{t+1}.

4. The simulated values (u_{1t}, u_{2t}) are used to update the time–varying dependence parameter ρ_{t+1}.

5. The simulated price and transformed load factor are obtained by adding the seasonal effect at time t . To obtain the load factor we unmap the transformed load factor by applying the logistic function.

6. Repeat steps 1-5 h times.

We note that when $h = 1$, a closed-form expression for the one-period ahead time–varying parameters exists for the score-driven models. At the start of the simulation we need the initial dependence parameter ρ_t. This is obtained by applying the score-driven filter for the copula with the estimated coefficients κ_c, A_c and B_c to the PIT from the marginal models. A similar procedure gives the initial parameters f_t of the conditional distribution for the marginal score-driven model.

The simulation approach allows us to construct an empirical distribution of prices and the load factor. We consider the simulation horizon h to be one month.[12] We simulate 10,000 paths from all copula models considered in this study for all 24 OOS months. We keep the model parameters fixed during the whole simulation exercise. This can be justified by the large in-sample dataset and therefore reestimation of the model should not change the model parameters much and is therefore unnecessary. Using the simulated values the empirical joint distribution for each OOS month is obtained. Figure 8.9 shows the joint empirical distribution function for August 2016 when the two-components score-driven model is used as marginal model for the price series and the Gaussian GAS copula is used for the dependence structure.

As [130] we note that even though the Gaussian copula is used, the resulting empirical distribution is clearly not Gaussian as it exhibits skewness and heavy tails. The heavy tails and the skewness arise as the marginal models are conditionally Student's t and Skew Normal, respectively.

[12] Therefore the length of the simulation differs between e.g. January and February.

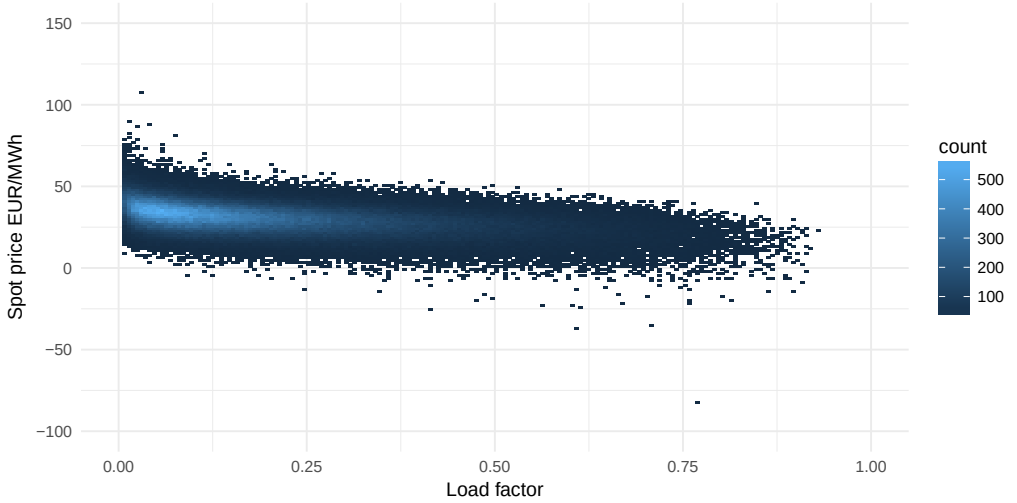

Figure 8.9: Simulated joint distribution function for daily spot prices and load factor in August 2016 using a Gaussian copula and a two-components score-driven model as marginal model for the price series.

We consider an energy trading company entering a PPA of fixed length. We consider monthly contracts, however, the length of the contract is arbitrary. The energy trading company pays a fixed price R for each MWh of wind power produced during the contract. The daily load factor L_t and the wind power production Q_t during the contract are unknown and thus the energy trading company faces volumetric risk. Moreover, the company faces price risk as the produced energy is sold on the day-ahead market at the current spot price S_t.

We assume that the two parties agree on the contract at least one day before the start of the contract period since bids to the day-ahead market have to be made one day in advance. We denote the settlement day by t_0, the start day by t_1 and the end date by t_2 where $t_0 < t_1 \leq t_2$. The length of the contract is $T = t_2 - t_1 + 1$ days. The profit of a contract with length T is given by:

$$\pi = \sum_{t=t_1}^{t_2} Q_t \left(S_t - R \right). \tag{8.11}$$

Following [130] we assume that the quantity Q_t bid to day-ahead market is given by:

$$Q_t = \mathbb{E}_{t-1} \left(Q_t \right), \tag{8.12}$$

where $\mathbb{E}_{t-1} \left(Q_t \right)$ is the conditional expectation of the one day-ahead production. Further, we assume no balance risk i.e. we assume that the energy trading

company can predict the following day's wind power production perfectly. Under this assumption the energy trading company does not trade on the intraday market to cover any imbalances between the bid and produced amount of electricity.

The fixed price contract deviates from a standard forward contract since the production is unknown [130]. Additionally, the correlation between Q_t and S_t introduces a correlation risk. We can express Equation (8.11) in terms of a forward price F and the price of correlation c [130]:

$$\pi = \sum_{t=t_1}^{t_2} Q_t \left(S_t - (F - c) \right), \tag{8.13}$$

where $c = c\left(t_0, T\right)$ is the price of correlation risk which captures the risk associated with the negative dependence between S_t and Q_t, and $F = F\left(t_0, T\right)$ is the forward price. Both quantities depend on the time the contract is settled t_0 and the length of the contract T. In the following the dependence is suppressed and we write only c and F. The fair value of c is obtained by setting the discounted conditional expected value of Equation (8.13) equal to zero. Under the assumption of a risk-free rate of zero we find c as [130]:

$$0 = \mathbb{E}_{t_0}^{\mathbb{Q}} \left(\sum_{t=t_1}^{t_2} Q_t \left(S_t - (F - c) \right) \right) \tag{8.14}$$

$$\Updownarrow$$

$$c = F - \frac{\mathbb{E}_{t_0}^{\mathbb{Q}} \left(\sum_{t=t_1}^{t_2} Q_t S_t \right)}{\mathbb{E}_{t_0}^{\mathbb{Q}} \left(\sum_{t=t_1}^{t_2} Q_t \right)}. \tag{8.15}$$

An estimate of c can be found by simulating from the proposed copula model [130]. However, as the model builds upon historical prices and wind power production this estimate will reflect the price of correlation under the physical measure $\mathbb{P}$ and not under the risk neutral measure $\mathbb{Q}$. The risk neutral measure reflects the risk premium charged by the energy trading company offering the PPA to wind farm owners. It is generally difficult to obtain the market price of risk associated with a PPA cf. the discussion in [130] and therefore we follow [130] and set $\mathbb{P} = \mathbb{Q}$. This means that we assume the market price of risk is equal to zero. The consequences of this is expected to have only a minor impact on the price of the PPA and therefore the overall conclusion is still valid [130].

The energy trading company can hedge against the risks associated with a PPA. However, since the market of wind forwards is incomplete a perfect hedge is not possible [130]. Instead a simple hedge can be done by taking a short position of H^* standard forward power contracts. We assume that the hedge is static and performed at time t_0. The hedge payoff is given by:

$$H^* \left(\mathbb{E}_{t_0}^{\mathbb{Q}} \left(\frac{1}{T} \sum_{t=t_1}^{t_2} S_t \right) - \frac{1}{T} \sum_{t=t_1}^{t_2} S_t \right) = H^* \left(F - \bar{S} \right), \tag{8.16}$$

where F is the forward price from Equation (8.13) and $\bar{S}$ denotes the average day-ahead spot price for the delivery period. H^* is found by minimizing the variance of the portfolio payoff:

$$\min_{H^*} \mathbb{V}_{t_0} \left[\sum_{t=t_1}^{t_2} \tilde{Q}_t \left(S_t - (F - c) \right) + H^* \left(F - \bar{S} \right) \right], \tag{8.17}$$

where $\tilde{Q}_t = 24 \cdot L_t \cdot \Lambda$, Λ denotes the installed capacity under the contract and L_t denotes the load factor i.e. the daily amount of energy produced relative to the total installed capacity in DK1. Hence $\tilde{Q}_t$ denotes the total MWh produced by the portfolio on a given day. Note that L_t is a relative measure for the whole price area DK1 and therefore we need to assume that it is representative for the load factor of the smaller portfolio. This is a realistic assumption if the portfolio is diversified properly according to turbine type and location. The hedge quantity minimizing Equation (8.17) is found as [130]:

$$H^* = \frac{\operatorname{cov}_{t_0} \left(\bar{S}, \sum_{t=t_1}^{t_2} \tilde{Q}_t S_t \right) - (F - c) \operatorname{cov}_{t_0} \left(\bar{S}, \sum_{t=t_1}^{t_2} \tilde{Q}_t \right)}{\mathbb{V}_{t_0} \left(\bar{S} \right)}. \tag{8.18}$$

The simple hedge provides protection on average but does not protect against worst case scenarios such as extremely high wind and low prices, something which is a likely outcome in DK1 [130]. The situation can be improved by adding options to the portfolio but as the market for options is very illiquid in DK1, the simple hedge is realistic [130]. When a hedge is performed, the profit of a PPA is given by:

$$\pi^H = \sum_{t=t_1}^{t_2} Q_t \left(S_t - (F - c) \right) + H^* \left(F - \bar{S} \right). \tag{8.19}$$

To find the fair price of a PPA or equivalently the price of the correlation risk we perform Monte Carlo simulations from the joint model of the day-ahead spot

price and the wind power production. We then use Equation (8.15) to find c. We follow [130] and perform the simulations as follows:

Given all information up to and including the settlement day t_0 we determine the price of the PPA R, the price of the correlation risk c and the optimal amount of hedging H^* by performing $10,000$ simulations from the joint model where the forecast horizon $h = T$ i.e. the length of the contract. The simulations are performed as described in the beginning of this section. This gives 10,000 different paths of length T for prices and the load factor. We calculate c and H^* using Equation (8.15) and Equation (8.18), respectively. The price of the PPA is then obtained as:

$$R = F - c, \tag{8.20}$$

where the simulated forward price F is obtained as the average across all 10,000 simulations i.e.:

$$F = \frac{1}{10,000} \sum_{s=1}^{10,000} \bar{S}_s. \tag{8.21}$$

To illustrate this we assume that we are on the last day of July 2016 and want to find the price of a PPA for August 2016 i.e. a 31 days contract. We consider a portfolio of size 500 MW. For each of the marginal models we simulate the joint distribution of wind power production and prices using the estimated Gaussian GAS copula. Using the simulated values we calculate c, F and R and use these quantities to obtain the corresponding simulated profits. We consider the cases with and without a price hedge. The simulated profits are calculated using Equation (8.19) and Equation (8.13), respectively. The 5% quantile of the simulated distributions is used as an estimate of the 5% Value-at-Risk. The results are presented in Table 8.9.

	Multiple components	ARMA-GARCH
R	27.79 EUR/MWh	31.24 EUR/MWh
c	2.88 EUR/MWh	2.12 EUR/MWh
F	30.67 EUR/MWh	33.35 EUR/MWh
$VaR(0.05)_t$ with hedge	-223,502.5 EUR	-248,161.93 EUR
$VaR(0.05)_t$ no hedge	-609,600.75 EUR	-608,485.41 EUR

Table 8.9: Simulation results for a PPA for August 2016. The results are based on 10,000 simulations and a Gaussian GAS copula for the dependence structure.

The results show that a price hedge performed by selling H^* amounts of forwards reduces the 5% Value-at-Risk significantly for both marginal models. This is

not surprising and it is equal to the findings in [130]. We note that the ARMA-GARCH model forecasts a higher forward price F and a lower price of correlation risk c than the score-driven model. This results in a higher price for the PPA cf. Equation (8.20).

We plot the mean and the 95% confidence interval of the simulated daily prices together with the actual prices for August 2016 for both models in Figure 8.10. We see that for both marginal models the variance of the forecast increases only moderately over the month.

In Figure 8.11 we compare the simulated profit distributions for the multiple components model and the ARMA-GARCH model for the case with and without a price hedge. We note that the profit distributions are not very different for both cases and when a price hedge is performed, the two distributions look almost equivalent. We clearly see how the price hedge decreases the variance of the profit distribution.

[130] illustrate the effect of the negative correlation between wind production and spot price by exchanging the estimated copula with the independence copula in the simulations. Under the assumption of the independence copula the energy trading company does not account for the dependence between wind power production and the price when determining the price of the PPA i.e. $R = F$. The distribution of profits under the independence assumption is compared with the distribution obtained by a Gaussian GAS copula in Figure 8.12. As [130] we see that ignoring the dependence between wind power production and prices leads to an underestimation of the 5% Value-at-Risk and the distribution of profits is more asymmetric when the dependence is modeled. Specifically the simulated 5% VaR is -562, 514 EUR under the assumption of wind and price being independent while it is $-609,601$ EUR when a Gaussian copula is used to model the dependence between the variables. The reduction in the 5% VaR amounts to 7.7% which is considerably smaller than the reduction of 15% presented in [130].

While Table 8.9 compared the two marginal models for a single month we show similar results averaged over all 24 months in the OOS period in Table 8.10. When comparing over the full OOS period we see that the VaR with and without hedge is substantially higher (numerically) for the two-components model. The same is seen for the price of correlation c. We notice that the two-components model yields a lower contract price R and forward price F on average. Additionally the variance is substantially lower for all quantities from the two-components model. These results in turn result in a higher average profit for the two-components model under the assumption that a customer accepts the calculated contract

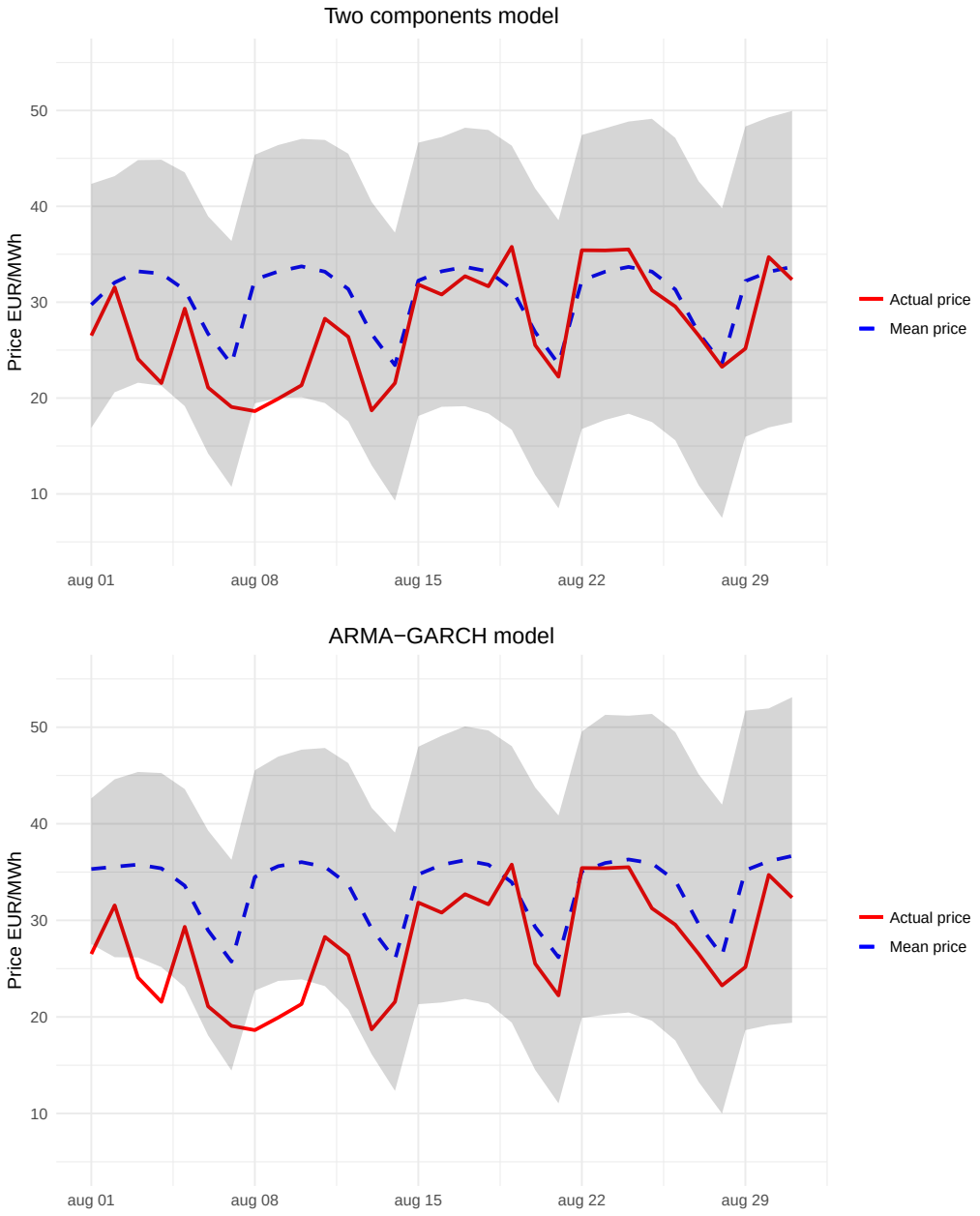

Figure 8.10: Comparison of the simulated and actual price for August 2016 for both marginal models for the price series when a Gaussian GAS copula is used for the dependence structure. 95% confidence intervals from the simulations are reported in gray.

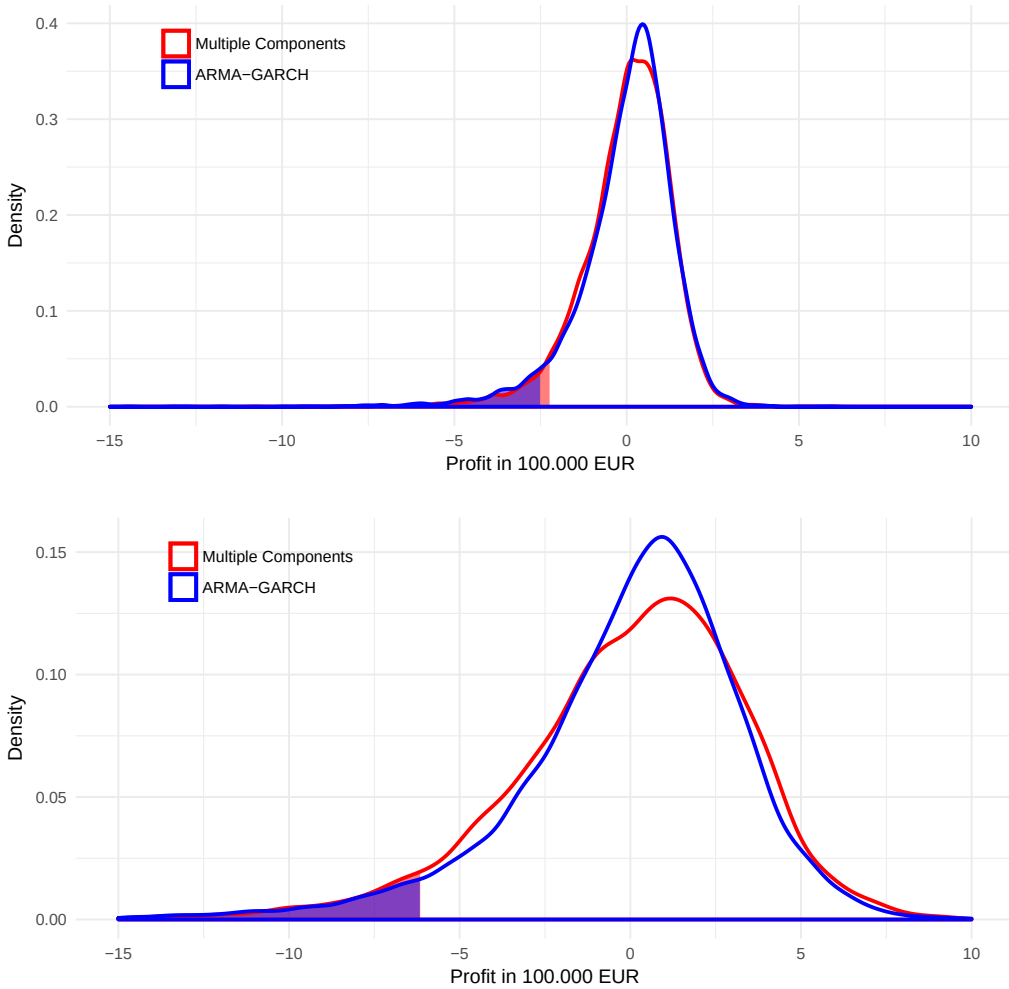

Figure 8.11: Comparison of the distribution of simulated monthly profits for August 2016 using a Gaussian GAS copula for the dependence structure. The upper figure shows the case with price hedging and the lower figure shows the case without price hedging. The colored areas represent the profits below the 5% VaR for each model.

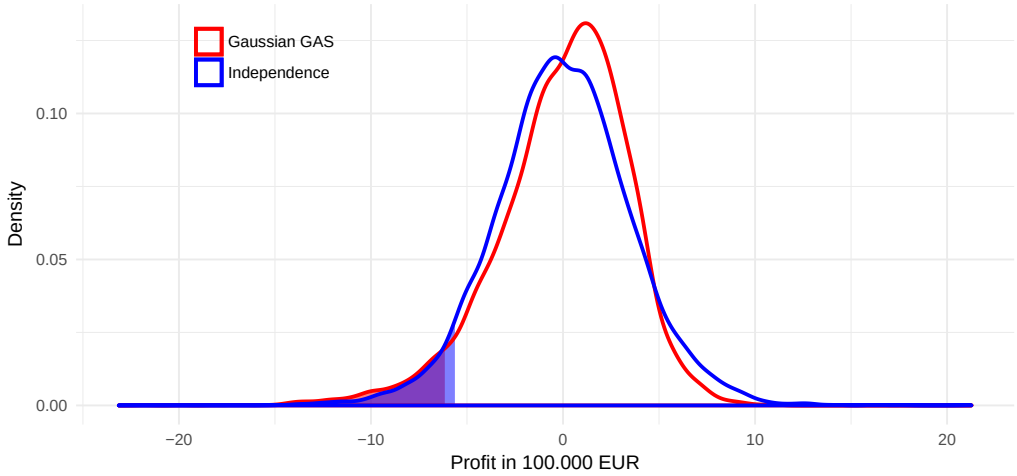

Figure 8.12: Comparison of the distribution of simulated monthly profits for August 2016 under different assumptions for the dependence structure. The two-components model is used as marginal model for the spot price. This is the case without a price hedge. The colored areas represent the profits below the 5% VaR for each model.

price.

	Mean R	sd R	Mean c	sd c	Mean F	sd F
Multiple components	25.27 EUR/MWh	4.96 EUR/MWh	2.73 EUR/MWh	0.22 EUR/MWh	28 EUR/MWh	4.98 EUR/MWh
ARMA-GARCH	26.32 EUR/MWh	5.63 EUR/MWh	2.25 EUR/MWh	0.43 EUR/MWh	28.57 EUR/MWh	5.67 EUR/MWh

	Mean $VaR(0.05)_t$ hedge	sd $VaR(0.05)_t$ hedge	Mean $VaR(0.05)_t$ no hedge	sd $VaR(0.05)_t$ no hedge
Multiple components	-282587.07 EUR	31755.94 EUR	-794962.94 EUR	135837.95 EUR
ARMA-GARCH	-366232.17 EUR	99449.03 EUR	-1019215.95 EUR	358495.85 EUR

Table 8.10: Simulation results for all 24 OOS months for the two competing models. The results are based on 10,000 simulations and a Gaussian GAS copula for the dependence structure.

8.4.2 VaR model comparison

The accuracy of the forecasted Value-at-Risk is of high importance for risk managers. To evaluate the downside risk prediction of the models we consider the Quantile Loss function (QL), which is a frequent choice for comparing the VaR prediction of two models [166]. Consider the prediction of Value-at-Risk at time t $VaR_t(\alpha)$ for a given risk level α.[13] The associated quantile loss, QL_t, is defined as follows [166]:

$$QL_t(\alpha) \equiv (\alpha - d_t)(r_t - VaR_t(\alpha)), \tag{8.22}$$

where $d_t \equiv \mathbf{1}\{r_t < VaR_t(\alpha)\}$ is an indicator function for the event of a return below the predicted $VaR_t(\alpha)$, usually called the hitting sequence [166], and r_t corresponds to the profit π described above in this section. A return below the $VaR_t(\alpha)$ is weighted with $(1-\alpha)$ while a return above is weighted with α. Hence a VaR exceedance is penalized more and therefore the loss function is asymmetric.

Assume that we consider a dataset of length T which is divided into an in-sample period of length $t^* = T - H$ and an out-of-sample period of length H. The model is estimated on the in-sample data and h-days ahead predictions of the return are performed using the estimated model. From these predictions the $VaR_t(\alpha)$ $t \in \{t^*+1, \ldots, t^*+H\}$ is extracted. For each $VaR_t(\alpha)$ we calculate $QL_t(\alpha)$ and then for a given model $\mathcal{A}$ the quantile losses are averaged over the forecasting period:

$$QL_{\mathcal{A}} = \frac{1}{H}\sum_{t=t^*}^{t^*+H} QL_{\mathcal{A}t}(\alpha). \tag{8.23}$$

The model with the lowest loss function is preferred and thus model $\mathcal{A}$ outperforms $\mathcal{B}$ when $QL_{\mathcal{A}} < QL_{\mathcal{B}}$.

In the following we compare the joint distributions obtained by applying each of the marginal models for spot prices and the different copulas considered. This is done by simulating h-days ahead predictions for wind power production and spot prices for each day in the OOS for all models. Specifically we consider $h = 31$ corresponding to a one month ahead prediction and perform $10,000$ simulations from each model.

Based on the simulated prices and wind power production we calculate the estimated forward prices as the average of the simulated prices, the fair con-

[13] The Value-at-Risk is defined as: $VaR_t(\alpha) \equiv F^{-1}(\alpha, \theta_t)$ where θ_t is the (time–varying) parameters of the conditional distribution [167] and thus it is the α-quantile of the profit distribution at time t.

tract price using Equation (8.20) and the minimum variance hedge quantity by Equation (8.18) for each day in the OOS. In total we perform $H = 700$ rolling 31-days ahead predictions and assume that on each day the energy company agrees on a PPA with a wind farm owner with a portfolio size of 500 MW and sells a quantity H^* of forwards.[14] Note that we keep the model parameters fixed during the whole forecasting exercise. This can be justified by the large in-sample dataset and therefore re-estimation of the model is not expected to change the estimated parameters much.

Using the estimated price of the PPA we calculate the profit on such a contract for each of the 10,000 simulated 31-days ahead predictions. This gives a simulated distribution of profits and the $VaR_t(\alpha)$ can be found as the α-quantile of the simulated distribution. For each of the contract prices the actual profit is calculated using the OOS data. The profit is then compared with the $VaR_t(\alpha)$ for each $t \in \{t^* + 1, \ldots, t^* + H\}$ using the loss function in Equation (8.22). The average loss QL for each model is then calculated and the two models are compared in Table 8.11. Here $\mathcal{A}$ refers to the two-components model and $\mathcal{B}$ refers to the ARMA-GARCH model from [130].

	t GAS	Gaussian GAS	Clayton GAS	Gumbel GAS	t	Gaussian	Clayton	Gumbel
$QL_{\mathcal{A}}/QL_{\mathcal{B}}$	0.79	0.70	0.86	0.85	0.87	0.87	0.87	0.88

Table 8.11: Comparison of QL for both marginal models.

It is clear from Table 8.11 that the two-components model outperforms the ARMA-GARCH model from [130] for all the different copula models considered. This might be caused by the fact that the estimated ARMA-GARCH model is close to non-stationary because of the extreme observations of prices. This can lead to inaccurate filtration of the data which affects the forecasts and therefore also the estimate of $VaR_t(\alpha)$ [152]. The two-components score-driven model is robust to extreme observations and therefore the filtration of the data is better.

Comparison of the loss functions does not provide any information on whether the difference in forecast ability differ significantly across the models. Therefore the comparison of the loss functions is accompanied by the Diebold-Mariano (DM)-test [164]. The test is intended for comparison of forecasts [168]. Generally the DM-test compares the loss differential i.e. the loss associated with a given forecast error e_t. The loss differential depends upon a loss function $L(e_t)$ e.g. in

[14] The OOS size is 731 and thus to evaluate the actual loss of the contract we consider $731 - 31 = 700$ forecasts.

our case $L(e_t) = QL_t$. The time t loss differential between a forecast from model $\mathcal{A}$ and model $\mathcal{B}$ is given by:

$$d_{\mathcal{AB}t} = L(e_{\mathcal{A}t}) - L(e_{\mathcal{B}t}). \tag{8.24}$$

The test requires that the loss differential is covariance stationary. The null hypothesis is equal predictive performance i.e. $H_0 : \mathbb{E}(d_{\mathcal{AB}t}) = 0$. When the loss differential is stationary, we have:

$$DM_{\mathcal{AB}} = \frac{\bar{d}_{\mathcal{AB}}}{\hat{\sigma}_{\mathcal{AB}}} \xrightarrow{d} N(0,1), \tag{8.25}$$

where $\bar{d}_{\mathcal{AB}} = \frac{1}{T}\sum_{t=1}^{T} d_{\mathcal{AB}t}$ is the sample average loss differential and $\hat{\sigma}_{\mathcal{AB}}$ is a consistent and robust estimator of the standard deviation for $\bar{d}_{\mathcal{AB}}$. We use the HAC-estimator.

As already indicated we use $QL_{\cdot t}$ as loss function for each model $\{\mathcal{A}, \mathcal{B}\}$ and compute $d_{\mathcal{AB}t}$ from Equation (8.24). The DM-assumption of $\bar{d}$ being stationary is tested using the ADF-test. The test rejects the null of a unit root for all loss differentials. The results of the DM-test are seen in Table 8.12 and they show that the two-components model is significantly better than the ARMA-GARCH model from [130] at predicting the 5% Value-at-Risk for all copulas.

According to the DM-test a two-components score-driven model for spot prices improves the risk management of PPAs significantly compared to the ARMA-GARCH model used in [130].

	t GAS	Gaussian GAS	Clayton GAS	Gumbel GAS	t	Gaussian	Clayton	Gumbel
$DM_{\mathcal{AB}}$	-9.99^a	-11.25^a	-7.49^a	-7.44^a	-8.74^a	-8.7^a	-8.57^a	-7.98^a

Table 8.12: The table reports the DM-test statistic for testing of equal forecast ability of $VaR(0.05)$ for both marginal models. *'a'* indicates that the forecasts of $VaR(0.05)$ are significantly different at a 5% significance level. A negative value means that the forecasts of model 1 are preferred to the forecasts of model 2 and vice versa for a positive value.

It is also of interest to study whether the time–varying copulas are significantly better at predicting the 5% VaR compared to the constant copulas. This is done using the DM-test and the results are presented in Table 8.13. We see that all time–varying copulas are significantly better than their constant counterparts at predicting the 5% Value-at-Risk hence time–varying copulas should be used in risk management of PPAs.

	t	Gaussian	Clayton	Gumbel
Multiple components	-10.98^a	-9.71^a	-11.87^a	-11.1^a
ARMA-GARCH	-11.2^a	-10.89^a	-10.68^a	-10.04^a

Table 8.13: The table reports the DM-test statistic for testing of equal forecast ability of $VaR(0.05)$ between the time–varying and constant copulas. *'a'* indicates that the forecasts of $VaR(0.05)$ are significantly different at a 5% significance level. A negative value means that the forecasts of the time–varying copula are preferred to the forecasts of the constant copula and vice versa for a positive value.

For both marginal models we investigate whether the Gaussian GAS copula is significantly better at predicting the 5% VaR compared to the other copulas using the DM-test. The results are presented in Table 8.14. A test of the DM-assumption using the ADF-test rejects the null of a unit root. We see that the Gaussian copula provides better VaR predictions for the multiple components model while it is outperformed by the other time–varying copulas when a ARMA-GARCH model is used to model the price series. For the ARMA-GARCH model the VaR forecasts of the Gaussian copula are preferred to the forecasts from the constant copulas.

	t GAS	Clayton GAS	Gumbel GAS	t	Gaussian	Clayton	Gumbel
Multiple Components	-8.74^a	-8.94^a	-8.81^a	-9.69^a	-9.71^a	-9.51^a	-9.68^a
ARMA-GARCH	10.82^a	5.12^a	10.81^a	-11.14^a	-10.89^a	-10.85^a	-10.95^a

Table 8.14: The table reports the DM-test statistic for testing of equal forecast ability of $VaR(0.05)$ between the Gaussian GAS copula and the other copulas for each of the models. *'a'* indicates that the forecasts of $VaR(0.05)$ are significantly different at a 5% significance level. A negative value means that the forecasts of the Gaussian GAS copula are preferred and vice versa for a positive value.

8.5 CONCLUSION

In this study we investigate the negative dependence between wind power production and electricity spot price by constructing a joint model using different copulas. We propose using a new generation of score-driven models as marginal model for the spot price of electricity as these are more robust to extreme events compared to ARMA-GARCH models. We apply the new model to pricing

and risk management of long-term power purchase agreements (PPAs) and benchmark against a previously published model of the ARMA-GARCH type.

In our simulation study we find that using the new score-driven model results in higher profit and lower VaR compared with the previous published ARMA-GARCH model. According to the DM-test this improvement of the risk management of PPAs is statistically significant compared to the previously published ARMA-GARCH model.

Ignoring the dependence between wind power production and electricity spot price leads to an underestimation of the VaR by 7.7%, which indicates the importance of using copulas to model the dependence structure. Comparing constant and time–varying copulas we find that all time–varying copulas are significantly better than their constant counterparts at predicting the 5% Value-at-Risk hence time–varying copulas should be used in risk management of PPAs.

Our simulation study is limited to consecutive monthly contracts. The forecast horizon is arbitrary, so the same approach can be used for risk management of quarterly or annual contracts. In case of a long forecast horizon for a long-term PPA the limiting factor in practice is the liquidity of the forward market for properly hedging the contract.

In this study we focus on a single market area, namely western Denmark. As a natural extension this new model could be used to quantify the risk associated with an international portfolio of PPAs spread across several market areas. A geographical dispersion of PPAs could potentially lead to a reduction of the overall portfolio risk due to the limited size of weather patterns. Such an investigation can be done by estimating a joint distribution for each price area of interest using the marginal models and the copulas considered in this study. The bivariate distributions for each price area can then be combined into a joint distribution for the whole portfolio using a copula. The overall portfolio risk can then be quantified by simulations similar to the ones carried out in this study.

We limit this study to wind power production. It could be extended to allow for different generation technologies like solar power to model the combined risk of a portfolio consisting of several generation technologies. Power purchase agreements for consumption could be included as well, in which case some amount of the produced electricity would be used to serve these contracts and thereby potentially limiting the price risk of selling directly in the spot market.

9

Concluding remarks

The frame of this dissertation is the rapidly increasing share of variable renewable electricity generation in the European electricity system. The purpose has been twofold: 1) investigate the optimal layout of generation capacities assuming cooperation between the European countries and allocate costs based on usage, and 2) improving risk management of long-term power purchase agreements (PPAs) for wind power.

ELECTRICITY SYSTEM MODELS

In an electricity system with a high share of variable renewable power generation, neighboring countries rely on imports and exports to balance the variability caused by the weather. Different flow tracing methods were introduced in Chapter 3 to investigate the allocation of transmission usage in a system with high share of renewable power generation. The different flow tracing methods produced different results for individual hours, but when averaged over a five-year time series with hourly resolution the results were similar. This is important for the subsequent applications of flow tracing, which are all based on averages of imports and exports.

Exploring optimal heterogeneous placement of renewable generation capacities, flow tracing was utilized to calculate levelized cost of electricity (LCOE) for each country, which served as a benchmark between the different layouts. In Chapter 4 it was found that an optimal placement of renewable capacities according to the best weather resources leads to a reduction of the overall system LCOE. Surprisingly, it also gave a reduction in the individual LCOE for all 30 countries considered in the model. In addition, the effect of different approaches to transmission allocation on the individual LCOEs was studied. The result of varying the transmission allocation between importers and exporters showed that for the variation of nodal LCOEs to be minimal, the transmission usage

would have to be allocated fully to the countries exporting excess generation. However, such an allocation is not likely to be accepted as fair.

Using a techno-economic model to jointly optimize generation capacity investments, their location, and their dispatch, it was found in Chapter 5 that solar PVs should predominantly be installed in Southern Europe, whereas onshore and offshore wind turbines should predominantly be installed in the western and northern parts. From the capacity layout it was clear that battery storage tended to follow solar PVs whereas hydrogen storage followed wind turbines. Flow tracing enabled me to confirm this intuition showing that battery storage is almost exclusively utilized by solar power to balance its diurnal pattern. Hydrogen storage is almost exclusively utilized by onshore and offshore wind to balance the synoptic patterns caused by large weather systems. Additionally, flow tracing was utilized to explore the distances traveled in the system when exporting power from the different generation and storage technologies. It was found that most of the power from all technologies except offshore wind is consumed locally. However, when power is exported it is usually transmitted several hundreds of kilometers and often exceeding 1000km in a system with a diameter of approximately 3500km. This is further evidence supporting the importance of cooperation between the European countries in balancing the variability of renewable electricity generation.

Moving away from model outputs and studying real system data, flow tracing was used in Chapter 6 to construct a new real-time carbon accounting method based on actual consumption. This study was a collaboration with Tomorrow to showcase the carbon accounting methodology of the electricityMap[1]. This method represents the underlying physics of the electricity system in contrast to the traditional input-output models used for carbon accounting. The new consumption-based accounting resulted in substantial differences when compared to a production-based accounting method, which is calculated as the carbon intensity from local generation within each country. This is the result of importing and exporting power from different technologies with very different carbon footprints, which emphasizes the importance of including cross-border flows for increased transparency regarding carbon emission accounting of electricity.

[1] www.electricitymap.org

RISK MANAGEMENT

Having modeled the entire European electricity system, the perspective was changed to that of an energy trading company within a single price area (West Denmark) in Chapter 8. Here, the negative correlation between wind power production and electricity spot price was investigated using a joint model based on copulas. The purpose was to improve risk management of long-term PPAs for wind power by finding the fair contract price, optimal hedge quantities and accurately predict the Value-at-Risk (VaR). It was found that when the negative dependence between wind power production and power spot price is ignored, the VaR is underestimated by 7.7%, which indicates the importance of using copulas to model the dependence structure. Additionally, when compared to constant copulas, the time-varying copulas outperform these in risk management applications. The new score-driven model shows a statistically significant improvement of risk management of long-term PPAs when benchmarked against a previously published model with a similar application to risk management of long-term PPAs in West Denmark. This result will help energy trading companies minimize the risk associated with long-term PPAs, which, in turn, benefits the investors in wind turbines. This encourages further investments in wind turbines leading to a higher share of renewable power generation in the European electricity system.

FINAL REMARKS

In this dissertation, I have applied physical and financial models to different aspects of the European electricity system. In the first part of the dissertation, I modeled the European electricity system from the perspective of a central planner assuming full cooperation in a selfless manner between the European countries. This enabled me to investigate optimal, pragmatic solutions to the layout of renewable generation capacities. In the second part, I took the perspective of an individual energy trading company seeking to minimize the risk associated with long-term PPAs for wind power, which has an immediate effect on the individual investors in wind turbines.

These are two very different perspectives. The central planning perspective is useful when exploring pragmatic solutions to the overall design of the European electricity system of the future but provides no guidance for the individual actors in the system. In contrast, the perspective of a trading company or an investor in a renewable power generating asset focuses on a set of individual business cases

with little regard to the impact of the asset in question on the overall electricity system.

The link between the two perspectives is the policy makers, who regulate the electricity system. The results from system models using the central planning perspective can be used by the policy makers as guidelines to provide the right incentives for investors, and other actors in the system, such that the current European electricity system develops towards the optimal and sustainable system of the future.

Appendices

A

A simplified model of a highly renewable European electricity network

We aggregate the European system to one node per country, with links between the nodes representing transmission capacity between the respective countries. This leads to a network with 30 nodes and 52 links; see Fig. 3.1. The depicted network topology was used, among others, in [35, 43, 69], and is based on the layout reported by ENTSO-E (European Network of Transmission System Operators for Electricity) [169]. The links between Sweden and Lithuania, and between Poland and Lithuania have been commissioned at the end of 2015 and were added in this network compared to the topology used in [35, 43, 69].

We demand that for every node n at any time t the following balancing condition is fulfilled:

$$G_n^R(t) - L_n(t) = P_n(t) + B_n(t) \; . \tag{A.1}$$

In this expression $G_n^R(t)$ denotes the renewable generation and $L_n(t)$ the load. The term $B_n(t)$ refers to the nodal balancing, and $P_n(t)$ to the import or exports injected into or withdrawn from the network. The left side of this equation is data-driven: The aggregated load per country $L_n(t)$ at hour t is given by historical data provided by the European Transmission System Operators [170], whereas the renewable generation $G_n^R(t)$ is based on data from a Renewable Energy Atlas [66, 171]. Both data sets comprise the years from 2010 to 2014 with hourly resolution, leading to 43822 different time steps. The renewable generation data is obtained by converting spatio-temporal wind velocity and solar radiation fields into wind and solar power generation time series, which are scaled in such a way that *on average* the load in each country is completely covered:

$$\langle L_n \rangle = \langle G_n^R \rangle = \langle G_n^W \rangle + \langle G_n^S \rangle \; . \tag{A.2}$$

Here G_n^W denotes the wind power generation, whereas G_n^S gives the solar power generation from photovoltaics. For the modeling underlying the results in the

present article a fixed wind fraction of $\langle G_n^W \rangle / \langle G_n^R \rangle = 0.7$ has been used. Other fluctuating forms of renewable generation are neglected, or assumed to be included into the backup generation capacity. Despite the relation in Eq. (A.2), at a specific hour t in general there will be a mismatch $\Delta_n(t)$ between the renewable generation $G_n^R(t)$ and the load $L_n(t)$:

$$\Delta_n(t) = G_n^R(t) - L_n(t) \; . \tag{A.3}$$

This mismatch has to be balanced by a combination of nodal power import or export $P_n(t)$, and nodal balancing $B_n(t)$. The latter describes dispatchable backup power generation $G_n^B(t) = -\min(B_n(t), 0)$ when $B_n(t) < 0$, or curtailment $C_n(t) = \max(B_n(t), 0)$ of excess power when $B_n(t) > 0$. The net power injection $P_n(t)$ refers to exports $P_n^+(t)$ for $P_n(t) > 0$, or to imports $P_n^-(t) = -P_n(t)$ for $P_n(t) < 0$.

Given a time series of renewable generation and load, different combinations of nodal balancing power and imports and exports will fulfill the balancing equation Eq. (A.1). For simplicity and to allow a comparison with previous studies we follow the approach of *synchronised balancing* [28], where the global mismatch is distributed to the individual nodes proportional to their average load:

$$B_n(t) = \left[\sum_m \Delta_m(t) \right] \frac{\langle L_n \rangle}{\sum_k \langle L_k \rangle} \; . \tag{A.4}$$

This choice of a balancing scheme fixes the power in- and outflows $P_n(t)$ at the individual nodes as

$$P_n = \Delta_n(t) - \alpha_n \Delta(t) \; , \tag{A.5}$$

where we have used the following abbreviations:

$$\Delta(t) = \sum_n \Delta_n(t) \; , \tag{A.6}$$

$$\alpha_n = \frac{\langle L_n \rangle}{\sum_k \langle L_k \rangle} \; . \tag{A.7}$$

Note that this set-up with Eq. (A.2) and Eq. (A.4) leads to $\langle P_n \rangle = 0$ or equivalently $\langle P_n^+ \rangle = \langle P_n^- \rangle$, that is the average power imports and exports of every node coincide [6].

B

Copulas

B.1 INFORMATION MATRICES

Information matrices for the copulas used in this study:

$$\mathcal{I}_{Ga}(\rho) = \frac{1+\rho^2}{(1-\rho^2)^2} \tag{B.1}$$

$$\mathcal{I}_{t}(\rho,\nu) = \frac{\nu+2+\nu\rho^2}{(\nu+4)(1-\rho^2)^2} \tag{B.2}$$

$$\mathcal{I}_{Gu}(\theta) = \theta^2\left(\frac{\pi^2}{9}-\frac{2}{3}\right)-\theta+\frac{2K_0}{\theta} \tag{B.3}$$

$$+\left(\theta^3+\theta^2+(K_0-1)\theta-2K_0+\frac{K_0}{\theta}\right)E_1(\theta-1)e^{\theta-1} \tag{B.4}$$

$$\mathcal{I}_{Cl}(\theta) = \frac{1}{\theta^2}+\frac{2}{\theta(\theta-1)(2\theta-1)}+\frac{4\theta}{3\theta-2}-\frac{2(2\theta-1)}{\theta-1}\rho(\theta) \tag{B.5}$$

where Ga refers to the Gaussian copula, t refers to the Student's t copula, Gu refers to the Gumbel copula and Cl refers to the Clayton copula.

For the Gumbel copula $K_0 = \left(5/6-\theta^2/18\right)$ and $E_1(\theta-1) = \int_{1-\theta}^{\infty} u^{-1}e^{-u}\mathrm{d}u$.

For the Clayton copula $\rho(\theta)$ is given by:

$$\begin{aligned}\rho(\theta) =& \frac{1}{(3\theta-2)(2\theta-1)} \\ &+\frac{\theta}{2(3\theta-2)(2\theta-1)(\theta-1)}\left[\Psi\left\{\frac{1}{2(\theta-1)}\right\}-\Psi\left\{\frac{\theta}{2(\theta-1)}\right\}\right] \\ &+\frac{1}{2(3\theta-2)(2\theta-1)(\theta-1)}\left[\Psi\left\{\frac{\theta}{2(\theta-1)}\right\}-\Psi\left\{\frac{2\theta-1}{2(\theta-1)}\right\}\right].\end{aligned} \tag{B.6}$$

Equation (B.1) and Equation (B.2) are found in [172, Supplementary material]. Equation (B.4) is from [173] and Equation (B.5) is from [174].

B.2 DERIVATIONS OF COPULA SCORES

The Gaussian copula has density [172]:

$$c_{Ga}\left(u_1, u_2\right) = \frac{\exp\left(\frac{2\rho x_2 x_1 - x_1^2 - x_2^2}{2(1-\rho^2)} + \frac{1}{2}\left(x_1^2 + x_2^2\right)\right)}{\sqrt{1-\rho^2}} \tag{B.7}$$

where $x_i = \Phi^{-1}\left(u_i\right)$ and $\Phi\left(\cdot\right)$ is the univariate standard Gaussian cdf. The log-likelihood for the Gaussian copula is achieved by taking the log of Equation (B.7):

$$\begin{aligned}
\log c_{Ga}\left(u_1, u_2\right) &= -\frac{1}{2}\log\left(1-\rho^2\right) + \left(\frac{2\rho x_2 x_1 - x_1^2 - x_2^2}{2\left(1-\rho^2\right)} + \frac{1}{2}\left(x_1^2 + x_2^2\right)\right) \\
&= -\frac{1}{2}\log\left(1-\rho^2\right) + \left(\frac{2\rho x_2 x_1 - x_1^2 - x_2^2 + \left(1-\rho^2\right)\left(x_1^2 + x_2^2\right)}{2\left(1-\rho^2\right)}\right) \\
&= -\frac{1}{2}\log\left(1-\rho^2\right) + \left(2\rho x_2 x_1 - x_1^2 - x_2^2 + \left(1-\rho^2\right)\left(x_1^2 + x_2^2\right)\right)\left(2\left(1-\rho^2\right)\right)^{-1}.
\end{aligned}$$

The score function is the partial derivative of the log-likelihood function w.r.t. ρ and it is given by:

$$\begin{aligned}
\nabla_{Ga} = \frac{\partial \log c_{Ga}}{\partial \rho} =& -\frac{1}{2\left(1-\rho^2\right)}\left(-2\rho\right) + \left(2x_2x_1 - 2\rho\left(x_1^2 + x_2^2\right)\right)\left(2\left(1-\rho^2\right)\right)^{-1} \\
&+ \left(2\rho x_2 x_1 - x_1^2 - x_2^2 + \left(1-\rho^2\right)\left(x_1^2 + x_2^2\right)\right)(-1)\left(2\left(1-\rho^2\right)\right)^{-2}(-4\rho) \\
=& \frac{\rho}{\left(1-\rho^2\right)} + \frac{\left(x_2x_1 - \rho\left(x_1^2 + x_2^2\right)\right)\left(1-\rho^2\right)}{\left(1-\rho^2\right)^2} \\
&+ \frac{\rho\left(2\rho x_2 x_1 - x_1^2 - x_2^2 + \left(1-\rho^2\right)\left(x_1^2 + x_2^2\right)\right)}{\left(1-\rho^2\right)^2} \\
=& \frac{\rho}{\left(1-\rho^2\right)} + \frac{\left(x_2x_1 - \rho\left(x_1^2 + x_2^2\right)\right)\left(1-\rho^2\right) + \rho\left(2\rho x_2 x_1 - \rho^2\left(x_1^2 + x_2^2\right)\right)}{\left(1-\rho^2\right)^2} \\
=& \frac{\rho}{\left(1-\rho^2\right)} + \frac{x_2x_1\left(1-\rho^2\right) - \rho\left(x_1^2 + x_2^2\right) + \rho^3\left(x_1^2 + x_2^2\right) + 2\rho^2 x_2 x_1 - \rho^3\left(x_1^2 + x_2^2\right)}{\left(1-\rho^2\right)^2} \\
=& \frac{\rho}{\left(1-\rho^2\right)} + \frac{\rho\left(2\rho x_2 x_1 - x_1^2 - x_2^2\right) + x_2x_1\left(1-\rho^2\right)}{\left(1-\rho^2\right)^2} \\
=& \frac{\rho}{\left(1-\rho^2\right)} + \frac{\rho\left(2\rho y - x\right) + y\left(1-\rho^2\right)}{\left(1-\rho^2\right)^2},
\end{aligned}$$

where $y = x_1x_2$ and $x = x_1^2 + x_2^2$.

Now considering the Student's t copula. The Student's t copula has density [172]:

$$\begin{aligned} c_t\left(u_1,u_2\right) = & \frac{\Gamma\left(\frac{\nu}{2}\right)\Gamma\left(\frac{\nu+2}{2}\right)}{\sqrt{1-\rho^2}\Gamma\left(\frac{\nu+1}{2}\right)^2} \\ & \times\left(1+\frac{x_1^2}{\nu}\right)^{\frac{\nu+1}{2}}\left(1+\frac{x_2^2}{\nu}\right)^{\frac{\nu+1}{2}}\left(1+\frac{x_1^2+x_2^2-2\rho x_2 x_1}{\nu\left(1-\rho^2\right)}\right)^{-\frac{1}{2}(\nu+2)} \end{aligned} \tag{B.8}$$

where $x_i = \mathcal{T}_\nu^{-1}\left(u_i\right)$ for $i = 1,2$ and $\mathcal{T}_\nu\left(\cdot\right)$ denotes the univariate Student's t cdf. And therefore the log-likelihood is:

$$\begin{aligned} \log c_t\left(u_1,u_2\right) = & \log\left(\Gamma\left(\frac{\nu}{2}\right)\right)+\log\left(\Gamma\left(\frac{\nu+2}{2}\right)\right)-\frac{1}{2}\log\left(1-\rho^2\right)-2\log\left(\Gamma\left(\frac{\nu+1}{2}\right)\right) \\ & +\frac{\nu+1}{2}\left[\log\left(1+\frac{x_1^2}{\nu}\right)+\log\left(1+\frac{x_2^2}{\nu}\right)\right]-\frac{1}{2}(\nu+2)\log\left(1+\frac{x_1^2+x_2^2-2\rho x_2 x_1}{\nu\left(1-\rho^2\right)}\right) \\ = & \log\left(\Gamma\left(\frac{\nu}{2}\right)\right)+\log\left(\Gamma\left(\frac{\nu+2}{2}\right)\right)-\frac{1}{2}\log\left(1-\rho^2\right)-2\log\left(\Gamma\left(\frac{\nu+1}{2}\right)\right) \\ & +\frac{\nu+1}{2}\left[\log\left(\frac{\nu+x_1^2}{\nu}\right)+\log\left(\frac{\nu+x_2^2}{\nu}\right)\right] \\ & -\frac{1}{2}(\nu+2)\log\left(\frac{\nu\left(1-\rho^2\right)+x_1^2+x_2^2-2\rho x_2 x_1}{\nu\left(1-\rho^2\right)}\right) \\ = & \log\left(\Gamma\left(\frac{\nu}{2}\right)\right)+\log\left(\Gamma\left(\frac{\nu+2}{2}\right)\right)-\frac{1}{2}\log\left(1-\rho^2\right)-2\log\left(\Gamma\left(\frac{\nu+1}{2}\right)\right) \\ & +\frac{\nu+1}{2}\left[\log\left(\nu+x_1^2\right)+\log\left(\nu+x_2^2\right)-2\log(\nu)\right] \\ & -\frac{1}{2}(\nu+2)\left(\log\left(\nu\left(1-\rho^2\right)+x_1^2+x_2^2-2\rho x_2 x_1\right)-\log\left(\nu\left(1-\rho^2\right)\right)\right). \end{aligned}$$

The score of the log-likelihood is therefore given as:

$$
\begin{aligned}
\nabla_t = \frac{\partial \log c_t}{\partial \rho} =& -\frac{1}{2}\frac{1}{1-\rho^2}\left(-2\rho\right) \\
& -\frac{1}{2}\left(\nu+2\right)\left[\frac{1}{\nu\left(1-\rho^2\right)+x_1^2+x_2^2-2\rho x_2 x_1}\left(-2\nu\rho-2x_2x_1\right)-\frac{1}{\nu\left(1-\rho^2\right)}\left(-2\rho\nu\right)\right] \\
=& \frac{\rho}{1-\rho^2}+\frac{1}{2}\left(\nu+2\right)\left[\frac{\left(2\nu\rho+2x_2x_1\right)}{\nu\left(1-\rho^2\right)+x_1^2+x_2^2-2\rho x_2x_1}-\frac{2\rho}{1-\rho^2}\right] \\
=& \frac{\rho}{1-\rho^2}-\left(\nu+2\right)\frac{\rho}{1-\rho^2}+\frac{\left(\nu+2\right)\left(\nu\rho+x_2x_1\right)}{\nu\left(1-\rho^2\right)+x_1^2+x_2^2-2\rho x_2x_1} \\
=& \frac{-\left(1+\nu\right)\rho}{1-\rho^2}+\frac{\left(\nu+2\right)\left(\nu\rho+x_2x_1\right)}{\nu\left(1-\rho^2\right)+x_1^2+x_2^2-2\rho x_2x_1} \\
=& \frac{-\left(1+\nu\right)\rho\left(\nu\left(1-\rho^2\right)+x_1^2+x_2^2-2\rho x_2x_1\right)+\left(1-\rho^2\right)\left(\nu+2\right)\left(\nu\rho+x_2x_1\right)}{\left(1-\rho^2\right)\left(\nu\left(1-\rho^2\right)+x_1^2+x_2^2-2\rho x_2x_1\right)} \\
=& \frac{-\left(1+\nu\right)\rho\nu\left(1-\rho^2\right)-\rho\left(1+\nu\right)\left(x_1^2+x_2^2\right)+2\left(1+\nu\right)\rho^2x_2x_1}{\left(1-\rho^2\right)\left(\nu\left(1-\rho^2\right)+x_1^2+x_2^2-2\rho x_2x_1\right)} \\
& +\frac{\left(1-\rho^2\right)\nu\left(\nu\rho+x_2x_1\right)+2\left(1-\rho^2\right)\left(\nu\rho+x_2x_1\right)}{\left(1-\rho^2\right)\left(\nu\left(1-\rho^2\right)+x_1^2+x_2^2-2\rho x_2x_1\right)} \\
=& \frac{\left[2\nu\rho+\rho\nu^2-\left(\rho\nu+\rho\nu^2\right)\right]\left(1-\rho^2\right)-\left(1+\nu\right)\rho\left(x_1^2+x_2^2\right)}{\left(1-\rho^2\right)\left(\nu\left(1-\rho^2\right)+x_1^2+x_2^2-2\rho x_2x_1\right)} \\
& +\frac{x_2x_1\left[2\rho^2+2\nu\rho^2+\nu-\nu\rho^2+2-2\rho^2\right]}{\left(1-\rho^2\right)\left(\nu\left(1-\rho^2\right)+x_1^2+x_2^2-2\rho x_2x_1\right)} \\
=& \frac{\left(\nu\rho^2+\nu+2\right)x_2x_1-\left(1+\nu\right)\rho\left(x_1^2+x_2^2\right)+\left(1-\rho^2\right)\rho\nu}{\left(1-\rho^2\right)\left(\nu\left(1-\rho^2\right)+x_1^2+x_2^2-2\rho x_2x_1\right)} \\
=& \frac{\left(\nu\rho^2+\nu+2\right)y-\left(1+\nu\right)\rho x+\left(1-\rho^2\right)\rho\nu}{\left(1-\rho^2\right)\left(\nu\left(1-\rho^2\right)+x-2\rho y\right)},
\end{aligned}
$$

where $y = x_1x_2$ and $x = x_1^2 + x_2^2$.

The Clayton copula has density [172]:

$$
c_{Cl}\left(u_1,u_2\right) = \left(\theta+1\right)\left(u_1u_2\right)^{-\left(\theta+1\right)}\left(u_1^{-\theta}+u_2^{-\theta}-1\right)^{-\left(\frac{1}{\theta}+2\right)}, \tag{B.9}
$$

where u_1 and u_2 are the PIT.

So the log-likelihood is:

$$\begin{aligned}
\log c_{Cl}(u_1,u_2) &= \log(\theta+1) - (\theta+1)\log(u_1u_2) - \left(\frac{1}{\theta}+2\right)\log\left(u_1^{-\theta}+u_2^{-\theta}-1\right) \\
&= \log(\theta+1) - (\theta+1)\log(u_1u_2) - \frac{1}{\theta}\log\left(u_1^{-\theta}+u_2^{-\theta}-1\right) - 2\log\left(u_1^{-\theta}+u_2^{-\theta}-1\right) \\
&= \log(\theta+1) - (\theta+1)\log(u_1u_2) - \frac{1}{\theta}\log\left(\frac{u_2^\theta+u_1^\theta-u_1^\theta u_2^\theta}{u_1^\theta u_2^\theta}\right) - 2\log\left(\frac{u_2^\theta+u_1^\theta-u_1^\theta u_2^\theta}{u_1^\theta u_2^\theta}\right) \\
&= \log(\theta+1) - (\theta+1)\log(u_1u_2) - \frac{1}{\theta}\left[\log\left(u_2^\theta+u_1^\theta-u_1^\theta u_2^\theta\right) - \theta\log(u_1u_2)\right] \\
&\quad - 2\left[\log\left(u_2^\theta+u_1^\theta-u_1^\theta u_2^\theta\right) - \theta\log(u_1u_2)\right] \\
&= \log(\theta+1) + (1-\theta-1+2\theta)\log(u_1u_2) - \frac{1}{\theta}\log\left(u_2^\theta+u_1^\theta-u_1^\theta u_2^\theta\right) \\
&\quad - 2\log\left(u_2^\theta+u_1^\theta-u_1^\theta u_2^\theta\right) \\
&= \log(\theta+1) + \theta\log(u_1u_2) - \frac{1}{\theta}\log\left(u_2^\theta+u_1^\theta-u_1^\theta u_2^\theta\right) - 2\log\left(u_2^\theta+u_1^\theta-u_1^\theta u_2^\theta\right).
\end{aligned}$$

The score of the log-likelihood is given by [172, Supplementary material]:

$$\nabla_{Cl} = \frac{c_{Cl}^N}{c_{Cl}^D}, \tag{B.10}$$

where

$$\begin{aligned}
c_{Cl}^N =& -\theta\left(2\theta^2+3\theta+1\right)\left(u_1^\theta\log(u_2)+u_2^\theta\log(u_1)\right) \\
&-\left(u_1^\theta\left(u_2^\theta-1\right)-(u_2)^\theta\right)\cdot\left(-\theta^2+(\theta+1)\,\theta^2\log(u_1u_2)-(\theta+1)\log\left(u_1^{-\theta}u_2^{-\theta}-1\right)\right) \\
c_{CL}^D =& \theta^2(\theta+1)\left(u_1^\theta\left(u_2^\theta-1\right)-u_2^\theta\right).
\end{aligned}$$

The Gumbel copula has density:

$$\begin{aligned}
c_{Gu}(u_1,u_2) =& \frac{1}{u_1u_2}\exp\left\{-\left((-\log u_1)^\theta+(-\log u_2)^\theta\right)^{\frac{1}{\theta}}\right\}\left[(-\log u_1)^\theta+(-\log u_2)^\theta\right]^{\frac{2}{\theta}-2} \\
&\times\left[1+(\theta-1)\left((-\log u_1)^\theta+(-\log u_2)^\theta\right)^{-\frac{1}{\theta}}\right]\times(\log u_1\log u_2)^{\theta-1}.
\end{aligned}$$

So the log-likelihood is:

$$\begin{aligned}
\log c_{Gu}(u_1,u_2) =& -\log(u_1u_2) - \left((-\log u_1)^\theta+(-\log u_2)^\theta\right)^{\frac{1}{\theta}} + \left(\frac{2}{\theta}-2\right)\left((-\log u_1)^\theta+(-\log u_2)^\theta\right) \\
&+\log\left(1+(\theta-1)\left((-\log u_1)^\theta+(-\log u_2)^\theta\right)^{-\frac{1}{\theta}}\right)+(\theta-1)\log(\log u_1\log u_2).
\end{aligned}$$

The Gumbel score is quite complicated and therefore the expression is omitted.

B.3 MAPPING FUNCTIONS COPULAS

The mapping function for the Clayton copula is given by ($\theta_t \in (0, \infty)$):

$$\theta_t = \exp\left(\tilde{f}_t\right) \iff \tilde{f}_t = \log\left(\theta_t\right), \tag{B.11}$$

The Jacobian is given by:

$$\frac{\partial \theta_t}{\partial \tilde{f}_t} = \frac{\partial \exp\left(\tilde{f}_t\right)}{\partial \tilde{f}_t} = \exp\left(\tilde{f}_t\right). \tag{B.12}$$

The mapping function for the Gumbel copula is given by ($\theta_t \in (1, \infty)$):

$$\theta_t = 1 + \exp\left(\tilde{f}_t\right) \iff \tilde{f}_t = \log\left(\theta_t - 1\right). \tag{B.13}$$

The Jacobian is given by:

$$\frac{\partial \theta_t}{\partial \tilde{f}_t} = \frac{\partial \left(1 + \exp\left(\tilde{f}_t\right)\right)}{\partial \tilde{f}_t} = \exp\left(\tilde{f}_t\right). \tag{B.14}$$

For the correlation parameter for the Gaussian and Student's t copulas we use the same mapping function as [153] namely:

$$\rho_t = \frac{1 - \exp\{-\tilde{f}_t\}}{1 + \exp\{-\tilde{f}_t\}} \iff \tilde{f}_t = \log\left(1 + \rho_t\right) - \log\left(1 - \rho_t\right). \tag{B.15}$$

The Jacobian is given by:

$$\frac{\partial \rho_t}{\partial \tilde{f}_t} = \exp\{-\tilde{f}_t\}\left(1 + \exp\{-\tilde{f}_t\}\right)^{-1} + \left(1 - \exp\{-\tilde{f}_t\}\right)\left(1 + \exp\{-\tilde{f}_t\}\right)^{-2}\exp\{-\tilde{f}_t\} \tag{B.16}$$

$$= \exp\{-\tilde{f}_t\}\left[\frac{1 + 1 - \exp\{-\tilde{f}_t\}}{\left(1 + \exp\{-\tilde{f}_t\}\right)^2}\right] \tag{B.17}$$

$$= \exp\{-\tilde{f}_t\}\left[\frac{2 - \exp\{-\tilde{f}_t\}}{\left(1 + \exp\{-\tilde{f}_t\}\right)^2}\right]. \tag{B.18}$$

For the degrees of freedom parameter ν for the Student's t copula we use the modified logistic transformation [167] to ensure $\nu \in (a, b)$:

$$\nu_t = a + \frac{b - a}{1 + \exp\left(-\tilde{f}_t\right)} \iff \tilde{f}_t = \log\left(\frac{\nu_t - a}{b - \nu_t}\right). \tag{B.19}$$

We follow [167] and set $a = 4$ and $b = 50$.

Since we do not consider time–varying degrees of freedom we do not need the Jacobian and therefore we do not report it. It can be found by differentiation.

C

Supplementary material

C.1 CARBON INTENSITIES

Carbon emission intensities are derived from the ecoinvent 3.4 database [120]. For each of the EU28 we calculate technology-specific factors extracted from the high-voltage level (for most technologies) and low-voltage level (for photovoltaic technologies), to generate their lifecycle carbon intensities in grams of CO_2 equivalents per kilowatthour. Furthermore, we also differentiate infrastructure-related impacts from operational impacts. This is done by grouping life cycle inventory inputs by unit, where the set {'meter', 'meter-year', 'unit', 'kilometer'} are assumed to denote infrastructure processes, whereas the rest, that is, 'kilowatthour', 'tonne-kilometer', etc., are accounted as operation and maintenance processes.

The values under "high-voltage mix" denote the global warming potential (GWP) score of the electricity mix directly from high-voltage technologies, while "low-voltage mix" values denote the GWP score of electricity at the consumer level, i.e. after transformation and distribution from high and medium-voltage (including losses), and integration of photovoltaic electricity into the grid. The high- and low-voltage GWP scores are extracted directly from ecoinvent 3.4, here only shown for information, and never used in the calculations.

Not all technology-area pairs are available in the database, in case of missing information, values have been proxied by the EU28 average intensity for the given technology, calculated from the areas for which the data exists, and weighted by their respective contribution to the EU28 mix. When the production source is unknown we assume an intensity averaged over the particular country's intensity for gas, oil and coal.

Table C.1–C.3 show the country-specific lifecycle, infrastructure, and operation intensities per technology in units of g CO_2 eq./kWh. EU28 averages are also

shown, in bold. The relation between the three tables is such that lifecycle = infrastructure + operation. The operation intensities in Table C.3 are the basis for the production as well as consumption-based carbon allocation in this study.

Table C.1: Lifecycle CO_2 equivalent intensity per technology and country, in g CO_2 eq./kWh. Values in italic indicate that the country-specific factor is not available, and was replaced by the European weighted average for that technology (shown in bold).

		AT	BE	BG	CZ	DE	DK	EE	ES	EU28	FI	FR	GB	GR	HU	IE	IT	LT	LV	ME	NL	NO	PL	PT	RO	RS	SE	SI	SK
category	**variant**																												
high-voltage mix	-	125	188	609	731	654	432	1030	336	**426**	262	41.9	801	980	400	513	469	551	520	*426*	616	15.9	1000	360	398	852	21.8	434	216
wind	-	17.8	16.2	19.5	19.4	20.0	13.8	19.8	14.2	**16.8**	23.0	15.6	*16.8*	15.1	13.6	13.7	19.7	13.3	18.2	*16.8*	16.3	14.4	16.5	13.7	25.3	*16.8*	16.2	*16.8*	*16.8*
nuclear	-	*12.4*	12.0	12.0	12.0	11.3	*12.4*	*12.4*	12.1	**12.4**	12.5	12.9	*12.4*	*12.4*	12.0	*12.4*	*12.4*	*12.4*	*12.4*	*12.4*	12.0	*12.4*	*12.4*	*12.4*	14.2	*12.4*	12.2	12.0	12.0
geothermal	-	*81.8*	*81.8*	*81.8*	*81.8*	81.8	*81.8*	*81.8*	*81.8*	**81.8**	*81.8*	*81.8*	*81.8*	*81.8*	*81.8*	*81.8*	81.8	*81.8*	*81.8*	*81.8*	*81.8*	*81.8*	*81.8*	81.8	*81.8*	*81.8*	*81.8*	*81.8*	*81.8*
biomass	**cogeneration**	53.8	53.8	56.8	53.8	53.8	53.8	56.8	53.8	**53.9**	53.8	53.8	53.8	*53.9*	53.8	53.8	53.8	56.8	56.8	*53.9*	53.8	*53.9*	53.8	53.8	53.8	*53.9*	53.8	53.8	53.8
hydropower	**pumped storage**	452	378	901	1140	965	*617*	*617*	546	**617**	*617*	*77.3*	*617*	1420	*617*	851	615	1040	*617*	*617*	*617*	41.7	1420	588	629	1220	*617*	617	684
	reservoir	6.97	*14.7*	*14.7*	51.4	51.4	*14.7*	*14.7*	51.4	**14.7**	51.4	6.97	*14.7*	*14.7*	*14.7*	*14.7*	6.97	*14.7*	*14.7*	*14.7*	*14.7*	6.97	*14.7*	51.4	*14.7*	6.97	51.4	*14.7*	51.4
	run-of-river	4.42	4.42	4.42	4.42	4.42	4.42	*4.42*	4.42	**4.42**	4.42	4.42	*4.42*	4.42	4.42	4.42	4.42	*4.42*	*4.42*	*4.42*	4.42	*4.42*	4.42	4.42	4.42	4.42	4.42	4.42	4.42
coal	-	986	1120	1180	1190	1170	*1160*	1300	1210	**1160**	1080	1090	1140	1300	1410	1070	1150	1180	*1160*	*1160*	1030	*1160*	*1160*	1140	1140	1340	1180	1200	*1160*
	cogeneration	1220	*1210*	1250	1710	1170	1050	*1210*	*1210*	**1210**	1100	*1210*	*1210*	1560	1240	*1210*	1260	*1210*	*1210*	*1210*	998	1490	1160	*1210*	1240	1240	1370	1250	1530
gas	-	614	472	746	697	533	*513*	*513*	492	**513**	839	588	521	682	750	462	532	*513*	*513*	*513*	465	407	*513*	441	615	*513*	*513*	1090	694
	cogeneration	529	503	936	840	351	455	423	173	**475**	530	671	*475*	173	648	173	496	629	599	*475*	450	523	542	*475*	686	810	555	436	652
oil	-	1160	913	1670	1060	877	1240	1180	866	**1020**	447	953	1320	993	1130	919	1060	*1020*	*1020*	*1020*	*1020*	*1020*	*1020*	834	1000	*1020*	854	1390	960
	cogeneration	959	854	965	1520	680	965	873	*935*	**935**	952	*770*	*935*	1080	873	*935*	904	1530	*935*	*935*	1080	*935*	880	610	1260	*935*	837	873	1400
low-voltage mix	-	323	239	675	794	657	393	921	369	**446**	244	54.9	805	973	487	588	443	729	780	738	610	30.5	1030	400	474	940	42.3	447	458
solar	-	107	112	*77.9*	118	110	*94.6*	*94.6*	71.4	**94.6**	*94.6*	90.9	*94.6*	76.3	*94.6*	*94.6*	81.3	109	*94.6*	*94.6*	109	*94.6*	*94.6*	69.3	88.1	82.8	110	83.0	90.7

Table C.2: CO_2 equivalent intensity per technology and country, embodied in infrastructure, in g CO_2 eq./kWh. Values in italic indicate that the country-specific factor is not available, and was replaced by the European weighted average for that technology (shown in bold).

		AT	BE	BG	CZ	DE	DK	EE	ES	**EU28**	FI	FR	GB	GR	HU	IE	IT	LT	LV	ME	NL	NO	PL	PT	RO	RS	SE	SI	SK
category	**variant**																												
high-voltage mix	-	5.48	3.10	3.10	2.39	4.49	7.41	3.64	5.23	**4.04**	3.16	3.02	1.18	3.60	2.63	4.17	6.18	6.17	3.80	*4.04*	2.40	6.55	2.82	6.66	5.42	3.36	4.41	2.32	2.56
wind	-	17.6	16.1	19.4	19.2	19.8	13.7	19.6	14.0	**16.7**	22.8	15.5	*16.7*	15.0	13.5	13.6	19.5	13.2	18.0	*16.7*	16.2	14.2	16.4	13.6	25.2	*16.7*	16.1	*16.7*	*16.7*
nuclear	-	*2.10*	1.93	1.93	1.93	1.89	*2.10*	*2.10*	1.95	**2.10**	1.99	2.27	*2.10*	*2.10*	1.93	*2.10*	*2.10*	*2.10*	*2.10*	*2.10*	1.93	*2.10*	*2.10*	*2.10*	1.86	*2.10*	1.96	1.93	1.93
geothermal	-	*81.8*	*81.8*	*81.8*	*81.8*	81.8	*81.8*	*81.8*	*81.8*	**81.8**	*81.8*	*81.8*	*81.8*	*81.8*	*81.8*	*81.8*	81.8	*81.8*	*81.8*	*81.8*	*81.8*	*81.8*	*81.8*	81.8	*81.8*	*81.8*	*81.8*	*81.8*	*81.8*
biomass	**cogeneration**	3.40	3.40	3.40	3.40	3.40	3.40	3.40	3.40	**3.40**	3.40	3.40	3.40	*3.40*	3.40	3.40	3.40	3.40	3.40	*3.40*	3.40	*3.40*	3.40	3.40	3.40	*3.40*	3.40	3.40	3.40
hydropower	**pumped storage**	6.52	6.52	6.52	6.52	6.52	*6.52*	*6.52*	6.52	**6.52**	*6.52*	6.52	*6.52*	6.52	*6.52*	6.52	6.52	6.52	*6.52*	*6.52*	*6.52*	6.52	6.52	6.52	6.52	6.52	*6.52*	6.52	6.52
	reservoir	6.52	*6.52*	*6.52*	6.52	6.52	*6.52*	*6.52*	6.52	**6.52**	6.52	6.52	*6.52*	*6.52*	*6.52*	*6.52*	6.52	*6.52*	*6.52*	*6.52*	*6.52*	6.52	*6.52*	6.52	*6.52*	6.52	6.52	*6.52*	6.52
	run-of-river	4.39	4.39	4.39	4.39	4.39	4.39	*4.39*	4.39	**4.39**	4.39	4.39	*4.39*	4.39	4.39	4.39	4.39	*4.39*	*4.39*	*4.39*	4.39	*4.39*	4.39	4.39	4.39	4.39	4.39	4.39	4.39
coal	-	1.37	1.58	2.41	2.46	2.13	*1.96*	2.34	1.69	**1.96**	1.87	1.58	1.55	2.38	3.01	1.84	1.57	2.40	*1.96*	*1.96*	1.46	*1.96*	*1.96*	1.56	2.45	2.82	2.40	2.59	*1.96*
	cogeneration	1.17	*1.82*	1.82	1.66	1.34	1.43	*1.82*	*1.82*	**1.82**	1.20	*1.82*	*1.82*	2.37	2.25	*1.82*	1.42	*1.82*	*1.82*	*1.82*	1.58	1.25	1.87	*1.82*	2.25	2.25	1.02	2.24	1.96
gas	-	0.916	0.927	0.469	0.559	0.818	*0.721*	*0.721*	1.15	**0.721**	1.82	1.25	0.354	1.08	0.962	0.880	0.964	*0.721*	*0.721*	*0.721*	0.809	0.704	*0.721*	1.15	0.386	*0.721*	*0.721*	0.688	0.878
	cogeneration	2.30	2.48	4.96	4.35	4.31	3.35	4.00	5.69	**3.19**	2.56	3.79	*3.19*	5.69	2.85	5.69	2.78	3.37	3.02	*3.19*	1.89	2.32	1.88	*3.19*	3.57	4.31	3.71	3.91	2.54
oil	-	2.64	2.08	3.75	2.39	1.99	2.76	2.65	1.94	**2.27**	1.02	2.14	2.97	2.19	2.60	2.06	2.32	*2.27*	*2.27*	*2.27*	*2.27*	*2.27*	*2.27*	1.89	2.24	*2.27*	1.95	3.12	2.16
	cogeneration	2.19	1.94	2.17	3.42	1.54	2.15	1.96	*2.08*	**2.08**	2.18	1.73	*2.08*	2.37	1.96	*2.08*	1.98	3.42	*2.08*	*2.08*	2.53	*2.08*	1.98	1.39	2.89	*2.08*	1.91	1.96	3.14
low-voltage mix	-	4.54	2.99	6.18	7.71	13.8	2.97	2.95	6.76	**6.41**	2.99	3.66	2.96	12.1	2.95	2.96	13.0	4.02	2.97	2.91	3.01	2.97	2.97	3.68	5.88	2.93	3.03	3.03	3.44
solar	-	107	112	77.9	118	110	*94.6*	*94.6*	71.4	**94.6**	*94.6*	90.9	*94.6*	76.3	*94.6*	*94.6*	81.3	109	*94.6*	*94.6*	109	*94.6*	*94.6*	69.2	88.1	82.7	110	83.0	90.7

Table C.3: CO_2 equivalent intensity per technology and country, embodied in operations, in g CO_2 eq./kWh. Values in italic indicate that the country-specific factor is not available, and was replaced by the European weighted average for that technology (shown in bold).

category	variant	AT	BE	BG	CZ	DE	DK	EE	ES	**EU28**	FI	FR	GB	GR	HU	IE	IT	LT	LV	ME	NL	NO	PL	PT	RO	RS	SE	SI	SK
high-voltage mix	-	119	185	606	729	649	425	1030	331	**422**	259	38.8	800	976	397	509	463	545	516	*422*	614	9.38	998	354	392	848	17.4	432	214
wind	-	0.149	0.156	0.149	0.166	0.165	0.126	0.165	0.122	**0.142**	0.156	0.133	*0.142*	0.121	0.114	0.116	0.161	0.110	0.159	*0.142*	0.133	0.120	0.140	0.117	0.192	*0.142*	0.141	*0.142*	*0.142*
nuclear	-	*10.3*	10.1	10.1	10.1	9.37	*10.3*	*10.3*	10.2	**10.3**	10.5	10.6	*10.3*	*10.3*	10.1	*10.3*	*10.3*	*10.3*	*10.3*	*10.3*	10.1	*10.3*	*10.3*	*10.3*	12.3	*10.3*	10.3	10.1	10.1
geothermal	-	*0.00664*	*0.00664*	*0.00664*	*0.00664*	0.00664	*0.00664*	*0.00664*	*0.00664*	**0.00664**	*0.00664*	*0.00664*	*0.00664*	*0.00664*	*0.00664*	*0.00664*	0.00664	*0.00664*	*0.00664*	*0.00664*	*0.00664*	*0.00664*	*0.00664*	0.00664	*0.00664*	*0.00664*	*0.00664*	*0.00664*	*0.00664*
biomass	**cogeneration**	50.4	50.4	53.4	50.4	50.4	50.4	53.4	50.4	**50.5**	50.4	50.4	50.4	*50.5*	50.4	50.4	50.4	53.4	53.4	*50.5*	50.4	*50.5*	50.4	50.4	50.4	*50.5*	50.4	50.4	50.4
hydropower	**pumped storage**	445	372	894	1140	958	*611*	*611*	539	**611**	*611*	70.8	*611*	1410	*611*	845	608	1030	*611*	*611*	*611*	35.2	1410	582	622	1210	*611*	610	678
	reservoir	0.445	*8.13*	*8.13*	44.8	44.8	*8.13*	*8.13*	44.8	**8.13**	44.8	0.445	*8.13*	*8.13*	*8.13*	*8.13*	0.445	*8.13*	*8.13*	*8.13*	*8.13*	0.445	*8.13*	44.8	*8.13*	0.445	44.8	*8.13*	44.8
	run-of-river	0.0253	0.0253	0.0253	0.0253	0.0253	0.0253	*0.0253*	0.0253	**0.0253**	0.0253	0.0253	*0.0253*	0.0253	0.0253	0.0253	0.0253	*0.0253*	*0.0253*	*0.0253*	0.0253	*0.0253*	0.0253	0.0253	0.0253	0.0253	0.0253	0.0253	0.0253
coal	-	984	1120	1180	1180	1160	*1160*	1300	1210	**1160**	1080	1090	1140	1300	1400	1070	1150	1170	*1160*	*1160*	1030	*1160*	*1160*	1140	1140	1340	1170	1190	*1160*
	cogeneration	1220	*1210*	1250	1710	1160	1050	*1210*	*1210*	**1210**	1100	*1210*	*1210*	1560	1230	*1210*	1260	*1210*	*1210*	*1210*	996	1490	1160	*1210*	1230	1230	1370	1240	1530
gas	-	613	471	745	696	533	*513*	*513*	491	**513**	837	587	521	681	749	461	531	*513*	*513*	*513*	464	406	*513*	440	615	*513*	*513*	1090	694
	cogeneration	527	501	932	835	347	452	419	167	**471**	528	668	*471*	167	645	167	493	625	596	*471*	449	520	540	*471*	682	805	551	432	649
oil	-	1150	911	1660	1060	875	1240	1180	864	**1010**	446	951	1320	990	1130	917	1060	*1010*	*1010*	*1010*	*1010*	*1010*	*1010*	832	997	*1010*	852	1380	958
	cogeneration	957	852	962	1520	678	963	871	*933*	**933**	949	768	*933*	1070	871	*933*	902	1530	*933*	*933*	1070	*933*	878	609	1250	*933*	835	871	1390
low-voltage mix	-	319	236	669	786	643	390	918	362	**440**	241	51.2	802	961	484	585	430	725	*777*	735	607	27.5	1030	396	468	937	39.3	444	455
solar	-	0.00580	0.00502	0.00423	0.00642	0.00448	*0.00349*	*0.00349*	0.00234	**0.00349**	*0.00349*	0.00370	*0.00349*	0.00415	*0.00349*	*0.00349*	0.00166	0.00591	*0.00349*	*0.00349*	0.00591	*0.00349*	*0.00349*	0.00185	0.00478	0.00445	0.00565	0.00453	0.00493

C.2 FLOW TRACING

C.2.1 Formulation

Nomenclature

α set of all generation/storage technologies.

L_n nodal load.

$F_{n\to k}$ nodal outflow to direct neighbors.

$F_{m\to n}$ nodal inflow from direct neighbors.

$G_{n,\alpha}$ nodal generation for all technologies.

$S^+_{n,\alpha}$ storage discharge for each storage technology α at node n.

S^-_n sum of storage charging at node n.

$q_{n,\alpha}$ nodal colormix.

The nodal color mix refers to the mixing of electricity at each node from different technologies and countries of origin, where each technology for each country has been assigned a unique color [43]. Note that this is an assumption, analogous to the mixing of water flows in pipes, used to approximate the mixing of power flows at nodes in the transmission system.

Figure C.1 shows a sketch of the flow tracing implementation. For every hour all imports, generation, and storage discharge are mixed equally in the node, which then determines the color mix of the exports and the power serving the local load. We do not keep track of the color mix flowing into storage, but track which storage type the power originated from when the storages are discharging. This mixing approach is called *average participation* or *proportional sharing* in the literature which was also proposed initially in [40]. For a discussion of different allocation methods, see [44]. For comprehensive reviews, see [50, 51].

The sketch in Figure C.1 describes the nodal power balance

$$L_n + S^-_n + \sum_k F_{n\to k} = \sum_\alpha \left(G_{n,\alpha} + S^+_{n,\alpha}\right) + \sum_m F_{m\to n}, \tag{C.1}$$

where the left-hand side and the right-hand side account for the flows out of and into a node, respectively. In this, and following equations, there is an implicit

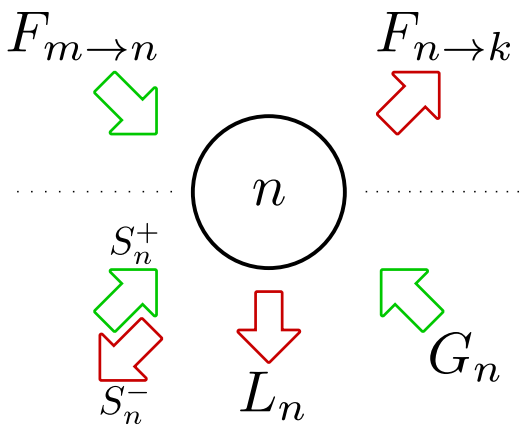

Figure C.1: Sketch of flow tracing methodology.

time index as the flow tracing is performed for every hour. We include nodal color mixes in the nodal power balance

$$q_{n,\alpha}\left(L_n + S_n^- + \sum_k F_{n\to k}\right) = G_{n,\alpha} + S_{n,\alpha}^+ + \sum_m q_{m,\alpha} F_{m\to n}, \tag{C.2}$$

which is now an equation per country n per technology type α. Rearranging Equation (C.2) we can write a matrix formula describing a unique solution for the nodal power mix $q_{n,\alpha}$ according to [46]:

$$\sum_m \left[\delta_{n,m}\left(L_m + S_m^- + \sum_k F_{m\to k}\right) - F_{m\to n}\right] q_{m,\alpha} = G_{n,\alpha} + S_{n,\alpha}^+. \tag{C.3}$$

Here $q_{m,\alpha}$ is the hourly nodal color mix for node m split into components for every technology for every country. The α set allows us to track originating technology as well as originating country e.g. we can trace who is consuming Danish wind power. Multiplying the nodal color mix with the nodal load and the carbon intensity of the originating generation/storage technologies allows us to calculate consumption-based carbon intensity allocation.

C.2.2 Handling of missing data

As we are using raw data directly from the power system there will be occurrences of missing values. In case of missing data for production or imports/-exports for a country the particular country is excluded from the flow tracing calculation for that specific hour.

Imports from countries not included in the topology are included (e.g. Switzerland), but do not have an effect on the nodal mix of the importer (they simply scale the color mix, but do not change the ratios). Exports to countries outside the considered topology are subtracted.

Figure C.2 shows $\sum_\alpha q_{n,\alpha}$ for every country for every hour. If Equation (C.3) is perfectly balanced it should be the case that $\sum_\alpha q_{n,\alpha} = 1$. Cases of partially missing data leads to $\sum_\alpha q_{n,\alpha} \neq 1$. This is usually caused by one country being excluded due to missing data (which explains the occurrence of 0's in Figure C.2), which affects the nodal balance of neighboring countries. See e.g. the effect of missing data for Ireland on Great Britain. We observe no cases of $\sum_\alpha q_{n,\alpha} > 1$. The missing data mostly occurs for small, satellite countries e.g. Ireland and Montenegro, which only have a small effect on the closest neighbors.

The total number of entries in Figure C.2:

$$hours \cdot nodes = 8760 \cdot 28 = 245280 \tag{C.4}$$

Of these there are 6367 occurrences of $q_{n,\alpha} = 0$ (due to missing data), which is only 2.6%. When the occurrences of 0 are subtracted there are 3742 occurrences where $q_{n,\alpha} < .9999$ which is only 1.5%. The cases where $0 < q_{n,\alpha} < .9999$ are all rather close to 1 (all except 3 are above .8 and most are above .9). The occurrences of 0 are predominantly for Ireland, Montenegro and Estonia, which are both small countries at the edge of the network.

C.3 ADDITIONAL RESULTS

Figure C.3 shows a comparison of hourly production intensity with hourly load for the full year of 2017 for every country. The production intensity is calculated based on the production within each country. The figure is split in two parts with large countries in the top panel and smaller countries in the bottom panel. In the top panel we see that Norway, Sweden and France have low intensities regardless of the level of consumption, which is due to a high share of hydro power in the Nordic countries and nuclear power in France. On the other hand, Poland has very high intensity due to a high share of coal power generation.

Figure C.4 shows the stacked average consumption intensity per kWh per hour in Austria for all of 2017. This figure does not tell anything about the amount of power being consumed by each technology.

Figure C.5 shows the total annual consumption intensity for Austria for 2017 based on flow tracing. From this figure we see that hydro is the technology

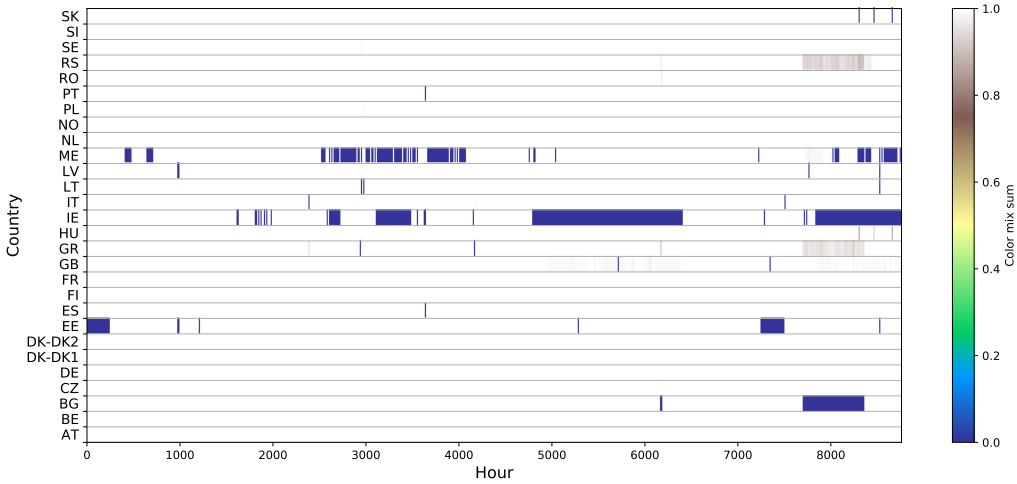

Figure C.2: Flow tracing consistency check. Dark blue means generation or import/export data is entirely missing for a country, lighter colors mean it is partially complete, and white means fully complete data.

providing most of the consumed power, but that the intensity from this consumption is among the lowest of the technologies. On the other hand coal power is one of the smaller contributors to the consumed power, but has the largest intensity.

Figure C.6 shows average hourly production/consumption carbon intensity plotted as duration curves for Austria and Denmark e.g. if a country runs on 100% coal the entire year the duration curve would be flat at that country's operational intensity for coal as seen in Table C.3. This figure shows that AT has a low production intensity, but a higher consumption intensity due to imports. DK is relying on imports for a low consumption intensity since it has a high production intensity for approximately half of the year.

Figure C.7 shows a comparison of average production (blue) and consumption (orange) intensity for each country. White dots mark the mean. The colored bars indicate 25%–75% quantiles and the gray bars 5%–95% quantiles. This is a summary of the duration curves for individual countries as shown in Figure C.6.

Figure C.8 shows the difference between production and consumption intensity as function of the share of non-fossil production of total production. Size of circles are proportional to average production. A value above zero corresponds to the country having a higher consumption intensity than production intensity. The

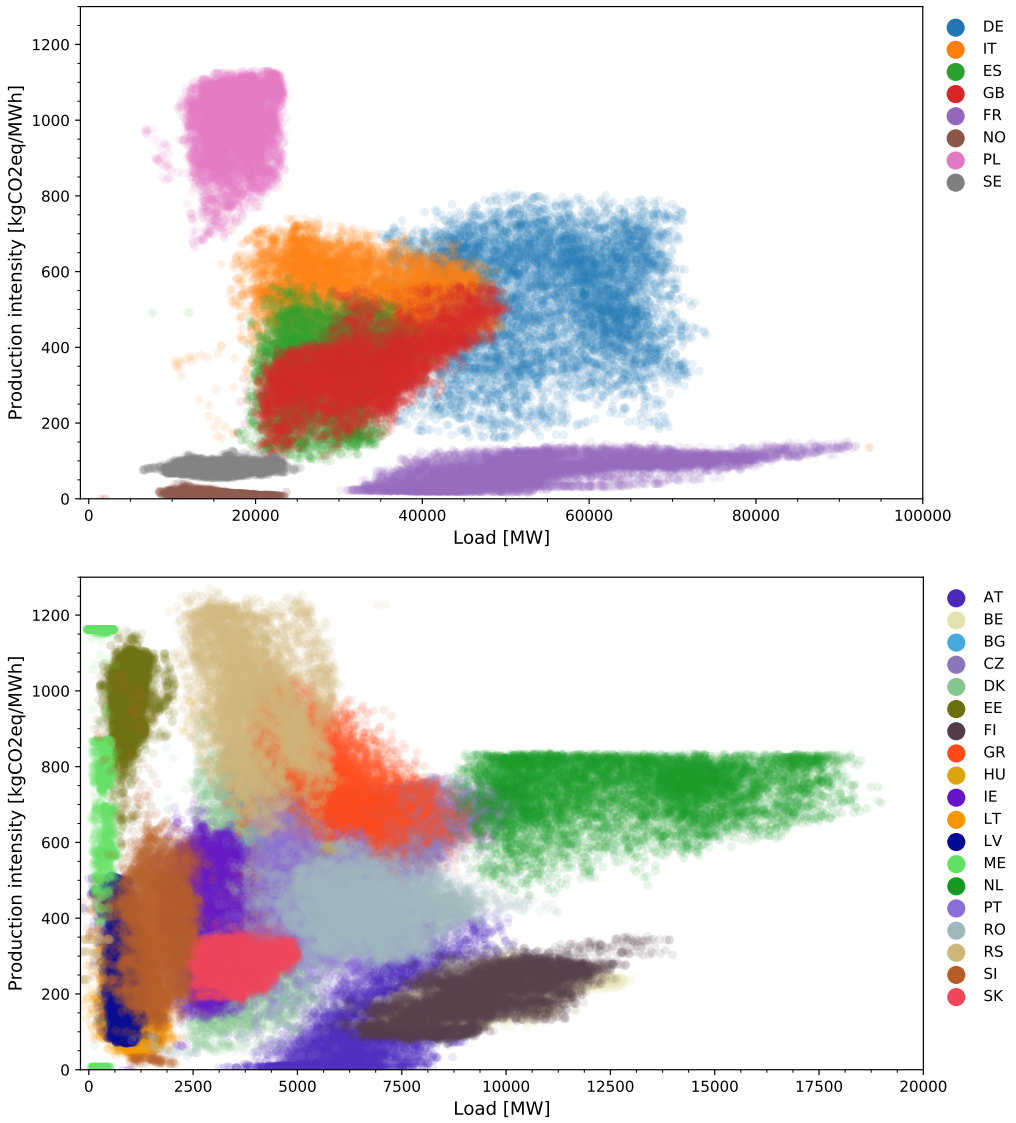

Figure C.3: Comparison of hourly production intensity with hourly load for every country.

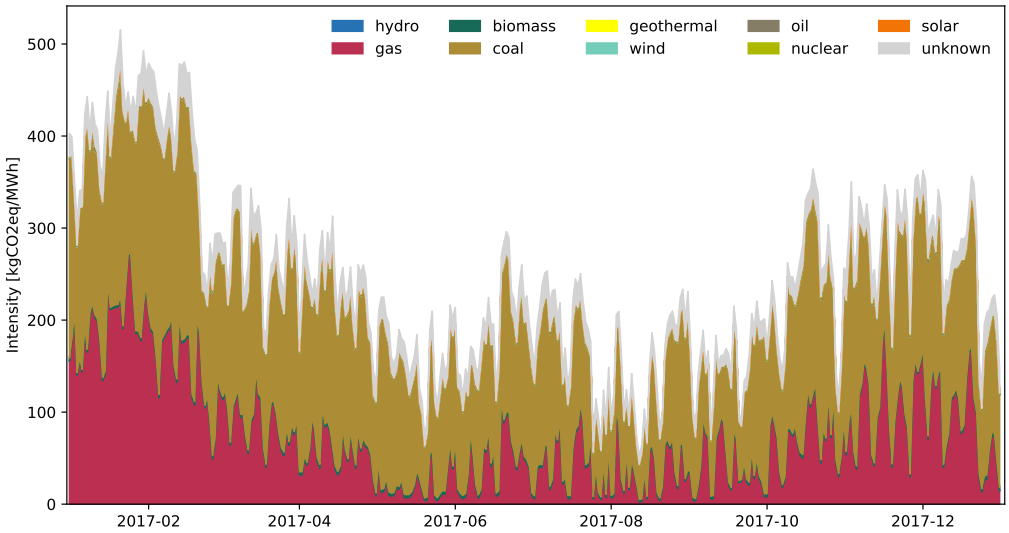

Figure C.4: Hourly intensity per consumed unit of energy for Austria downsampled to daily averages.

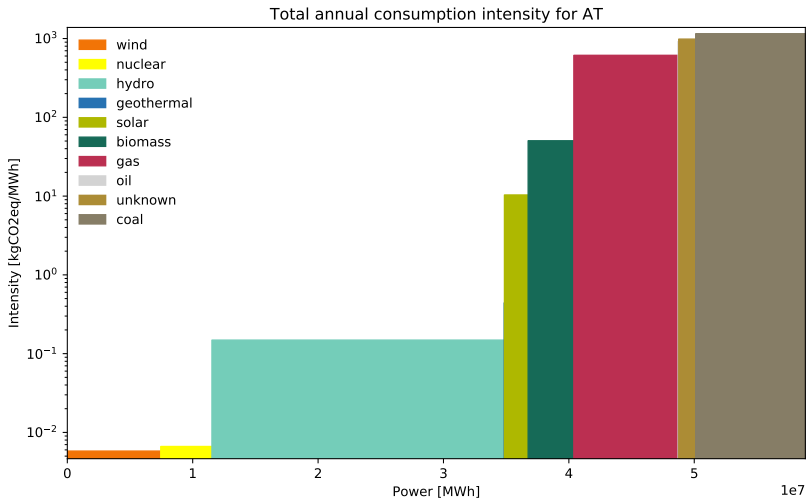

Figure C.5: Total annual consumption intensity for Austria for 2017.

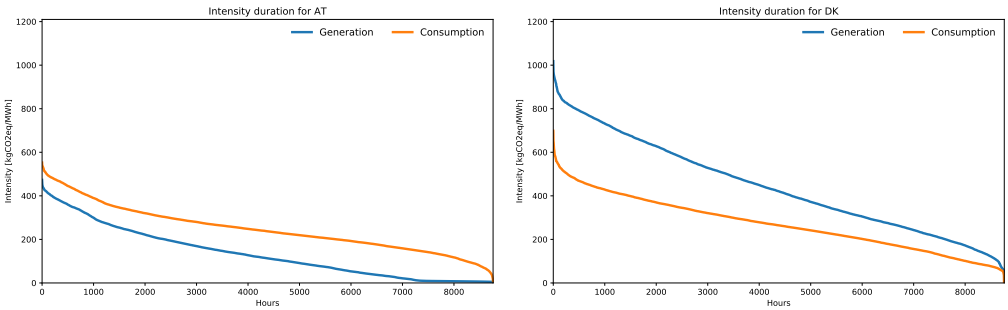

Figure C.6: Average hourly production/consumption carbon intensity duration curves for Austria and Denmark.

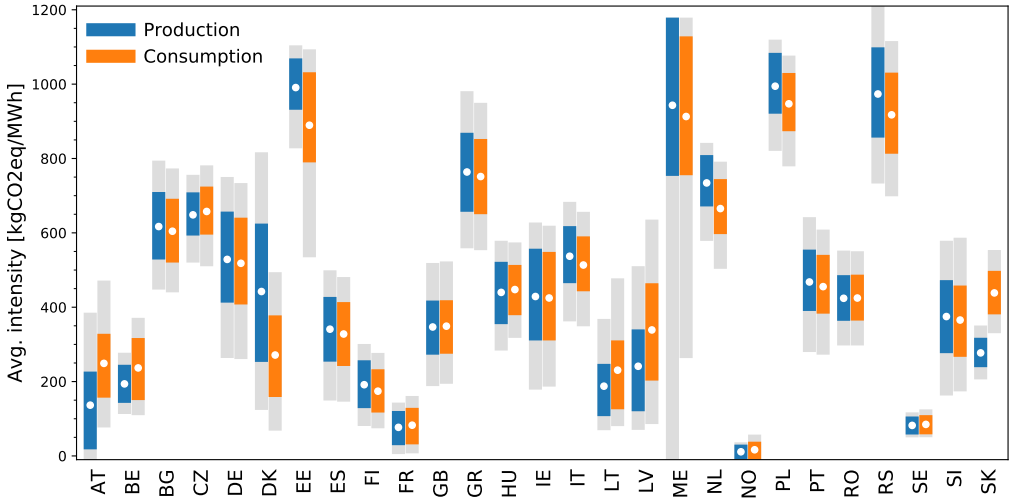

Figure C.7: Comparison of average production (blue) and consumption (orange) intensity. White dots mark the mean, colored bars 25%-75% quantiles and the gray bars 5%-95% quantiles.

figure shows a general trend that the higher the share of non-fossil production the higher the consumption intensity is compared to the production intensity. This can be explained by countries with high share of non-fossil production tend to import from countries with lower share of non-fossil production which results in the importing country's consumption intensity being higher than its production intensity.

Table C.4 shows average production and consumption intensity per country. These values are plotted in Figure 3 in the article, they are also shown as the white markers in Figure C.7, and the difference for each country is shown in Figure C.8.

Figure C.9 shows average intensity per imported/exported unit of energy. When calculating the average imported/exported intensity between two countries only hours with actual transfers have been used. A white entry means no data and only occurs for ME and RS. The figure should be read as NO exporting mostly low intensity hydro to all countries whereas EE and PL are exporting oil and coal to all countries. This figure doesn't say anything about the amount of energy being transferred e.g. most of the column for ME is based on data for very few hours as ME is a small, poorly connected country. The values in Figure C.9 are also shown in Table C.5.

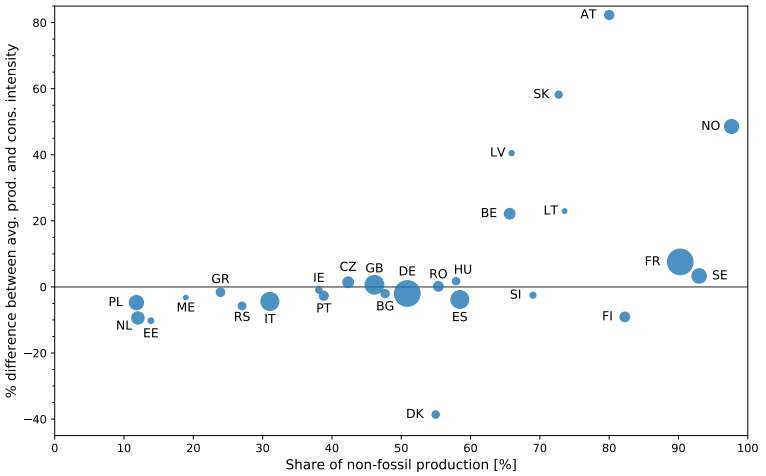

Figure C.8: Difference between production and consumption intensity as function of the share of non-fossil production of total production. Size of circles are proportional to average production.

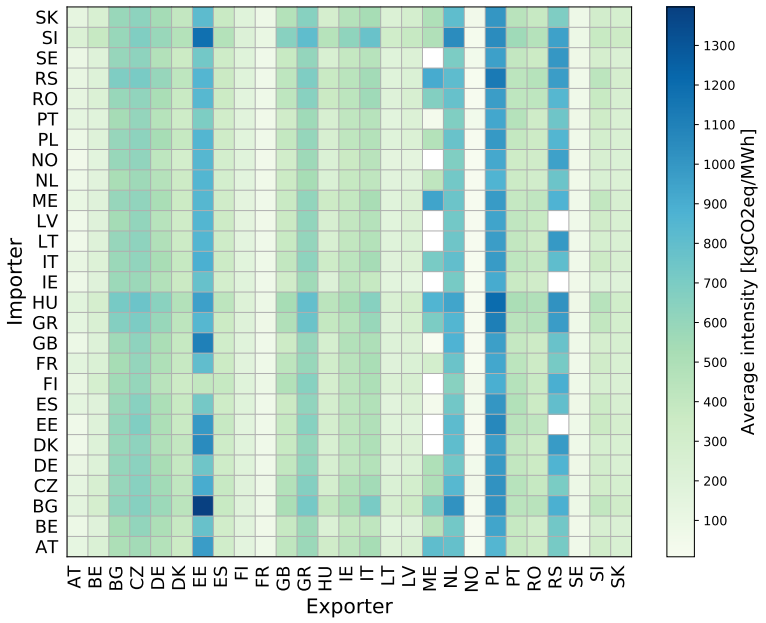

Figure C.9: Average imported/exported intensity. White cells indicating missing data. This figure doesn't say anything about the amount of energy being transferred e.g. most of the column for ME is based on data for very few hours as ME is a small, poorly connected country.

Table C.4: Average production and consumption intensity for each country. These values are plotted in Figure 3 in the article. Units are kgCO2eq/MWh.

	AT	BE	BG	CZ	DE	DK	EE	ES	FI	FR	GB	GR	HU	IE	IT	LT	LV	ME	NL	NO	PL	PT	RO	RS	SE	SI	SK
Consumption	248	236	604	657	518	271	889	327	174	82	349	751	447	424	513	230	338	912	665	16	947	455	424	917	84	365	438
Production	136	193	616	648	528	442	990	340	191	76	346	763	439	428	537	187	241	943	734	11	994	467	424	973	82	374	277

Table C.5: Average intensity of power imported and exported between countries. These values are plotted in Figure C.9. Columns are exporters and rows are importers. Units are kgCO2eq/MWh.

	AT	BE	BG	CZ	DE	DK	EE	ES	FI	FR	GB	GR	HU	IE	IT	LT	LV	ME	NL	NO	PL	PT	RO	RS	SE	SI	SK
AT	136	232	503	546	469	360	974	322	160	73	417	580	325	428	533	211	245	808	787	15	853	385	344	714	68	316	255
BE	91	193	533	615	506	381	774	316	181	65	377	572	227	394	417	174	195	452	734	19	938	384	322	736	67	265	237
BG	164	281	616	662	572	438	1397	372	196	85	513	719	395	518	708	273	342	690	1019	27	1021	447	450	891	91	406	324
CZ	143	258	599	648	552	413	904	377	196	86	479	668	285	480	549	234	294	501	843	59	1021	454	386	704	90	312	274
DE	121	206	599	640	528	391	748	336	192	73	406	613	263	412	470	193	234	493	739	55	989	406	360	869	82	302	244
DK	71	206	590	631	489	402	1050	335	182	69	375	600	256	420	491	210	221	-	808	20	969	399	343	981	75	275	256
EE	70	200	601	681	505	370	990	381	170	69	383	656	286	430	490	191	182	-	817	21	1066	451	413	-	76	363	281
ES	149	193	582	651	508	374	727	340	191	68	365	617	287	433	481	179	226	44	737	55	1003	484	359	795	83	351	260
FI	126	279	552	599	448	347	408	382	191	90	483	655	284	437	503	227	262	-	649	62	892	467	369	894	77	268	237
FR	167	231	533	610	496	382	804	356	181	76	429	594	307	450	518	193	235	292	766	14	925	432	348	715	68	327	256
GB	94	203	556	628	517	387	1106	322	183	69	346	594	277	477	501	208	221	8	871	21	965	389	345	772	77	283	272
GR	149	246	668	698	591	429	847	359	199	80	487	763	394	462	593	219	276	698	859	24	1113	448	469	976	75	409	293
HU	174	280	717	758	644	475	961	427	212	90	534	792	439	529	656	244	297	861	939	25	1206	515	489	1022	83	457	317
IE	86	197	577	581	480	361	782	297	185	70	326	561	214	427	386	169	154	-	717	18	913	367	326	-	63	205	203
IT	126	214	579	617	526	387	892	350	170	73	405	630	336	432	537	192	229	710	797	13	983	423	392	806	68	349	263
LT	68	199	596	630	486	354	856	337	165	68	371	605	255	406	469	187	235	-	750	20	973	405	346	992	70	274	244
LV	69	194	540	615	456	329	854	346	156	67	363	610	267	403	468	173	240	-	733	21	944	412	375	-	69	326	255
ME	114	194	594	618	522	359	848	325	158	69	371	613	349	396	526	183	241	942	759	22	984	388	413	872	70	408	262
NL	85	177	523	567	466	348	855	294	166	62	356	531	233	386	416	177	193	416	734	19	868	353	308	759	66	247	226
NO	57	167	589	620	422	298	845	291	183	59	313	569	234	364	448	159	159	-	684	11	920	341	327	957	66	261	231
PL	94	203	595	635	529	385	857	330	171	69	396	604	262	417	473	188	225	470	770	20	994	396	348	858	70	291	244
PT	145	182	537	606	463	334	693	314	177	66	327	565	268	414	458	166	221	44	683	55	926	467	333	746	82	329	245
RO	138	229	593	616	520	370	842	356	170	76	424	652	363	431	565	201	258	673	778	23	971	425	424	849	72	376	268
RS	127	206	691	709	596	420	853	363	189	71	425	686	367	444	549	187	234	913	815	13	1134	436	458	973	72	435	283
SE	97	198	599	631	477	357	731	335	191	71	372	608	254	389	454	191	224	-	701	55	961	404	355	997	82	282	241
SI	226	379	592	685	587	470	1184	472	217	111	652	805	463	622	772	322	379	486	1049	33	1048	565	466	955	92	374	347
SK	140	254	588	635	540	402	820	371	191	85	474	658	280	467	533	226	286	492	806	59	1002	449	380	690	87	305	277

Bibliography

[1] Mirko Schäfer, Bo Tranberg, Sabrina Hempel, Stefan Schramm, and Martin Greiner. Decompositions of injection patterns for nodal flow allocation in renewable electricity networks. *Eur. Phys. J. B*, 90(8):144, 2017, doi:10.1140/epjb/e2017-80200-y.

[2] Bo Tranberg, Leon J. Schwenk-Nebbe, Mirko Schäfer, Jonas Hörsch, and Martin Greiner. Flow-based nodal cost allocation in a heterogeneous highly renewable European electricity network. *Energy*, 150:122 – 133, 2018, doi:10.1016/j.energy.2018.02.129.

[3] Bo Tranberg, Mirko Schäfer, Tom Brown, Jonas Hörsch, and Martin Greiner. Flow-Based Analysis of Storage Usage in a Low-Carbon European Electricity Scenario. In *2018 15th International Conference on the European Energy Market (EEM)*, pages 1–5, June 2018, doi:10.1109/EEM.2018.8469951.

[4] Bo Tranberg, Olivier Corradi, Bruno Lajoie, Thomas Gibon, Iain Staffell, and Gorm Bruun Andresen. Real-Time Carbon Accounting Method for the European Electricity Markets. *Submitted to Energy Strategy Reviews*, 2018.

[5] Bo Tranberg, Rasmus Thrane Hansen, and Leopoldo Catania. Managing Volumetric Risk of Long-term Power Purchase Agreements. *Submitted to Energy Economics*, 2018.

[6] Mirko Schäfer, Sabrina Hempel, Jonas Hörsch, Bo Tranberg, Stefan Schramm, and Martin Greiner. Power flow tracing in complex networks. In *New Horizons in Fundamental Physics*, pages 357–373. Springer, 2017, doi:10.1007/978-3-319-44165-8_26.

[7] Emil H Eriksen, Leon J Schwenk-Nebbe, Bo Tranberg, Tom Brown, and Martin Greiner. Optimal heterogeneity in a simplified highly renewable European electricity system. *Energy*, 133:913–928, 2017, doi:10.1016/j.energy.2017.05.170.

[8] Mirko Schäfer, Leon Schwenk-Nebbe, Jonas Hörsch, Bo Tranberg, and Martin Greiner. Allocation of nodal costs in heterogeneous highly renewable European electricity networks. In *2017 14th International Con-*

ference on the European Energy Market (EEM), pages 1–6, June 2017, doi:10.1109/EEM.2017.7981964.

[9] Emil Thøgersen, Bo Tranberg, Jürgen Herp, and Martin Greiner. Statistical meandering wake model and its application to yaw-angle optimisation of wind farms. *Journal of Physics: Conference Series*, 854(1):012017, 2017, doi:10.1088/1742-6596/854/1/012017.

[10] Mirko Schäfer, Bo Tranberg, and Martin Greiner. Power flows in complex renewable energy networks. In *FIAS International Symposion on Discoveries at the Frontiers of Science*, To appear.

[11] IPCC. Special Report: Global Warming of 1.5°C, 2018.

[12] World Commission on Environment and Development. *Our Common Future*. Oxford University Press, 1987.

[13] United Nations. 7. a Kyoto Protocol to the United Nations Framework Convention on Climate Change. December 1997.

[14] European Union. A Roadmap for moving to a competitive low carbon economy in 2050. Communication from the Commission to the European Parliament, the Council, the European Economic and Social Committee and the Committee of the Regions, Low-carbon Economy Roadmap, Brussels, European Commission, 2011.

[15] United Nations. 7. d Paris Agreement. December 2015.

[16] EU Commission. A Clean Planet for all - A European strategic long-term vision for a prosperous, modern, competitive and climate neutral economy, COM(2018) 773, 2018.

[17] International Energy Agency. World Energy Balances 2018, 2018.

[18] Victor D. G., D. Zhou, E. H. M. Ahmed, P. K. Dadhich, J. G. J. Olivier, H-H. Rogner, K. Sheikho, and M. Yamaguchi. Introductory Chapter. In: Climate Change 2014: Mitigation of Climate Change. Contribution of Working Group III to the Fifth Assessment Report of the Intergovernmental Panel on Climate Change. Technical report, IPCC, 2014.

[19] H. Lund and B.V. Mathiesen. Energy system analysis of 100% renewable energy systems—the case of Denmark in years 2030 and 2050. *Energy*, 34(5):524 – 531, 2009, doi:10.1016/j.energy.2008.04.003. 4th Dubrovnik Conference.

[20] Mark Z. Jacobson and Mark A. Delucchi. Providing all global energy with wind, water, and solar power, part i: Technologies, energy resources, quantities and areas of infrastructure, and materials. *Energy Policy*, 39(3):1154 – 1169, 2011, doi:10.1016/j.enpol.2010.11.040.

[21] Mark A. Delucchi and Mark Z. Jacobson. Providing all global energy with wind, water, and solar power, part ii: Reliability, system and transmission costs, and policies. *Energy Policy*, 39(3):1170 – 1190, 2011, doi:j.enpol.2010.11.045.

[22] Stephan Singer et al. *The energy report: 100% renewable energy by 2050.* Ecofys, World Wildlife Fund, 2010.

[23] Mark Z. Jacobson, Mark A. Delucchi, Zack A.F. Bauer, Savannah C. Goodman, William E. Chapman, and Mary A. Cameron et al. 100% clean and renewable wind, water, and sunlight all-sector energy roadmaps for 139 countries of the world. *Joule*, 1(1):108 – 121, 2017, doi:10.1016/j.joule.2017.07.005.

[24] Manish Ram, Dmitrii Bogdanov, Arman Aghahosseini, Ayobami Oyewo, Ashish Gulagi, Michael Child, Hans-Josef Fell, and Christian Breyer. Global energy system based on 100% renewable energy - power sector. Technical report, Lappeenranta University of Technology, 2017.

[25] Kenneth Hansen, Brian Vad Mathiesen, and Iva Ridjan Skov. Full energy system transition towards 100% renewable energy in germany in 2050. *Renewable and Sustainable Energy Reviews*, 102:1 – 13, 2019, doi:10.1016/j.rser.2018.11.038.

[26] Florian Steinke, Philipp Wolfrum, and Clemens Hoffmann. Grid vs. storage in a 100% renewable europe. *Renewable Energy*, 50:826 – 832, 2013, doi:10.1016/j.renene.2012.07.044.

[27] David Schlachtberger, Tom Brown, Stefan Schramm, and Martin Greiner. Networks versus Storage in a Highly Renewable European Electricity System: A Continuous Parameter Sweep. In *11th Conference on Sustainable Development of Energy, Water and Environment Systems : SDEWES 2016*, 2016.

[28] Rolando A. Rodriguez, Magnus Dahl, Sarah Becker, and Martin Greiner. Localized vs. synchronized exports across a highly renewable pan-European transmission network. *Energy, Sustainability and Society*, 5(1):21, Jul 2015, doi:10.1186/s13705-015-0048-6.

[29] Tom Brown, Jonas Hörsch, and David Schlachtberger. PyPSA: Python for Power System Analysis. *Journal of Open Research Software*, 6(4), 2018, doi:10.5334/jors.188.

[30] Jonas Hörsch and Tom Brown. The role of spatial scale in joint optimisations of generation and transmission for European highly renewable scenarios. In *Proceedings of 14th International Conference on the European Energy Market (EEM 2017)*, 2017, doi:10.1109/EEM.2017.7982024.

[31] Tom Brown, David Schlachtberger, Alexander Kies, Stefan Schramm, and Martin Greiner. Synergies of sector coupling and transmission reinforcement in a cost-optimised, highly renewable European energy system. *Energy*, 160:720 – 739, 2018, doi:10.1016/j.energy.2018.06.222.

[32] Kun Zhu, Marta Victoria, Tom Brown, Gorm B. Andresen, and Martin Greiner. Impact of CO2 prices on the design of a highly decarbonised coupled electricity and heating system in Europe. *Applied Energy*, 236:622 – 634, 2019, doi:10.1016/j.apenergy.2018.12.016.

[33] Spyros Chatzivasileiadis, Damien Ernst, and Göran Andersson. The global grid. *Renewable Energy*, 57:372 – 383, 2013, doi:10.1016/j.renene.2013.01.032.

[34] Magnus Dahl, Rolando A. Rodriguez, Anders A. Søndergaard, Timo Zeyer, Gorm B. Andresen, and Martin "Walterson" Greiner. *Infrastructure Estimates for a Highly Renewable Global Electricity Grid*, pages 333–356. Springer International Publishing, 2017, doi:10.1007/978-3-319-44165-8_25.

[35] Sarah Becker, Rolando A. Rodriguez, Gorm B. Andresen, Stefan Schramm, and Martin Greiner. Transmission grid extensions during the build-up of a fully renewable pan-European electricity supply. *Energy*, 64(Supplement C):404 – 418, 2014, doi:10.1016/j.energy.2013.10.010.

[36] Michael Child, Dmitrii Bogdanov, and Christian Breyer. The Baltic Sea Region: Storage, grid exchange and flexible electricity generation for the transition to a 100% renewable energy system. *Energy Procedia*, 155:390 – 402, 2018, doi:10.1016/j.egypro.2018.11.039. 12th International Renewable Energy Storage Conference, IRES 2018, 13-15 March 2018, Düsseldorf, Germany.

[37] Sgouris Sgouridis, Denes Csala, and Ugo Bardi. The sower's way: quantifying the narrowing net-energy pathways to a global energy transition. *Environmental Research Letters*, 11(9):094009, 2016.

[38] B.P. Heard, B.W. Brook, T.M.L. Wigley, and C.J.A. Bradshaw. Burden of proof: A comprehensive review of the feasibility of 100% renewable-electricity systems. *Renewable and Sustainable Energy Reviews*, 76:1122 – 1133, 2017, doi:10.1016/j.rser.2017.03.114.

[39] Tom W. Brown, Tobias Bischof-Niemz, Kornelis Blok, Christian Breyer, Henrik Lund, and Brian V. Mathiesen. Response to 'Burden of proof: A comprehensive review of the feasibility of 100% renewable-electricity systems'. *Renewable and Sustainable Energy Reviews*, 92:834 – 847, 2018, doi:10.1016/j.rser.2018.04.113.

[40] Janusz W. Bialek. Tracing the flow of electricity. *IEEE Proceedings - Generation, Transmission and Distribution*, 143(4):313–320, 1996.

[41] Daniel Kirschen, Ron Allan, and Goran Strbac. Contributions of individual generators to loads and flows. *IEEE Transactions on Power Systems*, 12:52–60, 1997.

[42] Tiago Soares, Fábio Pereira, Hugo Morais, and Zita Vale. Cost allocation model for distribution networks considering high penetration of distributed energy resources. *Electric Power Systems Research*, 124:120–132, 2015, doi:10.1016/j.epsr.2015.03.008.

[43] Bo Tranberg, Anders B. Thomsen, Rolando A. Rodriguez, Gorm B. Andresen, Mirko Schäfer, and Martin Greiner. Power flow tracing in a simplified highly renewable European electricity networks. *New Journal of Physics*, 17:105002, 2015, doi:10.1088/1367-2630/17/10/105002.

[44] Tom Brown. Transmission network loading in Europe with high shares of renewables. *IET Renewable Power Generation*, 9(1):57–65, 2015, doi:10.1049/iet-rpg.2014.0114.

[45] Janusz W. Bialek and Paul A. Kattuman. Proportional sharing assumption in tracing methodology. *IEE Proceedings - Generation, Transmission and Distribution*, 151(4):526–532, July 2004, doi:10.1049/ip-gtd:20040351.

[46] Jonas Hörsch, Mirko Schäfer, Sarah Becker, Stefan Schramm, and Martin Greiner. Flow tracing as a tool set for the analysis of networked large-scale renewable electricity systems. *International Journal of Electrical Power & Energy Systems*, 96:390 – 397, 2018, doi:10.1016/j.ijepes.2017.10.024.

[47] ACER - Agency for the Cooperation of the Energy Regulators. Inter-TSO compensation mechanism. https://www.acer.europa.eu/en/Electricity/Infrastructure_and_network%20development/Pages/Inter-TSO-compensation-mechanism-and-transmission-charging.aspx, Accessed December 2018.

[48] EU Commission. Regulation on laying down guidelines relating to the inter-transmission system operator compensation mechanism and a common regulatory approach to transmission charging, No. 838/2010, 2010.

[49] Samson Yemane Hadush, Cedric De Jonghe, and Ronnie Belmans. The implication of the European inter-TSO compensation mechanism for cross-border electricity transmission investments. *International Journal of Electrical Power & Energy Systems*, 73:674 – 683, 2015, doi:10.1016/j.ijepes.2015.05.041.

[50] Ignacio Pérez-Arriaga, Luis Olmos Camacho, and Francisco Javier Rubio Odériz. Report on cost components of cross border exchanges of electricity. Technical report, Universidad Pontificia Comillas, 2002.

[51] CONSENTEC and Frontier Economics. Study on the further issues relating to the inter-tso compensation mechanism. Final Report, Study commissioned by the European Commission Directorate-General Energy and Transport, 2006.

[52] Dimo Stoilov, Yulian Dimitrov, and Bruno François. Challenges facing the European power transmission tariffs: The case of inter-TSO compensation. *Energy Policy*, 39(9):5203 – 5210, 2011, doi:10.1016/j.enpol.2011.05.044.

[53] On a new regulatory framework for the inter-transmission system operator compensation. Technical report, ACER, 2013.

[54] Luis Olmos Camacho and Ignacio J. Pérez-Arriaga. An assessment of inter-TSO compensation algorithms in the Internal Electricity Market of the European Union. *International Journal of Electrical Power & Energy Systems*, 29(10):699 – 712, 2007, doi:10.1016/j.ijepes.2007.05.004.

[55] Ralph Sims, Pedro Mercado, Wolfram Krewitt, Gouri Bhuyan, Damian Flynn, Hannele Holttinen, Gilberto Jannuzzi, Smail Khennas, Yongqian Liu, Lars J Nilsson, Joan Ogden, Kazuhiko Ogimoto, Mark O'Malley, Hugh Outhred, Øystein Ulleberg, and Frans van Hulle. *Integration of Renewable Energy into Present and Future Energy Systems*. IPCC Special Report on

Renewable Energy Sources and Climate Change Mitigation. Cambridge University Press, 2011.

[56] 10-year network development plan 2016. Technical report, ENTSO-E, 2016.

[57] Paul Schultz, Jobst Heitzig, and Jürgen Kurths. A random growth model for power grids and other spatially embedded infrastructure networks. *The European Physical Journal Special Topics*, 223(12):2593–2610, Oct 2014, doi:10.1140/epjst/e2014-02279-6.

[58] Réka Albert, István Albert, and Gary L. Nakarado. Structural vulnerability of the north american power grid. *Phys. Rev. E*, 69:025103, Feb 2004, doi:10.1103/PhysRevE.69.025103.

[59] Ricard V. Solé, Martí Rosas-Casals, Bernat Corominas-Murtra, and Sergi Valverde. Robustness of the European power grids under intentional attack. *Phys. Rev. E*, 77:026102, Feb 2008, doi:10.1103/PhysRevE.77.026102.

[60] Giovanni Filatrella, Arne H. Nielsen, and Niels F. Pedersen. Analysis of a power grid using a Kuramoto-like model. *The European Physical Journal B*, 61(4):485–491, Feb 2008, doi:10.1140/epjb/e2008-00098-8.

[61] Takashi Nishikawa and Adilson E. Motter. Comparative analysis of existing models for power-grid synchronization. *New Journal of Physics*, 17(1):015012, January 2015, doi:10.1088/1367-2630/17/1/015012.

[62] Pedro H.J. Nardelli, Nicolas Rubido, Chengwei Wang, Murilo S. Baptista, Carlos Pomalaza-Raez, Paulo Cardieri, and Matti Latva-aho. Models for the modern power grid. *The European Physical Journal Special Topics*, 223(12):2423–2437, Oct 2014, doi:10.1140/epjst/e2014-02219-6.

[63] Adilson E. Motter, Seth A. Myers, Marian Anghel, and Takashi Nishikawa. Spontaneous synchrony in power-grid networks. *Nature Physics*, 9(3):191–197, 2013, doi:10.1038/nphys2535.

[64] Martin Rohden, Andreas Sorge, Marc Timme, and Dirk Witthaut. Self-organized synchronization in decentralized power grids. *Phys. Rev. Lett.*, 109:064101, Aug 2012, doi:10.1103/PhysRevLett.109.064101.

[65] Dirk Witthaut, Martin Rohden, Xiaozhu Zhang, Sarah Hallerberg, and Marc Timme. Critical links and nonlocal rerouting in complex supply networks. *Phys. Rev. Lett.*, 116:138701, Mar 2016, doi:10.1103/PhysRevLett.116.138701.

[66] Dominik Heide, Lueder Von Bremen, Martin Greiner, Clemens Hoffmann, Markus Speckmann, and Stefan Bofinger. Seasonal optimal mix of wind and solar power in a future, highly renewable Europe. *Renewable Energy*, 35(11):2483–2489, 2010, doi:10.1016/j.renene.2010.03.012.

[67] Dominik Heide, Martin Greiner, Lüder von Bremen, and Clemens Hoffmann. Reduced storage and balancing needs in a fully renewable European power system with excess wind and solar power generation. *Renewable Energy*, 36(9):2515 – 2523, 2011, doi:10.1016/j.renene.2011.02.009.

[68] Tue Vissing Jensen and Martin Greiner. Emergence of a phase transition for the required amount of storage in highly renewable electricity systems. *European Physical Journal Special Topics*, 223:2475–2481, October 2014, doi:10.1140/epjst/e2014-02216-9.

[69] Rolando A. Rodríguez, Sarah Becker, Gorm B. Andresen, Dominik Heide, and Martin Greiner. Transmission needs across a fully renewable European power system. *Renewable Energy*, 63(Supplement C):467 – 476, 2014, doi:10.1016/j.renene.2013.10.005.

[70] Rachel Baïle and Jean-Fran çois Muzy. Spatial intermittency of surface layer wind fluctuations at mesoscale range. *Phys. Rev. Lett.*, 105:254501, Dec 2010, doi:10.1103/PhysRevLett.105.254501.

[71] Patrick Milan, Matthias Wächter, and Joachim Peinke. Turbulent character of wind energy. *Phys. Rev. Lett.*, 110:138701, Mar 2013, doi:10.1103/PhysRevLett.110.138701.

[72] Debsankha Manik, Martin Rohden, Henrik Ronellenfitsch, Xiaozhu Zhang, Sarah Hallerberg, Dirk Witthaut, and Marc Timme. Network susceptibilities: Theory and applications. *Phys. Rev. E*, 95:012319, Jan 2017, doi:10.1103/PhysRevE.95.012319.

[73] Mark Newman. *Networks: an introduction*. Oxford university press, 2010.

[74] Marc Durand and Denis Weaire. Optimizing transport in a homogeneous network. *Phys. Rev. E*, 70:046125, Oct 2004, doi:10.1103/PhysRevE.70.046125.

[75] Eleni Katifori, Gergely J. Szöllősi, and Marcelo O. Magnasco. Damage and fluctuations induce loops in optimal transport networks. *Phys. Rev. Lett.*, 104:048704, Jan 2010, doi:10.1103/PhysRevLett.104.048704.

[76] S. Gómez, A. Díaz-Guilera, J. Gómez-Gardeñes, C. J. Pérez-Vicente, Y. Moreno, and A. Arenas. Diffusion dynamics on multiplex networks. *Phys. Rev. Lett.*, 110:028701, Jan 2013, doi:10.1103/PhysRevLett.110.028701.

[77] Allen J. Wood and Bruce F. Wollenberg. *Power Generation, Operation, and Control*. John Wiley and Sons, 3 edition, 2013.

[78] Goran Strbac, Daniel Kirschen, and Syed Ahmed. Allocating transmission system usage on the basis of traceable contributions of generators and loads to flows. *IEEE Transactions on Power Systems*, 13(2):527–534, 1998.

[79] Konrad Purchala, Leonardo Meeus, Daniel Van Dommelen, and Ronnie Belmans. Usefulness of DC power flow for active power flow analysis. In *Power Engineering Society General Meeting, 2005. IEEE*, pages 454–459. IEEE, 2005, doi:10.1109/PES.2005.1489581.

[80] Ignacio J. Pérez-Arriaga, F. Jetal Rubio, J. F. Puerta, J. Arceluz, and Javier Marín. Marginal pricing of transmission services: An analysis of cost recovery. *IEEE Transactions on Power Systems*, 10(1):546–553, 1995, doi:10.1109/59.373981.

[81] Hugh Rudnick, Rodrigo Palma, and José E. Fernández. Marginal pricing and supplement cost allocation in transmission open access. *IEEE Transactions on Power Systems*, 10(2):1125–1132, 1995.

[82] Damien Challet, Matteo Marsili, and Yi-Cheng Zhang. *Minority Games*. Oxford University Press, 2005.

[83] European Union. A 2030 framework for climate and energy policies. Climate & Energy Framework, Brussels, European Commission, 2013.

[84] Katrin Schaber, Florian Steinke, and Thomas Hamacher. Transmission grid extensions for the integration of variable renewable energies in Europe: Who benefits where? *Energy Policy*, 43:123–135, 2012, doi:10.1016/j.enpol.2011.12.040.

[85] Jonas Egerer, Casimir Lorenz, and Clemens Gerbaulet. European electricity grid infrastructure expansion in a 2050 context. In *10th International Conference on the European Energy Market (EEM), 2013*, pages 1–7. IEEE, 2013.

[86] David Schlachtberger, Tom Brown, Stefan Schramm, and Martin Greiner. The benefits of cooperation in a highly renewable European electricity network. *Energy*, 134:469 – 481, 2017, doi:http://dx.doi.org/10.1016/j.energy.2017.06.004.

[87] Rolando A. Rodriguez, Sarah Becker, and Martin Greiner. Cost-optimal design of a simplified, highly renewable pan-European electricity system. *Energy*, 83:658 – 668, 2015, doi:10.1016/j.energy.2015.02.066.

[88] Steven Stoft. *Power System Economics – Designing Markets for Electricity*. Wiley-IEEE Press, 2002.

[89] Juan M. Morales, Antonio J. Conejo, Henrik Madsen, Pierre Pinson, and Marco Zugno. *Integrating renewables in electricity markets: Operational problems*. Springer Science & Business Media, 2013.

[90] Christoph Weber. Adequate intraday market design to enable the integration of wind energy into the European power systems. *Energy Policy*, 38(7):3155 – 3163, 2010, doi:10.1016/j.enpol.2009.07.040.

[91] Paul M. Sotkiewicz and J. Mario Vignolo. Allocation of fixed costs in distribution networks with distributed generation. *IEEE transactions on power systems*, 21(2):639–652, 2006, doi:10.1109/TPWRS.2006.873112.

[92] Stefan Bofinger, Lüder von Bremen, Kaspar Knorr, Katharina Lesch, Kurt Rohrig, Yves-Marie Saint-Drenan, and Markus Speckmann. Raum-zeitliche Erzeugungsmuster von Wind- und Solarenergie in der UCTE-Region und deren Einfluss auf elektrische Transportnetze. Abschlussbericht, Institut für Solare Energieversorgungstechnik, ISET e.V., 2008.

[93] Eurostat. Energy statistics: supply, transformation and consumption, Table nrg_105a, 2016.

[94] Eurostat. Infrastructure: electricity: annual data, Table nrg_113a, 2016.

[95] Katrin Schaber, Florian Steinke, Pascal Mühlich, and Thomas Hamacher. Parametric study of variable renewable energy integration in Europe: Advantages and costs of transmission grid extensions. *Energy Policy*, 42:498–508, 2012.

[96] European Transmission System Operators. Indicative values for Net Transfer Capacities (NTC) in Continental Europe. Technical report, ENTSO-E, 2011.

[97] Jan-Erik Skog, Kees Koreman, Bo Pääjärvi, Thomas Worzyk, and Thomas Andersröd. The NorNed HVDC cable link: a power transmission highway between Norway and the Netherlands. Technical report, ABB, 2007.

[98] BritNed Development Limited. BritNed Construction. http://www.britned.com/.

[99] Christoph Kost, Johannes N. Mayer, Jessica Thomsen, Niklas Hartmann, Charlotte Senkpiel, and Simon Philipps et al.'. Levelized cost of electricity renewable energies. *Fraunhofer Institute for Solar Energy Systems ISE, Heidenhofstraße*, 2012.

[100] Walter Short, Daniel J. Packey, and Thomas Holt. *A manual for the economic evaluation of energy efficiency and renewable energy technologies*. University Press of the Pacific, 2005.

[101] Thomas H. Cormen, Charles E. Leiserson, Ronald L. Rivest, and Clifford Stein. *Introduction to algorithms second edition*. The MIT Press, 2001. Chapter 16: Greedy Algorithms.

[102] Stefan Pfenninger, Adam Hawkes, and James Keirstead. Energy systems modeling for twenty-first century energy challenges. *Renewable and Sustainable Energy Reviews*, 33:74–86, 2014, doi:10.1016/j.rser.2014.02.003.

[103] Baowei Li, Yonghua Song, and Zechun Hu. Carbon flow tracing method for assessment of demand side carbon emissions obligation. *IEEE Transactions on Sustainable Energy*, 4(4):1100–1107, Oct 2013, doi:10.1109/TSTE.2013.2268642.

[104] Jonas Hörsch, Fabian Hofmann, David Schlachtberger, and Tom Brown. PyPSA-Eur: An open optimisation model of the European transmission system. *Energy Strategy Reviews*, 22:207 – 215, 2018, doi:10.1016/j.esr.2018.08.012.

[105] Jonas Hörsch, Henrik Ronellenfitsch, Dirk Witthaut, and Tom Brown. Linear optimal power flow using cycle flows. *Electric Power Systems Research*, 158:126–135, 2018, doi:10.1016/j.epsr.2017.12.034.

[106] David P. Schlachtberger, Tom Brown, Mirko Schäfer, Stefan Schramm, and Martin Greiner. Cost optimal scenarios of a future highly renewable European electricity system: Exploring the influence of weather data, cost parameters and policy constraints. *Energy*, 163:100 – 114, 2018, doi:10.1016/j.energy.2018.08.070.

[107] International Energy Agency. Global EV Outlook 2018, 2018.

[108] Matthew Brander, Michael Gillenwater, and Francisco Ascui. Creative accounting: A critical perspective on the market-based method for reporting purchased electricity (scope 2) emissions. *Energy Policy*, 112:29 – 33, 2018, doi:10.1016/j.enpol.2017.09.051.

[109] World Resource Institute. GHG Protocol Scope 2 Guidance, 2015.

[110] Scott Jiusto. The differences that methods make: Cross-border power flows and accounting for carbon emissions from electricity use. *Energy Policy*, 34(17):2915 – 2928, 2006, doi:10.1016/j.enpol.2005.05.002.

[111] Hanne Lerche Raadal. Greenhouse gas (GHG) emissions from electricity generation systems. Tracking and claiming in environmental reporting, 2013. Available at https://www.ostfoldforskning.no/media/1727/thesis-hanne-final_excl-appendices.pdf.

[112] Jing-Li Fan, Yun-Bing Hou, Qian Wang, Ce Wang, and Yi-Ming Wei. Exploring the characteristics of production-based and consumption-based carbon emissions of major economies: A multiple-dimension comparison. *Applied Energy*, 184:790 – 799, 2016, doi:10.1016/j.apenergy.2016.06.076.

[113] Zengkai Zhang and Jintai Lin. From production-based to consumption-based regional carbon inventories: Insight from spatial production fragmentation. *Applied Energy*, 211:549 – 567, 2018, doi:10.1016/j.apenergy.2017.11.047.

[114] John Clauß, S. Stinner, C. Solli, Karen B. Lindberg, Henrik Madsen, and Laurent Georges. A generic methodology to evaluate hourly average CO2eq. intensities of the electricity mix to deploy the energy flexibility potential of Norwegian buildings. In *10th International Conference on System Simulation in buildings*, 2018.

[115] Jörgen Sjödin and Stefan Grönkvist. Emissions accounting for use and supply of electricity in the nordic market. *Energy Policy*, 32(13):1555 – 1564, 2004, doi:10.1016/S0301-4215(03)00129-0.

[116] Manfred Lenzen, Joy Murray, Fabian Sack, and Thomas Wiedmann. Shared producer and consumer responsibility — theory and practice. *Ecological Economics*, 61(1):27 – 42, 2007, doi:10.1016/j.ecolecon.2006.05.018.

[117] Glen P. Peters. From production-based to consumption-based national emission inventories. *Ecological Economics*, 65(1):13 – 23, 2008, doi:10.1016/j.ecolecon.2007.10.014.

[118] Tomorrow. electricityMap Database. https://data.electricitymap.org, 2016.

[119] Tomorrow. electricityMap. https://github.com/tmrowco/electricitymap-contrib, 2016.

[120] Gregor Wernet, Christian Bauer, Bernhard Steubing, Jürgen Reinhard, Emilia Moreno-Ruiz, and Bo Weidema. The ecoinvent database version 3 (part I): overview and methodology. *The International Journal of Life Cycle Assessment*, 21(9):1218–1230, 2016, doi:10.1007/s11367-016-1087-8.

[121] Friedrich Kunz. Quo vadis? (un)scheduled electricity flows under market splitting and network extension in central Europe. *Energy Policy*, 116:198 – 209, 2018, doi:10.1016/j.enpol.2018.01.051.

[122] WindEurope. Wind in power 2017. Technical report, Wind Europe, 2018. Available at https://windeurope.org/about-wind/statistics/european/wind-in-power-2017/.

[123] WindEurope. Wind energy in Europe: Outlook to 2020. Technical report, Wind Europe, 2017. Available at https://windeurope.org/about-wind/reports/wind-energy-in-europe-outlook-to-2020/.

[124] Tue Vissing Jensen. *Exploring market models for a European electricity grid with a high peneration of renewable resources*. PhD thesis, 2017.

[125] Lion Hirth. The market value of variable renewables. *Energy Economics*, 38:218–236, jul 2013, doi:10.1016/j.eneco.2013.02.004.

[126] Florentina Paraschiv, David Erni, and Ralf Pietsch. The impact of renewable energies on EEX day-ahead electricity prices. *Energy Policy*, 73:196 – 210, 2014, doi:10.1016/j.enpol.2014.05.004.

[127] Tryggvi Jónsson, Pierre Pinson, and Henrik Madsen. On the market impact of wind energy forecasts. *Energy Economics*, 32(2):313–320, mar 2010, doi:10.1016/j.eneco.2009.10.018.

[128] Andrew D. Mills and Ryan H. Wiser. Changes in the economic value of photovoltaic generation at high penetration levels: A pilot case study of california. In *2012 IEEE 38th Photovoltaic Specialists Conference (PVSC) PART 2*, pages 1–9. IEEE, 2012.

[129] David Ruppert and David S. Matteson. *Statistics and Data Analysis for Financial Engineering with R Examples*. Springer, 2nd edition, 2015.

[130] Anca Pircalabu, Thomas Hvolby, Jesper Jung, and Esben Høg. Joint price and volumetric risk in wind power trading: A copula approach. *Energy Economics*, 62:139–154, feb 2017, doi:10.1016/j.eneco.2016.11.023.

[131] ENTSO-E. Electricity in Europe 2016. Technical report, ENTSO-E, 2017.

[132] Janina C. Ketterer. The impact of wind power generation on the electricity price in Germany. *Energy Economics*, 44:270 – 280, 2014, doi:10.1016/j.eneco.2014.04.003.

[133] Dylan Mcconnell and Mike Sandiford. Winds of change - an analysis of recent changes in the south australian electricity market. Technical report, Melbourne Energy Institute, 2016.

[134] Enzo Fanone, Andrea Gamba, and Marcel Prokopczuk. The case of negative day-ahead electricity prices. *Energy Economics*, 35:22 – 34, 2013, doi:10.1016/j.eneco.2011.12.006. Quantitative Analysis of Energy Markets.

[135] Andrew J. Patton. A review of copula models for economic time series. *Journal of Multivariate Analysis*, 110:4 – 18, 2012, doi:10.1016/j.jmva.2012.02.021. Special Issue on Copula Modeling and Dependence.

[136] Sjur Westgaard. Energy spread modeling using copulas. In *Energy Pricing Models: Recent Advances, Methods, and Tools*, chapter 4. Palgrave Macmillan, 2015.

[137] Karl Friedrich Siburg, Pavel Stoimenov, and Gregor N.F. Weiß. Forecasting portfolio-value-at-risk with nonparametric lower tail dependence estimates. *Journal of Banking & Finance*, 54:129 – 140, 2015, doi:10.1016/j.jbankfin.2015.01.012.

[138] Yumi Oum and S Oren. Var constrained hedging of fixed price load-following obligations in competitive electricity markets. *Risk and Decision Analysis*, 1:43–56, 01 2009, doi:10.3233/RDA-2008-0005.

[139] Yumi Oum and Shmuel S. Oren. Optimal static hedging of volumetric risk in a competitive wholesale electricity market. *Decision Analysis*, 7:107–122, 03 2010, doi:10.1287/deca.1090.0167.

[140] Michael Coulon, Warren B. Powell, and Ronnie Sircar. A model for hedging load and price risk in the texas electricity market. *Energy Economics*, 40:976 – 988, 2013, doi:10.1016/j.eneco.2013.05.020.

[141] Anca Pircalabu and Jesper Jung. A mixed c-vine copula model for hedging price and volumetric risk in wind power trading. *Quantitative Finance*, 17(10):1583–1600, 2017, doi:10.1080/14697688.2017.1307511.

[142] Alexander J. McNeil, Rüdiger Frey, and Paul Embrechts. *Quantitative Risk Management: Concepts, Techniques and Tools (Princeton Series in Finance)*. Princeton University Press, 2015.

[143] Leopoldo Catania and Stefano Grassi. Modelling crypto-currencies financial time-series. *SSRN Electronic Journal*, 2017, doi:10.2139/ssrn.3028486.

[144] Andrew C. Harvey. *Dynamic Models for Volatility and Heavy Tails: With Applications to Financial and Economic Time Series (Econometric Society Monographs)*. Cambridge University Press, 2013.

[145] Francisco Blasques, Siem Jan Koopman, and Andre Lucas. Maximum likelihood estimation for generalized autoregressive score models. *SSRN Electronic Journal*, 2014, doi:10.2139/ssrn.2404276.

[146] Alessandro G. Laporta, Luca Merlo, and Lea Petrella. Selection of value at risk models for energy commodities. *Energy Economics*, 74:628 – 643, 2018, doi:10.1016/j.eneco.2018.07.009.

[147] Harry Joe. *Dependence modeling with copulas*. Chapman and Hall/CRC, 2014.

[148] Abe Sklar. Fonctions de répartition à n dimensions et leurs marges. vol. 8. *Institut Statistique de l'Université de Paris*, 1959.

[149] Andrew J. Patton. Estimation of multivariate models for time series of possibly different lengths. *Journal of Applied Econometrics*, 21(2):147–173, 2006, doi:10.1002/jae.865.

[150] Christopher G. Lamoureux and William D. Lastrapes. Persistence in variance, structural change, and the GARCH model. *Journal of Business & Economic Statistics*, 8(2):225–234, 1990.

[151] Andrew Harvey and Alessandra Luati. Filtering with heavy tails. *Journal of the American Statistical Association*, 109(507):1112–1122, 2014.

[152] Laurent E. Calvet, Veronika Czellar, and Elvezio Ronchetti. Robust filtering. *Journal of the American Statistical Association*, 110(512):1591–1606, 2015, doi:10.1080/01621459.2014.983520.

[153] Drew Creal, Siem Jan Koopman, and André Lucas. Generalized autoregressive score models with applications. *Journal of Applied Econometrics*, 28(5):777–795, jan 2013, doi:10.1002/jae.1279.

[154] Andrew Harvey and Genaro Sucarrat. EGARCH models with fat tails, skewness and leverage. *Computational Statistics & Data Analysis*, 76:320–338, aug 2014, doi:10.1016/j.csda.2013.09.022.

[155] Carmen Fernández and Mark F. J. Steel. On bayesian modeling of fat tails and skewness. *Journal of the American Statistical Association*, 93(441):359–371, 1998.

[156] Dongming Zhu and John W. Galbraith. A generalized asymmetric student-t distribution with application to financial econometrics. *Journal of Econometrics*, 157(2):297–305, 2010, doi:10.1016/j.jeconom.2010.01.013.

[157] Andrew Patton. Copula methods for forecasting multivariate time series. In *Handbook of Economic Forecasting*, pages 899–960. Elsevier, 2013, doi:10.1016/b978-0-444-62731-5.00016-6.

[158] Harry Joe. *Multivariate Models and Multivariate Dependence Concepts (Chapman & Hall/CRC Monographs on Statistics & Applied Probability)*. Chapman and Hall/CRC, 1997.

[159] Dimitris N. Politis and Joseph P. Romano. The stationary bootstrap. *Journal of the American Statistical Association*, 89(428):1303–1313, dec 1994, doi:10.1080/01621459.1994.10476870.

[160] Douglas Rivers and Quang Vuong. Model selection tests for nonlinear dynamic models. *The Econometrics Journal*, 5(1):1–39, jun 2002, doi:10.1111/1368-423x.t01-1-00071.

[161] Cees Diks, Valentyn Panchenko, and Dick van Dijk. Out-of-sample comparison of copula specifications in multivariate density forecasts. *Journal of Economic Dynamics and Control*, 34(9):1596–1609, sep 2010, doi:10.1016/j.jedc.2010.06.021.

[162] Sais E. Said and David A. Dickey. Testing for unit roots in autoregressive-moving average models of unknown order. *Biometrika*, 71(3):599–607, 1984, doi:10.1093/biomet/71.3.599.

[163] G. S. Maddala and In-Moo Kim. *Unit Roots Cointegration and Structural Change*. Cambridge University Press, 1999, doi:10.1017/cbo9780511751974.

[164] Francis X. Diebold, Todd A. Gunther, and Anthony S. Tay. Evaluating density forecasts with applications to financial risk management. *International Economic Review*, 39(4):863, nov 1998, doi:10.2307/2527342.

[165] Robert F. Engle. Autoregressive conditional heteroscedasticity with estimates of the variance of United Kingdom inflation. *Econometrica*, 1982.

[166] David Ardia, Kris Boudt, and Leopoldo Catania. Downside risk evaluation with the R package GAS. *The R Journal, Forthcoming*, 2018, doi:10.2139/ssrn.2871444.

[167] David Ardia, Kris Boudt, and Leopoldo Catania. Generalized Autoregressive Score models in R: The GAS package. *Journal of Statistical Software, Forthcoming*, 2018, doi:10.2139/ssrn.2825380.

[168] Francis X. Diebold. Comparing predictive accuracy, twenty years later: A personal perspective on the use and abuse of diebold–mariano tests. *Journal of Business & Economic Statistics*, 33(1):1–1, jan 2015, doi:10.1080/07350015.2014.983236.

[169] ENTSO-E. Statistical factsheet 2015, 2016.

[170] Country-specific hourly load data. https://www.entsoe.eu/data/data-portal/consumption, 2016.

[171] Gorm B. Andresen, Anders A. Søndergaard, and Martin Greiner. Validation of Danish wind time series from a new global renewable energy atlas for energy system analysis. *Energy*, 93(Part 1):1074 – 1088, 2015, doi:10.1016/j.energy.2015.09.071.

[172] Mauro Bernardi and Leopoldo Catania. Switching generalized autoregressive score copula models with application to systemic risk. *Journal of Applied Econometrics*, 0(0), 2018, doi:10.1002/jae.2650.

[173] David Oakes Amita K. Manatunga. Fisher information for a bivariate extreme value distribution. *Biometrika*, 79(4):827–832, 1992, doi:10.1093/biomet/79.4.827.

[174] David Oakes. A model for association in bivariate survival data. *Journal of the Royal Statistical Society. Series B (Methodological)*, 44(3):414–422, 1982.